Molecular Mechanisms of Estrogenic Xenobiotica

Dissertation zur Erlangung des Grades
„Doktor der Naturwissenschaften“ im Promotionsfach Pharmazie

am Fachbereich Chemie, Pharmazie, Geographie und Geowissenschaften
der Johannes Gutenberg-Universität Mainz

Madeleine Söngen
geb. in Essen

Mainz, den 16. Juni 2020

D77 (Dissertation Johannes Gutenberg-Universität Mainz)

First report	*(in online-Version entfernt)*
Second report	*(in online-Version entfernt)*
Oral examination	March 2nd, 2021

Contents

1 Introduction **7**

2 Material and methods **9**

2.1 Chemicals 9

2.2 Virtual screening 9

2.3 Molecular docking 9

2.4 Cell culture 10

2.5 Generating ERα overexpressing HEK293 cells 10

2.6 RNA extraction 11

2.7 RNA sequencing 11

2.8 Ingenuity pathway analysis 11

2.9 RT-qPCR 12

2.10 Microscale thermophoresis 12

2.11 Cytotoxicity assay 13

2.12 ER transcription factor activation assay 13

2.13 Cell cycle analysis 14

3 Bisphenols **17**

3.1 Abstract 17

3.2 Introduction 18

3.3 Results 19

3.4 Discussion 41

3.5 Conclusion 45

3.6 Acknowledgement 46

3.7 Supplementary material 46

4 Phthalates **53**

4.1 Abstract . . . 53
4.2 Introduction . . . 54
4.3 Results . . . 54
4.4 Discussion . . . 65
4.5 Conclusion . . . 67
4.6 Acknowledgement . . . 68
4.7 Supplementary material . . . 68

5 Organophosphate ester **73**

5.1 Abstract . . . 73
5.2 Introduction . . . 74
5.3 Results . . . 75
5.4 Discussion . . . 83
5.5 Conclusion . . . 85
5.6 Acknowledgement . . . 86
5.7 Supplementary material . . . 86

6 Polycyclic aromatic hydrocarbons **93**

6.1 Abstract . . . 93
6.2 Introduction . . . 94
6.3 Results . . . 95
6.4 Discussion . . . 107
6.5 Conclusion . . . 110
6.6 Acknowledgement . . . 110
6.7 Supplementary material . . . 110

7 Summary **115**

Bibliography **117**

Publications and presentations **143**

Abbreviations

4MeBPA	tetramethyl bisphenol A
AF	activation function
BBP	benzyl butyl phthalate
BCP	benzyl cyclohexyl phthalate
BOP	butyl octyl phthalate
BPA	bisphenol A
BPB	bisphenol B
BPZ	bisphenol Z
E2	17-β-estradiol
EDC	endocrine-disrupting chemical
ER	estrogen receptor
ERα	estrogen receptor α
ESR1	estrogen receptor 1
FSC-A	forward-scatter area
FSC-H	forward-scatter height
GFP	green fluorescence protein
H-bond	hydrogen bond
Indpy	indeno[1,2,3-*cd*]pyrene
IPA	Ingenuity pathway analysis
LBD	ligand binding domain
MST	microscale thermophoresis
NGS	next-generation sequencing
PAH	polycyclic aromatic hydrocarbon
PI	propidium iodide
Pice	picene
POP	persistent organic pollutant
RT-qPCR	real-time quantitative polymerase chain reaction
SD	standard deviation
SSC-A	side-scatter area
TOCP	tri-*o*-cresyl phosphate

1 Introduction

Microplastic: From human waste to human health

There is a large, and steadily increasing amount of plastic in the oceans [1, 2]. This environmental pollution has manyfold consequences, for example for marine animals: Animals can get entangled in macroscopic pieces of waste and can ingest pieces of plastic, often leading to their death [3–5]. As large plastic pieces break down, smaller particles are easily mistaken for food by fish and other marine animals. This so-called "microplastic" (with a size below 5 mm [6]) was found to have a negative effect on feeding, fertility and lifespan of marine animals *in vitro* [7–13].

Plasticizers leaching out of the plastic over time are suspected as the main origin of these adverse health effects [14–16]. A possible, yet to be tested hypothesis for the adverse health effects is the similarity between the molecular structure of plasticizers and those of hormones, like estrogen. As marine animals enter the human food chain, the effects of microplastic on humans are of increasing concern, yet details remain unknown [17–23].

Therefore, I investigate in this thesis the effect of xenobiotic compounds associated with microplastic on the human estrogen receptor α.

Methodology

For a systematic study, I screened 1845 molecules for their binding affinity towards the human estrogen receptor α (ERα) using virtual screening and molecular docking. Compounds with a high binding affinity were selected for *in vitro* experiments in immortalized human cell cultures. I used the ERα positive breast cancer cell line MCF-7 and generated an *ESR1*-overexpressing HEK293 cell line, named HEK-ESR1. I analyzed the compounds' ability to bind to ERα, to activate the receptor, their effect on the cell cycle proliferation and finally their ability to alter the gene expression by employing next-generation sequencing. All experimental methods are detailed in chapter 2.

The four compound groups

As a result of the screening, I identified ten compounds for *in vitro* measurements. Of these compounds, eight compounds are used as plasticizers and two compounds

are known as environmental pollutants. Thereby, two major concerns regarding microplastic and health are responded to: (1) the leaching of plasticizers out of the microplastic over time, and (2) microplastic as carrier of accumulated environmental toxins, present in the water.

This thesis is structured into four main chapters, each dealing with one compound group: Chapter 3 deals with the four bisphenol compounds bisphenol A, bisphenol B, bisphenol Z and tetramethyl bisphenol A. Chapter 4 is about the three phtalates benzyl butyl phthalate, butyl cyclohexyl phthalate, and butyl octyl phthalate. In chapter 5 I discuss the effects of the organophosphate ester tri-*o*-cresyl phosphate. Finally, in chapter 6 I focus on two polycyclic aromatic hydrocarbons: indeno[1,2,3-*cd*]pyrene and picene.

In this study I demonstrate that all investigated compounds bind *in silico* and *in vitro* to ERα. I observe the activation of the receptor by seven compounds. Additionally, four compounds show an influence on the cell cycle proliferation. RNA sequencing resulted in several differentially expressed genes with *ESR1* as upstream regulator. The gene expression pattern indicates an influence of all compounds on tumorigenesis with individual emphasis on invasion, migration, apoptosis, cell proliferation, angiogenesis and poor outcome in therapy. All compounds interfere with the human estrogen receptor α and, therefore, have the potential to induce adverse health effects in humans.

2 Material and methods

2.1 Chemicals

2,2-Bis(4-hydroxyphenyl)propane (bisphenol A, CAS 80-05-7, >99%), 2,2-bis(4-hydroxyphenyl)butane (bisphenol B, CAS 77-40-7, >98%), 1,1-bis(4-hydroxyphenyl)cyclohexane (bisphenol Z, CAS 843-55-0, >98%), 2,2-bis(4-hydroxy-3,5-dimethylphenyl)propane (tetramethyl bisphenol A, CAS 5613-46-7, >98%), picene (CAS 213-46-7, 99.9%), and tri-*o*-cresyl phosphate (TOCP, CAS 78-30-8, > 97.0%) were purchased from TCI Deutschland GmbH, Eschborn, Germany. 17-β-Estradiol (CAS 50-28-2, 96%), indeno[1,2,3-cd]-pyrene (CAS 193-39-5, 98%), and butyl cyclohexyl phthalate (BCP, CAS 84-64-0, 98%) were purchased from Toronto Research Chemicals, ON, Canada. Benzyl butyl phthalate (BBP, CAS 85-68-7, 98%) was purchased from Oxchem Corporation, IL, USA. Butyl octyl phthalate (BOP, CAS 84-78-6, 99.0%) was purchased from LGC Standards GmbH, Wesel, Germany.

2.2 Virtual screening

We screened 1845 compounds associated as environmental toxin and/or with plastic production to the whole ERα-LBD with the Virtual Screening Tool PyRx 0.9. Ligands were selected based on the list of environmental chemicals provided by CDC (cdc.gov/biomonitoring/environmental_chemicals.html) and the Toxin and Toxin Target Database (t3db.ca). The three-dimensional ligand structures were downloaded from PubChem (NCBI, MD, USA) [24] as standard data files. The crystal structure of ERα-LBD was downloaded from the Protein Data Bank (http://www.rcsb.org/) [25] as PDB file (PDB code: 5U2D) [26]. The binding affinity of all compounds to the whole ERα-LBD was calculated. Based on the lowest binding energy, four bisphenolic, three phthalate, one phosphate, and two PAH compound were selected for further investigation.

2.3 Molecular docking

We analyzed the *in silico* binding of the selected compounds and E2 to the ERα-LBD with AutoDock 4.2.6 (The Scripps Research Institute, CA, USA) [27]. AutoDockTools 1.5.6 was used to prepare the molecular docking. Ligand and protein files were converted to Protein Data Bank Partial Charge and Atom Type (PDBQT) files. A grid

box was set first around the whole protein (blind docking) and subsequently around the E2-binding pocket in the ERα-LBD (defined docking). The blind docking was performed with the center of the grid box at x=-15.057, y=16.023, z=2.325 and the number of grid points in x, y, and z direction set to 148, 130, and 136 with a spacing of 0.375 Å. For the defined docking, the center of the grid box was located at x=-4.989, y=22.471, z=5.499 and the number of grid points in x, y, and z direction set to 58, 46, and 46 with a spacing of 0.375 Å. The AutoDock build-in Lamarckian Algorithm has been used for the calculation with 250 runs and 25 Mio evaluations each. Results were obtained from the RMSD cluster analysis from AutoDock, using an RMSD-tolerance of 2.0 Å. Interacting amino acids were identified with AutoDockTools. Visual Molecular Dynamics 1.9.3 (VMD) was used to create the visualizations (http://www.ks.uiuc.edu/Research/vmd/) [28]. Parts of this research were conducted using the supercomputer Mogon and advisory services offered by Johannes Gutenberg University Mainz (hpc.uni-mainz.de), which is a member of the AHRP (Alliance for High Performance Computing in Rhineland Palatinate, www.ahrp.info) and the Gauss Alliance e.V.

2.4 Cell culture

MCF-7 and HEK-ESR1 cells were grown in phenol red free, high glucose Dulbecco's Modified Eagle Medium (DMEM, 21063029, GibcoTM) supplemented with 10% fetal bovine serum (10270106, GibcoTM) and 1% penicillin/ streptomycin (15144120, GibcoTM). Cells were grown at 37°C, 90% humidity and a 5% CO2 atmosphere. Cells were detached after washing with Dulbecco's phosphate-buffered saline (DPBS, 14190094, GibcoTM) and applying phenol red free Trypsin-EDTA 0.5% (15400054, GibcoTM).

2.5 Generating ERα overexpressing HEK293 cells

HEK-ESR1 cells were generated by transfection of HEK293 cells with the Precision LentiORFTM plasmid OHS5898-224630674 (Horizon Discovery Group, Cambridge, UK), containing the information for ERα, green fluorescence protein (GFP) and the antibiotic blasticidin S HCl. The transfection was performed with the DharmaFECT kb transfection reagent T-2006-01 from the Horizon Discovery Group, according to the manufacturer's instruction. For stable transfection the cells were grown in phenol red free DMEM medium (21063029, GibcoTM) with blasticidin S HCl (R21001, GibcoTM) for three weeks. Stable transfected cells expressing GFP were isolated by fluorescence-activated cell sorting (FACS) by the flow cytometry core facility at IMB, Mainz, Germany. Briefly, the transfected cells were collected in sorting buffer (1 mM EDTA, 1% FBS, in PBS buffer) and sorted on a BD FACSAria III cell sorter with a nozzle size of 100 µm and a sheath pressure of 23 psi into 96 well plates using the single

cell sort precision. After sorting, the single cells were kept in conditioned medium, containing 50% sterile filtered cell culture supernatant from the same cell line and 20% FBS. Growing HEK-ESR1 cell clones were further cultured in phenol red free DMEM medium containing 10 µg mL^{-1} blasticidin S HCl.

2.6 RNA extraction

Aliquots of $3.5 \cdot 10^5$ MCF-7 cells were seeded into 6-well-plates 24 h before treatment. Cells were treated with the bisphenol, phthalate and phosphate compounds resulting in a final concentration of 25 µM and with the PAH compounds resulting in a final concentration of 0.5 µM. Control cells were treated with 0.2% DMSO. After 8 h incubation, the cells were harvested with phenol red free trypsin 0.5% (GibcoTM). RNA extraction was performed with the InviTrap®Spin Cell RNA Mini Kit (Invitek Molecular GmbH, Berlin, Germany), according to the manufacturer's instruction. Briefly, the cell pellet was lysed with 350 µL Lysis Solution, treated with β-mercaptoethanol. After DNA removal, 350 µL 70% ethanol were added and the sample applied onto the RNA-RTA Spin Filter. After several washing steps, RNA was eluted with 60 µL of RNAse free water (New England Biolabs, MA, USA) and the concentration and purity measured with NanoDrop.

2.7 RNA sequencing

Next-generation sequencing was carried out by StarSEQ GmbH, Mainz, Germany. The quality of the extracted RNA was verified by the company with a 2100 Bioanalyzer system (Agilent Technologies, CA, USA). After mRNA isolation and library preparation using the NEBNext© Ultra™ II Directional RNA Library Prep Kit (New England Biolabs, MA, USA) RNA sequencing was performed with the Illumina NextSeq 500™ system using 25 Mio paired-end reads (2 × 150 nt). Fold changes were calculated by StarSEQ GmbH using the STAR Alignment workflow, followed by a pairwise comparison with DESeq2. Thereby, the expressions of the samples were compared to the DMSO control, respectively. Each sample was measured in biological duplicates.

2.8 Ingenuity pathway analysis

The differentially expressed genes based on NGS were analyzed with the Ingenuity Pathway Analysis (IPA) software (Qiagen, MD, USA). Core analysis was performed for all expressed genes with a p-value ≤ 0.05. The analysis settings were adjusted to the following values: reference set: ingenuity knowledge base (genes only); relationship to include: direct and indirect; include endogenous chemicals: true; filter summary:

species = human, confidence = experimentally observed, cell lines = all, node types = all, mutation = all, data sources = all. Networks were created based on the upstream analysis using *ESR1* as upstream regulator. Networks were displayed with the IPA Path Designer.

2.9 RT-qPCR

Aliquots of 1 µg of the extracted RNA was converted into cDNA with the Luna ScriptTM RT SuperMix Kit (E3010) from New England Biolabs GmbH, according to the manufacturer's instruction. Real-time quantitative polymerase chain reaction (RT-qPCR) was performed with the 5 x Hot Start Taq EvaGreen® qPCR Mix (No Rox) from Axon-Labortechnik (Kaiserslautern, Germany) according to the manufacturer's instruction. PCR primers were ordered from Eurofins Genomics Germany GmbH, Ebersberg, Germany. The primers were designed with the Primer-BLAST tool from NCBI and were double-checked for suitability with the Oligo Analyse Tool from Eurofins Genomics. Primer sequences are listed in Table 2.1. *GAPDH* and *HSP90AB1* were both selected as reference genes as they were not differentially expressed in the NGS data. The RT-qPCR was carried out with the CFX384TM Real-Time PCR Detection System (Bio-Rad Laboratories GmbH, Feldkirchen, Germany). Each sample was measured in biological triplicates with technical duplicates. The fold change *FC* was calculated based on the absolute value of the threshold cycles of the gene of interest (gene) and the reference gene (ref) from the sample (smp) as well as the control (cntr):

$$\Delta C_\mathrm{t} = C_\mathrm{t,gene} - C_\mathrm{t,ref} \tag{2.1}$$

$$\Delta\Delta C_\mathrm{t} = C_\mathrm{t,smp} - C_\mathrm{t,cntr} \tag{2.2}$$

$$FC = \log_2\left(2^{-\Delta\Delta C_\mathrm{t}}\right) \tag{2.3}$$

The fold change was calculated as fold change and plotted against the fold change of the NGS data. A linear regression was calculated with Origin 7.5. The comparison was performed for both reference genes.

2.10 Microscale thermophoresis

Microscale thermophoresis (MST) was performed with ERα as fluorescently labeled protein and the bisphenolic, phthalate, organophosphate ester, and PAH compounds and E2 as ligands. ERα was purchased as recombinant human protein (TP313277) from OriGene Technologies Inc., MD, USA. The protein had a concentration of 0.55 µg µL^{-1} (lot: WX1018M11). It was stained with the Monolith Protein Labeling Kit RED-NHS 2nd Generation (MO-L011) from NanoTemper Technologies GmbH, Munich, Germany. The concentration of the protein after buffer exchange was 7.55 µM. The protein was

stained according to the manufacturer's instruction using the dye with five times the protein concentration. After staining, the proteins were split into 10 µL aliquots and flash-frozen in liquid nitrogen. The MST experiments were performed with the Monolith NT.115 system using standard treated capillaries (MO-K022) according to the manufacturer's instruction. The results were obtained with an LED power of 95% and an MST power of 20%. The NT Analysis Software was used to analyze the results.

2.11 Cytotoxicity assay

Cytotoxicity of the bisphenolic compounds, phthaltes, TOCP and E2 on HEK-ESR1 cells was analyzed with resazurin reduction assay. 10^4 HEK-ESR1 cells were seeded per well in a 96-well-plate in 100 µL DMEM. Two columns were filled only with medium as control. After 24 h, the cells were treated with different concentrations of the compounds diluted in 100 µL DMEM medium, respectively. Each concentration was tested six times. 100 µL DMSO containing medium were added to one row as control. After 72 h incubation time, 20 µL of a 0.01% resazurin solution were added to all wells. The fluorescence signal was measured 4 h later using an Infinite M2000 Pro plate reader (Tecan, Crailsheim, Germany) with an excitation wavelength of 544 nm and an emission wavelength of 590 nm. The survival rate *SR* was calculated with the mean fluorescence of the respective samples , medium and DMSO as control as follows:

$$SR = \frac{m_{\text{smp}} - m_{\text{medium}}}{m_{\text{DMSO}} - m_{\text{medium}}} \cdot 100\% \tag{2.4}$$

The survival rate was plotted against the concentration of the compounds and thereof the 50% inhibition concentration IC_{50} calculated as mean ± standard deviation (SD) based on three independent experiments (biological replicates).

2.12 ER transcription factor activation assay

$3 \cdot 10^5$ HEK-ESR1 cells were seeded per well in 2 mL phenol red free DMEM using 6-well-plates. After 24 h the compounds were added to a final concentration of 25 µM. The compounds were diluted in DMSO, resulting in a final DMSO concentration of 0.2%. Nuclear extraction was performed 4 h and 8 h after the treatment, using a cell scraper to detach the cells. The NE-PER™ nuclear and cytoplasmic extraction reagents kit (78833, Thermo Scientific) was used to prepare nuclear extracts mainly according to the manufacturer's instructions. However, instead of vortexing after addition of the nuclear extraction reagent, the samples were treated four times with 5 s of sonication with a 10 s break on ice between each cycle. The protein concentration was measured with NanoDrop. The nuclear extracts were used in the estrogen receptor

transcription factor assay kit (ab207203, Abcam plc, Cambridge, UK) according to the manufacturer's instruction. 10 µg of the prepared nuclear extracts were applied per well. The absorbance was measured with the Infinite M2000 Pro plate reader (Tecan, Crailsheim, Germany). The estrogen receptor activation was calculated based on the averaged absorbance $\bar{A}$ of the samples (smp) at the measurement (ms) wavelength at 450 nm and the reference (rf) wavelength at 655 nm. DMSO treated cells were used as control (cntr) as follows:

$$ER_{\text{act}} = \left(\bar{A}_{\text{ms,smp}} - \bar{A}_{\text{rf,smp}}\right) - \left(\bar{A}_{\text{ms,cntr}} - \bar{A}_{\text{rf,cntr}}\right) \tag{2.5}$$

2.13 Cell cycle analysis

$3 \cdot 10^5$ HEK-ESR1 and $4 \cdot 10^5$ MCF-7 cells were seeded 24 h before treatment in 2 mL phenol red free medium in 6-well-plates. The bisphenol compounds, phthalate compounds, TOCP, and E2 were added with a final concentration of 25 µM and 50 µM, each. The PAH compounds with a final concentration of 0.5 µM and 0.1 µM, each. Compounds were diluted in DMSO, resulting in a final DMSO concentration of 0.2%. After 4 h and 8 h of treatment, respectively, the cells were harvested using trypsin 0.5% and centrifuged at 350 g for 5 min at 10 °C. The cell pellet was washed with 900 µL ice cold PBS. 900 µL ice cold 70% ethanol was added dropwise to the cell pellet while vortexing on the highest setting. The fixed cells were stored at −20 °C. In order to stain the cells with propidium iodide (PI), the cells were centrifuged at 350 g for 5 min at 10 °C and the cell pellet washed once with 900 µL ice cold PBS. The cell pellet was dissolved with 5 µg RNAse (Merck KGaA, Darmstadt, Germany) and 0.05 µg mL^{-1} PI (Merck KGaA) diluted in PBS. The cell suspension was passed through the cell strainers pluriStrainer® with a 40 µm mesh (pluriSelect Life Science, Leipzig, Germany) to prevent clumping of cells in the flow cytometer. The filtrate was kept dark and on ice until measurement. The measurement was carried out with a BD Accuri™ C6 Flow Cytometer (Becton Dickinson and Company, NJ, USA). At least 10 000 cells were measured with a flow rate of 14 µL min^{-1} and a 10 µm core size. Gating was performed with the software Kontrast (Söngen & Blachnik GmbH, Ingelheim, Germany). The major cell population was gated in a side scatter area (SSC-A) vs forward scatter area (FSC-A) plot. Aggregates and doublets were removed in a height (H) vs area (A) plot (Supplementary Material). Finally, the selected cells were gated based on their PI content detected by the FL2-A detector into four groups: sub G1, G1/G0, S, and G2/M phase of the cell cycle. The number of cells in each cell cycle gate was used for analysis.

Gene	NCBI RefSeq	Forward Primer	Reverse Primer
BCAS3	NM_001099432	GCTCGGTCCCTGTGTATGTT	GCCAGGTGGACGATCAACTC
CEBPB	NM_005194.4	CGCCGCCTGCCTTTAAATC	AAGCAGTCCGCCTCGTAGTA
GAPDH	NM_002046.7	CTGTTCGACAGTCAGCCGCATC	GCGCCCAATACGACCAAATCCG
HSP90AB1	NM_001271969.1	AAACTCTATGTCCGCCGTGT	TGTTCAGGGGCAGATCCTCA
HSPA13	NM_006948.5	TGGCCTATGGTCTCCACAAG	TAGAGTTCCTCCGCCCAAGT
IGF1R	NM_000875.5	GGGGAGCCGCTCATTCATTT	GACGCAGTTCGCAAGATCG
PHF19	NM_015651.3	GGCCAGACGAAGGCATTGAC	CCAACACCTGGTACTTCTCCC
PGR	NM_001202474.3	AGGCAAAAAGGAGTTGTGTCG	GAAATTCAACACTCAGTGCCCG
PRKCD	NM_001354676.2	AGTTCCTGAACGAGAAGGCG	ACAAAGGAGAAGCCAGCGAA
SIAH2	NM_005067.7	CACTTGACAGGCTGTTGCAC	ACCAATATGGGAAGGCAGGC
SLC7A5	NM_003486.7	AGTAGATCACCTCCTCGAACC	TGAGGGATGAGATTCGTACCAG
SLC7A11	NM_014331.4	TGTCGGAGAAAATAACCAGAACA	TCCCTATTTTGTGTCTCCCCTT
STC2	NM_003714.2	TGTAGTAGTTGAGCGCAGGC	AAGGAGTCGAGCAGGTGTTG
TFAP2C	NM_003222.4	TGGTTGGTTTTTGTGTCCGC	TGCCTCCTACCAGAGGACTT

Table 2.1: Sequence of primers ($5' \rightarrow 3'$) designed for RT-qPCR

3 Bisphenolic compounds alter gene expression in MCF-7 cells through interaction with estrogen receptor α

Chapter 3 is based on the article "Bisphenolic compounds alter gene expression in MCF-7 cells through interaction with estrogen receptor α" by M. Böckers, N. W. Paul and T. Efferth, which is published in *Toxicology and Applied Pharmacology* [29]. I performed and analyzed the experiments, prepared the figures and wrote the article with contributions from all authors. The RNA sequencing experiment was performed by StarSEQ GmbH, Mainz, Germany. The article is reproduced verbatim. Minor modifications were made for consistency within this thesis, such as combining the abbreviations and the method section from all manuscripts into a single chapter, respectively.

3.1 Abstract

Plasticizers released from microplastic are increasingly viewed with concern. While adverse health effects induced by bisphenol A and its analogues on marine animals is well documented in the literature, the endocrine potential of bisphenolic compounds on human health remains elusive. We applied next-generation sequencing (NGS) with the estrogen receptor α (ERα) positive human breast cancer cell line MCF-7 treated with 17-β-estradiol (E2), bisphenol A (BPA), bisphenol B (BPB), bisphenol Z (BPZ) and tetramethyl bisphenol A (4MeBPA). We used molecular docking, microscale thermophoresis, ERα activation assay, and cell cycle experiments on MCF-7 and ERα overexpressing HEK293 cells to verify the impact of the compounds on ERα. 14 genes were found upregulated (*ADORA1*, *DDIT4*, *CELSR2*, *FOSL2*, *JUN*, *HSPA13*, *IER3*, *IGF1R*, *PGR*, *RUNX2*, *SLC7A11*, *SLC7A2*, *SLC7A5*, *STC2*) and 3 genes were downregulated (*BCAS3*, *PHF19*, *PRKCD*) in almost all samples. These genes are associated with cell growth, invasion, migration, apoptosis and cancer development. We further confirmed the binding, activation and proliferative effect of BPA, BPB, BPZ, and 4MeBPA on ERα. We provide evidence for the endocrine potential of bisphenolic compounds and give insights into their molecular effects in MCF-7 cells.

3.2 Introduction

A significant amount of plastic can be found in the environment, mostly due to waste disposal [6, 30]. For example, the great pacific garbage patch is estimated to contain approximately 79 000 tons of synthetic material [31]. In the ocean, larger chunks or garbage are broken down into so called "microplastic" with a size of less than 5 mm [6]. Microplastic ingested by marine animals can end up in the human food supply [18–22]. Moreover, chemical compounds such as plasticizers or other additives added during plastic production can leach from the plastic particles [16, 32–34].

Plasticizers are added during the production of synthetic polymers to gain specific characteristics of the final plastic material [34]. A widely used plasticizer is bisphenol A, which is used in the production of epoxy resins and polycarbonate plastics [35]. After increasing evidence of endocrine potential of BPA [14, 36, 37], several analogs of BPA were used as replacement. Among these analogs are BPB [38, 39], BPZ [14, 40] and 4MeBPA [41]. The latter is used in the polycarbonate TMPC [42–44]. However, research indicates endocrine effects by the analogs as well [40, 41].

Marine animals can accidentally consume microplastic by mistaking it with food [17]. Studies revealed that the uptake of microplastic by sea animals caused impaired feeding, growth, reproduction and lifespan [7–13]. While the actual impact of microplastic to the environment is still under discussion [45], the results above raise the question, whether consumption of microplastics/plasticizers may result in (long-term) adverse effects on human health as well.

Plasticizers are expected to function as endocrine-disrupting chemicals (EDC). EDCs mimic hormones and thereby interfere with the normal hormone system, causing long-term consequences such as developmental and reproductive problems [46]. As plasticizers such as BPA induce endocrine functions regarding reproduction, an interaction with the estrogen receptor is likely [47]. Estrogens play an essential role in growth, differentiation and development of the reproductive system [48, 49].

Estrogens mediate their actions inside the cell by binding estrogen receptors (ER). ERs occur in two isoforms encoded by independent genes: ERα/*ESR1* and ERβ/*ESR2* [50] and function as ligand-activated transcription factors. The receptor isoforms differ partly in tissue distribution. ERα is mainly expressed in the mammary gland, uterus, ovary, kidneys and others, while ERβ is found in the prostate, lung, and others [51–53]. ERs are composed of six domains A-F. Domains A/B contain the activation function (AF) 1, domain C contains the DNA-binding domain with 97% homology between ERα and ERβ, domain D contains a hinge region, and the E/F domains are composed of the ligand binding domain (LBD) and AF-2 with only 60% homology between the ER subtypes [52, 54, 55]. After 17-β-estradiol (E2) binds to the LBD, the receptor undergoes a conformational change and heat shock proteins are released from the ER monomer [56]. The ligand-bound receptor homo- or heterodimerizes with another ERα or ERβ and locates to the nucleus [54]. Together with transcriptional

coregulators recruited by the AF domains and DNA-binding proteins, the expression of target genes is induced [54, 57]. ERs mediate transcription in three different ways: (1) direct binding of DNA through targeting estrogen responsive elements, (2) indirect binding through targeting other transcription factors which bind to the DNA instead and (3) non-genomic actions [58]. Ligands with similar physicochemical properties as E2 can bind to ERs as well, resulting in activation of the receptors without the presence of endogenous hormones.

Despite some general knowledge of BPA-inducing hormonal response, little is known about the molecular effects of BPA and its analogues in the cell. In this study we investigated the molecular effects of BPA, BPB, BPZ, and 4MeBPA on the human estrogen receptor ERα. By employing next-generation sequencing, we obtained detailed insights in bisphenol-mediated gene expression in the ERα positive human breast cancer cell-line MCF-7.

3.3 Results

3.3.1 Molecular Docking

Molecular docking was performed to measure the binding affinity of all ligands to the ligand binding domain of the estrogen receptor α in *in silico*. As a first step, the docking was performed for the whole ligand binding domain of the estrogen receptor. All ligands bind to the same binding pocket as estradiol (Figure 3.1, upper left). As a second step, we performed a defined docking by decreasing the size of the grid box and focused only on the binding pocket. The results are listed in Table 3.1. E2 was calculated to exert the strongest binding affinity towards the protein, followed by the ligands BPZ and 4MeBPA. All bisphenol ligands share some amino acids of ERα-LBD involved in hydrophobic and hydrogen (H)-bond interactions. H-bonds with the amino acids Glu353 and Arg394 of ERα-LBD were formed in all cases. Leu346, Leu387, Phe404, Ala350 and Leu384 were found as interacting amino acids for almost all bisphenols. Visualizations of each ligand in the binding pocket of ERα-LBD are shown in Figure 3.1. Each molecular docking was performed 250 times and all runs resulted in the same cluster, indicating a low deviation of the docking. Based on the molecular docking experiment, all ligands bind to ERα-LBD in *in silico*.

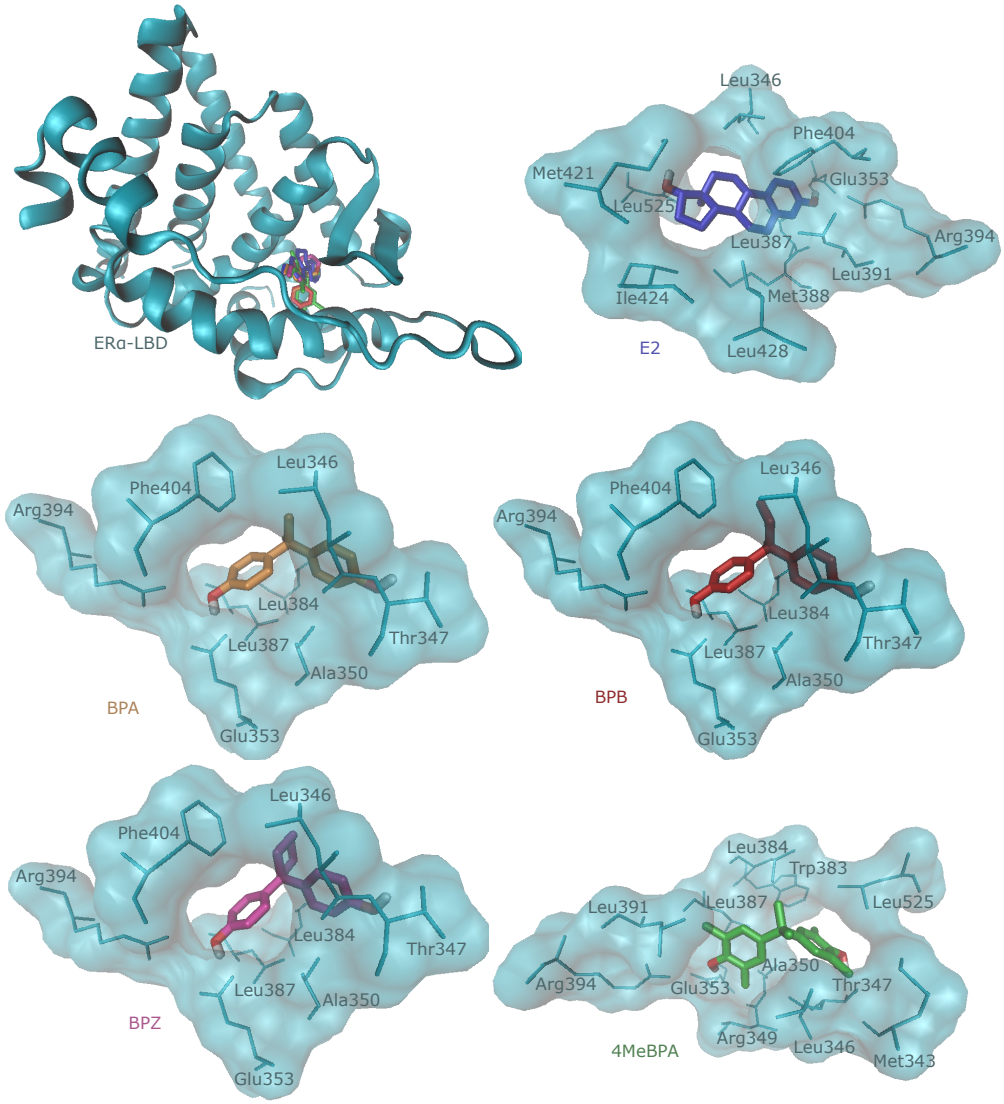

Figure 3.1: Visualization of the molecular docking result. The upper left image shows the result of the blind docking, with all ligands binding in the same pocket of ERα-LBD. The others images show the result of the defined docking for the ligands E2 (blue), BPA (orange), BPB (red), BPZ (magenta), and 4MeBPA (green), respectively. Each ligand is displayed with the interacting amino acids of ERα-LBD.

Table 3.1: Result of molecular docking. For each ligand, the lowest and mean binding energy and the predicted inhibitory constant $K_{i,pred}$ are given. The torsdof parameter Td indicates the torsional degree of freedom of each ligand. The amino acids of ERα-LBD involved in hydrophobic interactions and hydrogen bonds (H-bonds) are listed.

	lowest binding energy / kcal mol^{-1}	mean binding energy / kcal mol^{-1}	$K_{i,pred}$ / nM	Td	Runs in 1st cluster	Amino acids involved in hydrophobic interactions	Amino acids involved in H-bonds
E2	−9.48	−9.45	112.95	2	250/250	Leu346 Leu387 Met388 Leu391 Phe404 Met421 Ile424 Leu428 Leu525	Glu353 Arg394
BPA	−8.01	−7.98	1350	4	250/250	Leu346 Ala350 Leu384 Leu387 Phe404	Thr347 Glu353 Arg394
BPB	−8.19	−8.14	999.36	5	250/250	Leu346 Ala350 Leu384 Leu387 Phe404	Thr347 Glu353 Arg394
BPZ	−9.35	−9.31	140.46	4	250/250	Leu346 Ala350 Leu384 Leu387 Phe404	Thr347 Glu353 Arg394
4MeBPA	−9.24	−9.18	167.29	4	250/250	Met343 Leu346 Leu349 Ala350 Trp383 Leu384 Leu387 Leu391 Arg394 Leu525	Thr347 Glu353

3.3.2 RNA sequencing

In order to analyze the molecular effects induced by the bisphenols, we sequenced the mRNA of treated MCF-7 cells. The cells were treated with BPA, BPB, BPZ, 4MeBPA and E2 as control. We performed upstream target analyses using the Ingenuity Pathway Analysis (IPA) software using differentially expressed genes with a p-value ≤ 0.05. *ESR1* was identified as upstream target for all ligands, which supports the idea of the bisphenol compounds mediate their actions via ER-signaling. (Table 3.2). In addition, TP53 was also identified as possible upstream regulator.

	E2	BPA	BPB	BPZ	4MeBPA
1	TP53	TP53	TP53	ESR1	TP53
2	AR	ATF4	ESR1	TRIB3	E2F1
3	SYVN1	ESR1	ATF4	ATF4	ERBB2
4	ESR1	AR	LIN9	TP53	E2F4
5	OGA	SREBF1	Gsk3	AR	ESR1

Table 3.2: Upstream target analysis by IPA. Shown are the top five upstream regulators for the expressed gene pattern.

As *ESR1* was identified as possible upstream regulator, the question remains which genes are activated via the *ESR1*-signaling pathway. Therefore, the differentially expressed genes with a p-value ≤ 0.05 were further used for a core analysis in IPA. For all ligands a network was designed including genes that were directly or indirectly regulated by ESR1 (figures 3.2-3.6). Most frequently expressed were 14 upregulated genes (*ADORA1*, *DDIT4*, *CELSR2*, *FOSL2*, *JUN*, *HSPA13*, *IER3*, *IGF1R*, *PGR*, *RUNX2*, *SLC7A11*, *SLC7A2*, *SLC7A5*, *STC2*) and three downregulated genes (*BCAS3*, *PHF19*, *PRKCD*).

3.3.3 Ligand-specific gene expression

Besides genes differentially expressed by all ligands and associated with *ESR1*-mediated signaling, each ligand induced the regulation of an individual set of genes. We selected the genes that were not associated with *ESR1*, not regulated by E2 treated cells and expressed with a log2 fold change of at least 1 or -1 for BPA, BPB and BPZ (Tables 3.3-3.5). As 4MeBPA induced more than 200 genes unrelated to *ESR1*, we only show those with a log2 fold change of at least 2 or -2 (Table 3.6).

The RNA sequencing result demonstrates *ESR1* as upstream regulator and name several differentially expressed genes mediated by *ESR1*. In addition, further non-ESR1 associated genes were identified, indication additional effects of the tested compounds in the cells.

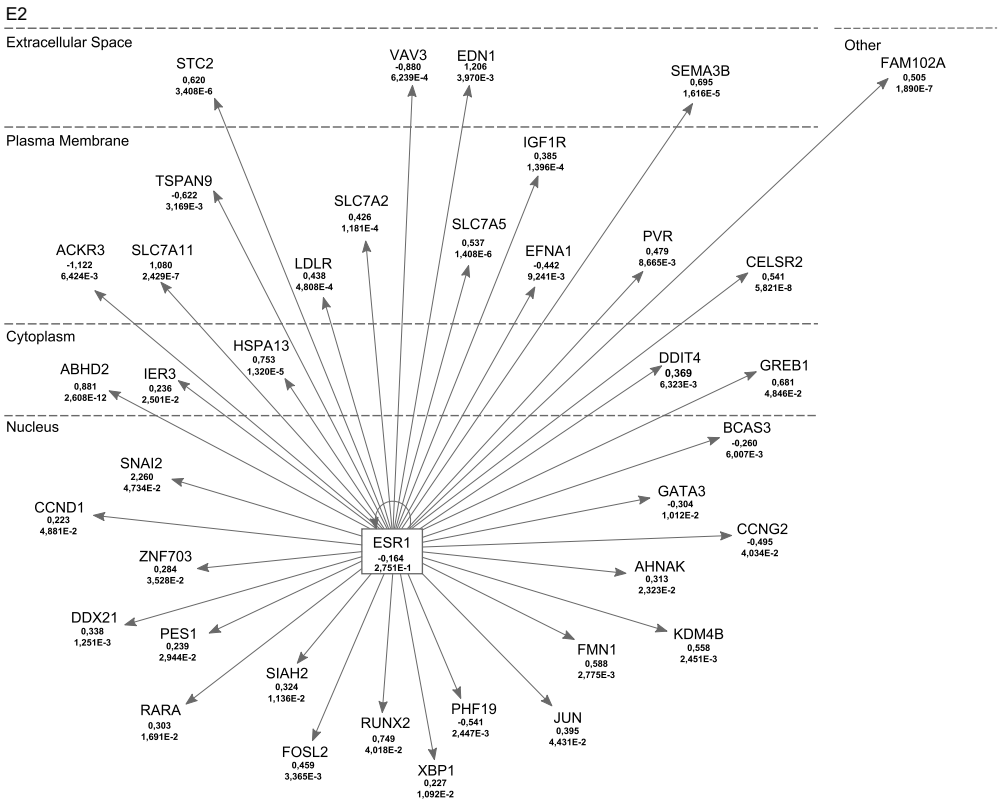

Figure 3.2: Upstream analysis with Ingenuity Pathway Analysis software (Qiagen). Differentially expressed genes induced by E2 in connection with *ESR1* signaling are shown. For each gene the log2 fold change and p-value is given.

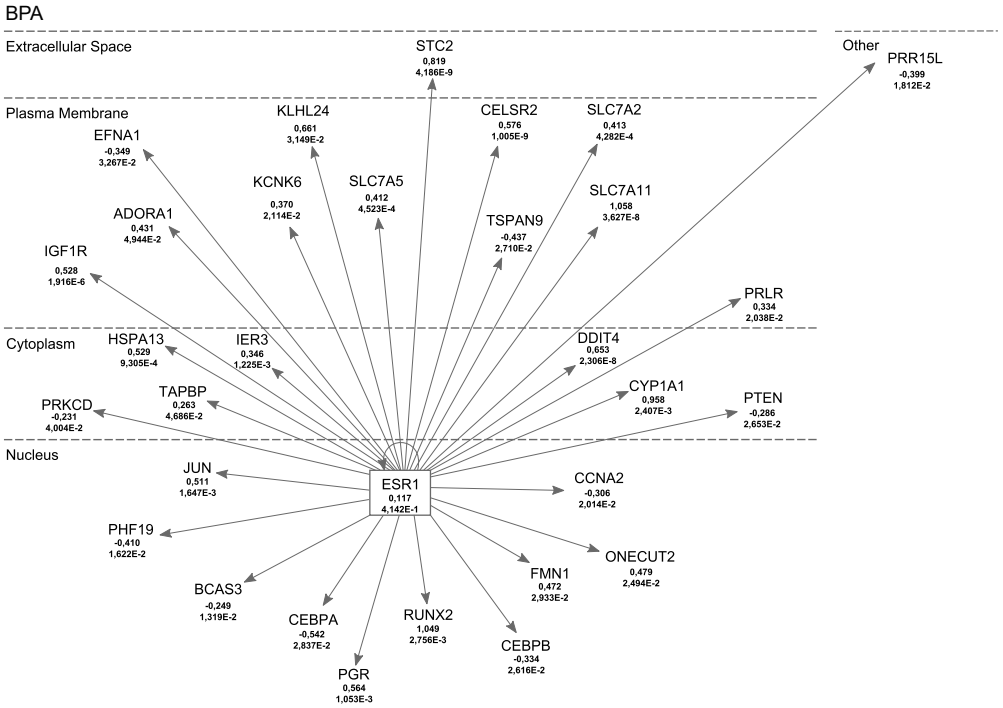

Figure 3.3: Upstream analysis with Ingenuity Pathway Analysis software (Qiagen). Differentially expressed genes induced by BPA in connection with *ESR1* signaling are shown. For each gene the log2 fold change and *p*-value is given.

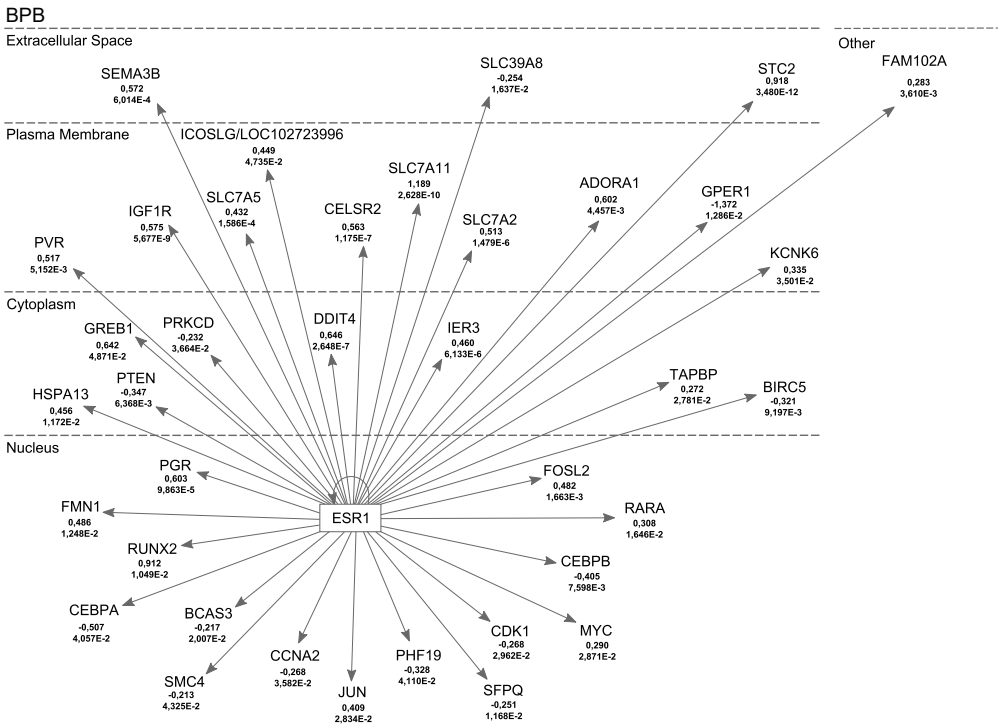

Figure 3.4: Upstream analysis with Ingenuity Pathway Analysis software (Qiagen). Differentially expressed genes induced by BPB in connection with *ESR1* signaling are shown. For each gene the log2 fold change and p-value is given.

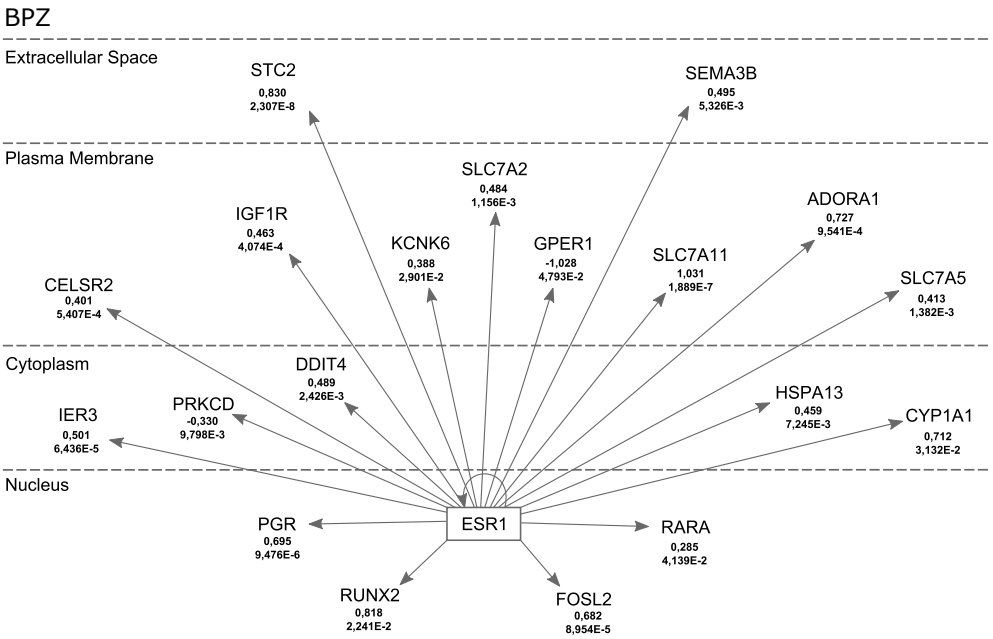

Figure 3.5: Upstream analysis with Ingenuity Pathway Analysis software (Qiagen). Differentially expressed genes induced by BPZ in connection with *ESR1* signaling are shown. For each gene the log2 fold change and p-value is given.

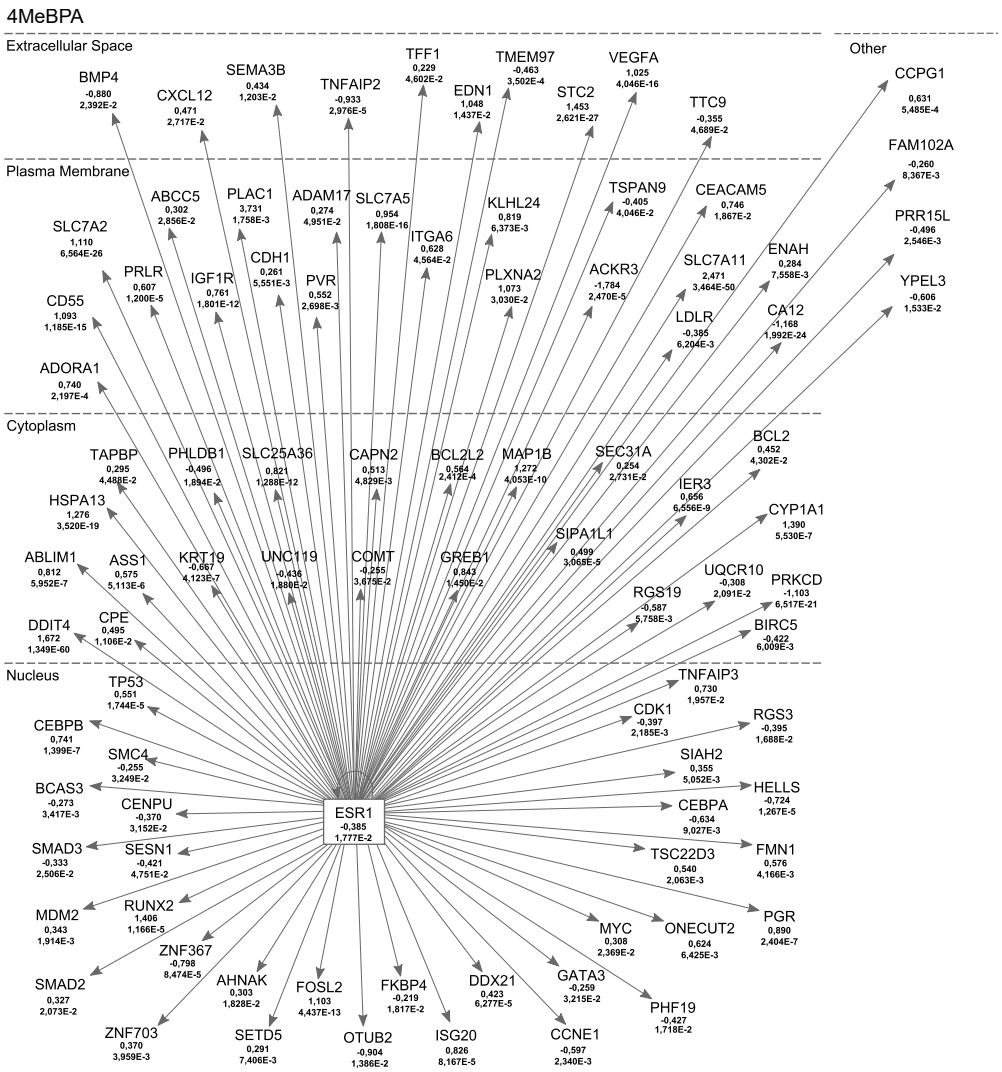

Figure 3.6: Upstream analysis with Ingenuity Pathway Analysis software (Qiagen). Differentially expressed genes induced by 4MeBPA in connection with *ESR1* signaling are shown. For each gene the log2 fold change and *p*-value is given.

Table 3.3: Specific gene expression induced by BPA. For each gene the fold change $\log_2\left(\frac{E_{\mathrm{BPA}}}{E_{\mathrm{c}}}\right)$ with corresponding standard error $\Delta\log_2\left(\frac{E_{\mathrm{BPA}}}{E_{\mathrm{c}}}\right)$ and p-value are listed. ID refers to the name of the gene, E to the expression induced by the respective ligand, and E_c to the expression under control conditions. p-values indicate the comparison with the DMSO-control.

ID	$\log_2\left(\frac{E_{\mathrm{BPA}}}{E_{\mathrm{c}}}\right)$	$\Delta\log_2\left(\frac{E_{\mathrm{BPA}}}{E_{\mathrm{c}}}\right)$	p	Entrez Gene Name
TMEM133	5.785	1.963	$3.21 \cdot 10^{-3}$	Rho GTPase activating protein 42
SNORD3B-2	5.653	2.022	$5.18 \cdot 10^{-3}$	small nucleolar RNA, C/D box 3B-2
U2AF1L5	4.367	1.880	$2.02 \cdot 10^{-2}$	U2 small nuclear RNA auxiliary factor 1
TBC1D3K	2.983	1.470	$4.25 \cdot 10^{-2}$	TBC1 domain family member 3F
IRAK1BP1	1.864	0.791	$1.84 \cdot 10^{-2}$	interleukin 1 receptor associated kinase 1 binding protein 1
SNORD3A	1.714	0.772	$2.63 \cdot 10^{-2}$	small nucleolar RNA, C/D box 3A
ZNF460	1.709	0.511	$8.26 \cdot 10^{-4}$	zinc finger protein 460
SNAI3-AS1	1.316	0.620	$3.37 \cdot 10^{-2}$	SNAI3 antisense RNA 1
CCDC144B	1.231	0.614	$4.50 \cdot 10^{-2}$	coiled-coil domain containing 144B (pseudogene)
RN7SK	1.122	0.455	$1.37 \cdot 10^{-2}$	RNA, 7SK small nuclear
LOC100190986	1.069	0.342	$1.78 \cdot 10^{-3}$	uncharacterized LOC100190986
RPPH1	1.048	0.500	$3.62 \cdot 10^{-2}$	ribonuclease P RNA component H1
ZNF483	1.024	0.320	$1.39 \cdot 10^{-3}$	zinc finger protein 483
LOC105373989	−1.179	0.417	$4.74 \cdot 10^{-3}$	putative cuticle collagen 91
GPR27	−1.500	0.593	$1.14 \cdot 10^{-2}$	G protein-coupled receptor 27
SLC25A21	−1.504	0.733	$4.01 \cdot 10^{-2}$	solute carrier family 25 member 21
TMEM238	−2.264	0.448	$4.43 \cdot 10^{-7}$	transmembrane protein 238
LOC107986035	−2.845	0.806	$4.16 \cdot 10^{-4}$	basic proline-rich protein-like
FAM72C	−3.027	1.185	$1.06 \cdot 10^{-2}$	family with sequence similarity 72 member D
TSNAX-DISC1	−5.495	2.281	$1.60 \cdot 10^{-2}$	TSNAX-DISC1 readthrough (NMD candidate)

Table 3.4: Specific gene expression induced by BPB. For each gene the fold change $\log_2\left(\frac{E_{\mathrm{BPB}}}{E_{\mathrm{c}}}\right)$ with corresponding standard error $\Delta\log_2\left(\frac{E_{\mathrm{BPB}}}{E_{\mathrm{c}}}\right)$ and p-value are listed. ID refers to the name of the gene, E to the expression induced by the respective ligand, and E_c to the expression under control conditions. p-values indicate the comparison with the DMSO-control.

Table 3.4: Specific gene expression by BPB.

ID	$\log_2\left(\frac{E_{\mathrm{BPB}}}{E_{\mathrm{c}}}\right)$	$\Delta\log_2\left(\frac{E_{\mathrm{BPB}}}{E_{\mathrm{c}}}\right)$	p	Entrez Gene Name
MAGED4	8.213	1.558	$1.35 \cdot 10^{-7}$	MAGE family member D4B
RNA18S5	4.856	2.412	$4.41 \cdot 10^{-2}$	RNA, 18S ribosomal 5
LOC107986903	4.844	2.346	$3.89 \cdot 10^{-2}$	uncharacterized LOC107986903
LOC105379271	4.008	1.895	$3.45 \cdot 10^{-2}$	uncharacterized LOC105379271
TNFSF4	2.779	1.260	$2.74 \cdot 10^{-2}$	TNF superfamily member 4
MUC2	1.383	0.594	$1.98 \cdot 10^{-2}$	mucin 2, oligomeric mucus/gel-forming
ZNF460	1.265	0.563	$2.48 \cdot 10^{-2}$	zinc finger protein 460
LOC100190986	1.201	0.335	$3.32 \cdot 10^{-4}$	uncharacterized LOC100190986
LOC105376781	1.095	0.477	$2.16 \cdot 10^{-2}$	uncharacterized LOC105376781
LOC105378936	1.015	0.440	$2.10 \cdot 10^{-2}$	uncharacterized LOC105378936
TTC28-AS1	−1.046	0.446	$1.90 \cdot 10^{-2}$	TTC28 antisense RNA 1
CHURC1-FNTB	−1.081	0.323	$8.32 \cdot 10^{-4}$	CHURC1-FNTB readthrough

Table 3.4: Specific gene expression by BPB.

ID	$\log_2\left(\frac{E_{\text{BPB}}}{E_{\text{c}}}\right)$	$\Delta\log_2\left(\frac{E_{\text{BPB}}}{E_{\text{c}}}\right)$	p	Entrez Gene Name
ZNF771	−1.169	0.590	$4.75 \cdot 10^{-2}$	zinc finger protein 771
LOC105373989	−1.448	0.427	$6.92 \cdot 10^{-4}$	putative cuticle collagen 91
C4orf48	−1.534	0.297	$2.35 \cdot 10^{-7}$	chromosome 4 open reading frame 48
KCNQ2	−1.597	0.764	$3.66 \cdot 10^{-2}$	potassium voltage-gated channel subfamily Q member 2
SLC25A21	−1.700	0.664	$1.05 \cdot 10^{-2}$	solute carrier family 25 member 21
RNA45S5	−2.222	0.695	$1.38 \cdot 10^{-3}$	RNA, 45S pre-ribosomal 5
TMEM238	−2.507	0.482	$2.02 \cdot 10^{-7}$	transmembrane protein 238
SENP3-EIF4A1	−3.146	1.295	$1.51 \cdot 10^{-2}$	SENP3-EIF4A1 readthrough (NMD candidate)
LOC105369850	−3.259	1.331	$1.43 \cdot 10^{-2}$	uncharacterized LOC105369850
LOC107986035	−3.768	0.929	$4.96 \cdot 10^{-5}$	basic proline-rich protein-like
CD36	−4.454	2.101	$3.40 \cdot 10^{-2}$	CD36 molecule
PRH1-PRR4	−5.201	2.326	$2.53 \cdot 10^{-2}$	PRH1-PRR4 readthrough

Table 3.5: Specific gene expression induced by BPZ. For each gene the fold change $\log_2\left(\frac{E_{\text{BPZ}}}{E_{\text{c}}}\right)$ with corresponding standard error $\Delta\log_2\left(\frac{E_{\text{BPZ}}}{E_{\text{c}}}\right)$ and p-value are listed. ID refers to the name of the gene, E to the expression induced by the respective ligand, and E_c to the expression under control conditions. p-values indicate the comparison with the DMSO-control.

ID	$\log_2\left(\frac{E_{\text{BPZ}}}{E_{\text{c}}}\right)$	$\Delta\log_2\left(\frac{E_{\text{BPZ}}}{E_{\text{c}}}\right)$	p	Entrez Gene Name
MEF2B	5.892	1.958	$2.61 \cdot 10^{-3}$	myocyte enhancer factor 2B
SCARNA10	5.781	2.106	$6.04 \cdot 10^{-3}$	small Cajal body-specific RNA 10
EIF4EBP3	5.648	2.143	$8.39 \cdot 10^{-3}$	eukaryotic translation initiation factor 4E binding protein 3
HIST1H2AH	5.500	2.239	$1.40 \cdot 10^{-2}$	histone cluster 1 H2A family member h
PABPC5	5.013	2.292	$2.87 \cdot 10^{-2}$	poly(A) binding protein cytoplasmic 5
SNORD3A	4.800	1.860	$9.87 \cdot 10^{-3}$	small nucleolar RNA, C/D box 3A
RN7SK	4.072	1.809	$2.44 \cdot 10^{-2}$	RNA, 7SK small nuclear
RPPH1	3.802	1.692	$2.46 \cdot 10^{-2}$	ribonuclease P RNA component H1
RMRP	3.469	1.667	$3.75 \cdot 10^{-2}$	RNA component of mitochondrial RNA processing endoribonuclease
RN7SL2	2.846	1.351	$3.52 \cdot 10^{-2}$	RNA, 7SL, cytoplasmic 2
CACNB2	2.724	1.036	$8.53 \cdot 10^{-3}$	calcium voltage-gated channel auxiliary subunit beta 2
SCARNA2	2.706	1.290	$3.60 \cdot 10^{-2}$	small Cajal body-specific RNA 2
ZNF460	1.461	0.557	$8.69 \cdot 10^{-3}$	zinc finger protein 460
PPFIA4	1.286	0.410	$1.69 \cdot 10^{-3}$	PTPRF interacting protein alpha 4
ADAMTS13	1.125	0.545	$3.91 \cdot 10^{-2}$	ADAM metallopeptidase with thrombospondin type 1 motif 13
LOC105376781	1.043	0.506	$3.93 \cdot 10^{-2}$	uncharacterized LOC105376781
TTLL3	1.015	0.490	$3.84 \cdot 10^{-2}$	tubulin tyrosine ligase like 3
TMEM238	−1.296	0.555	$1.96 \cdot 10^{-2}$	transmembrane protein 238
LOC107986035	−1.472	0.744	$4.79 \cdot 10^{-2}$	basic proline-rich protein-like
RGPD6	−3.422	0.428	$1.20 \cdot 10^{-15}$	RANBP2-like and GRIP domain containing 5
RORA-AS1	−3.484	1.665	$3.64 \cdot 10^{-2}$	RORA antisense RNA 1

Table 3.6: Specific gene expression induced by 4MeBPA. For each gene the fold change $\log_2\left(\frac{E_{\text{4MeBPA}}}{E_c}\right)$ with corresponding standard error $\Delta\log_2\left(\frac{E_{\text{4MeBPA}}}{E_c}\right)$ and p-value are listed. ID refers to the name of the gene, E to the expression induced by the respective ligand, and E_c to the expression under control conditions. p-values indicate the comparison with the DMSO-control.

ID	$\log_2\left(\frac{E_{\text{4MeBPA}}}{E_c}\right)$	$\Delta\log_2\left(\frac{E_{\text{4MeBPA}}}{E_c}\right)$	p	Entrez Gene Name
RNA18S5	6.876	1.783	$1.15 \cdot 10^{-4}$	RNA, 18S ribosomal 5
LOC102724843	6.452	1.856	$5.07 \cdot 10^{-4}$	uncharacterized LOC389831
LHX4-AS1	5.392	2.072	$9.26 \cdot 10^{-3}$	LHX4 antisense RNA 1
RNU4-2	4.839	2.468	$4.99 \cdot 10^{-2}$	RNA, U4 small nuclear 2
LOC100507373	4.771	2.373	$4.44 \cdot 10^{-2}$	uncharacterized LOC100507373
LOC105379426	4.732	2.360	$4.50 \cdot 10^{-2}$	ankyrin repeat domain-containing protein 20A2
INHBE	4.498	1.098	$4.18 \cdot 10^{-5}$	inhibin subunit beta E
LINC00473	4.255	1.947	$2.89 \cdot 10^{-2}$	long intergenic non-protein coding RNA 473
LGR6	4.225	1.939	$2.93 \cdot 10^{-2}$	leucine rich repeat containing G protein-coupled receptor 6
SNORA73A	4.181	2.022	$3.86 \cdot 10^{-2}$	small nucleolar RNA, H/ACA box 73A
BEST1	4.129	1.797	$2.16 \cdot 10^{-2}$	bestrophin 1
DLGAP1-AS2	4.059	2.013	$4.38 \cdot 10^{-2}$	DLGAP1 antisense RNA 2
SCN4A	3.783	1.031	$2.44 \cdot 10^{-4}$	sodium voltage-gated channel alpha subunit 4
FAM129A	3.731	0.558	$2.36 \cdot 10^{-11}$	family with sequence similarity 129 member A
CACNB2	3.651	0.882	$3.51 \cdot 10^{-5}$	calcium voltage-gated channel auxiliary subunit beta 2
BCAT1	3.534	1.195	$3.09 \cdot 10^{-3}$	branched chain amino acid transaminase 1
TM4SF19-AS1	3.381	1.536	$2.77 \cdot 10^{-2}$	TM4SF19 antisense RNA 1
DNAH17	3.241	1.333	$1.50 \cdot 10^{-2}$	dynein axonemal heavy chain 17
LOC107984261	3.225	1.570	$4.00 \cdot 10^{-2}$	uncharacterized LOC107984261
LINC00341	3.184	1.582	$4.41 \cdot 10^{-2}$	spectrin repeat containing nuclear envelope family member 3
C2CD4A	3.175	0.526	$1.54 \cdot 10^{-9}$	C2 calcium dependent domain containing 4A
KLHDC7B	3.104	1.028	$2.53 \cdot 10^{-3}$	kelch domain containing 7B
RASIP1	3.017	0.913	$9.47 \cdot 10^{-4}$	Ras interacting protein 1
VLDLR-AS1	2.914	1.095	$7.79 \cdot 10^{-3}$	VLDLR antisense RNA 1
PSAT1	2.907	1.052	$5.73 \cdot 10^{-3}$	phosphoserine aminotransferase 1
DDIT3	2.858	0.225	$4.23 \cdot 10^{-37}$	DNA damage inducible transcript 3
IZUMO1	2.542	1.203	$3.47 \cdot 10^{-2}$	izumo sperm-egg fusion 1
CCNA1	2.515	0.900	$5.20 \cdot 10^{-3}$	cyclin A1
ANK2	2.480	0.445	$2.50 \cdot 10^{-8}$	ankyrin 2
LOC105372580	2.449	0.845	$3.77 \cdot 10^{-3}$	uncharacterized LOC105372580
NCR3LG1	2.346	0.659	$3.68 \cdot 10^{-4}$	natural killer cell cytotoxicity receptor 3 ligand 1
LOC647070	2.344	1.128	$3.77 \cdot 10^{-2}$	uncharacterized LOC647070
GEM	2.335	0.879	$7.90 \cdot 10^{-3}$	GTP binding protein overexpressed in skeletal muscle
SCG2	2.269	0.934	$1.52 \cdot 10^{-2}$	secretogranin II
ADM2	2.262	0.265	$1.41 \cdot 10^{-17}$	adrenomedullin 2
CLGN	2.113	0.594	$3.78 \cdot 10^{-4}$	calmegin
SLC43A1	2.095	0.490	$1.89 \cdot 10^{-5}$	solute carrier family 43 member 1
ALDH1L2	2.092	0.346	$1.54 \cdot 10^{-9}$	aldehyde dehydrogenase 1 family member L2
F7	2.056	0.708	$3.68 \cdot 10^{-3}$	coagulation factor VII
GPRC5B	−2.066	0.709	$3.55 \cdot 10^{-3}$	G protein-coupled receptor class C group 5 member B
C2orf54	−2.101	0.671	$1.76 \cdot 10^{-3}$	mab-21 like 4
LOC105373989	−2.365	0.468	$4.39 \cdot 10^{-7}$	putative cuticle collagen 91
TMEM238	−2.518	0.448	$1.94 \cdot 10^{-8}$	transmembrane protein 238
KDR	−2.625	0.958	$6.13 \cdot 10^{-3}$	kinase insert domain receptor
TMEFF1	−3.043	1.510	$4.39 \cdot 10^{-2}$	transmembrane protein with EGF like and two follistatin like domains 1

Table 3.6: Specific gene expression induced by 4MeBPA. For each gene the fold change $\log_2\left(\frac{E_{\text{4MeBPA}}}{E_{\text{c}}}\right)$ with corresponding standard error $\Delta\log_2\left(\frac{E_{\text{4MeBPA}}}{E_{\text{c}}}\right)$ and p-value are listed. ID refers to the name of the gene, E to the expression induced by the respective ligand, and E_c to the expression under control conditions. p-values indicate the comparison with the DMSO-control.

ID	$\log_2\left(\frac{E_{\text{4MeBPA}}}{E_{\text{c}}}\right)$	$\Delta\log_2\left(\frac{E_{\text{4MeBPA}}}{E_{\text{c}}}\right)$	p	Entrez Gene Name
LOC107986035	−3.246	0.838	$1.06 \cdot 10^{-4}$	basic proline-rich protein-like

3.3.4 RT-qPCR

Real-time quantitative PCR was performed for three up- and three downregulated genes to confirm the NGS results. *GAPDH* and *HSP90AB1* were both used as reference gene (Figure 3.7). Linear regression of the RT-qPCR against the NGS results was performed for each reference gene. The expression profile of both experiments matches each other. The deviation of the linear fit was smaller using *GAPDH* as reference (R-value = 0.96), indicating a lower effect of the tested compounds than on *HSP90AB1* (R-value = 0.94). RT-qPCR lead to the same expression result for the selected genes, confirming the NGS result.

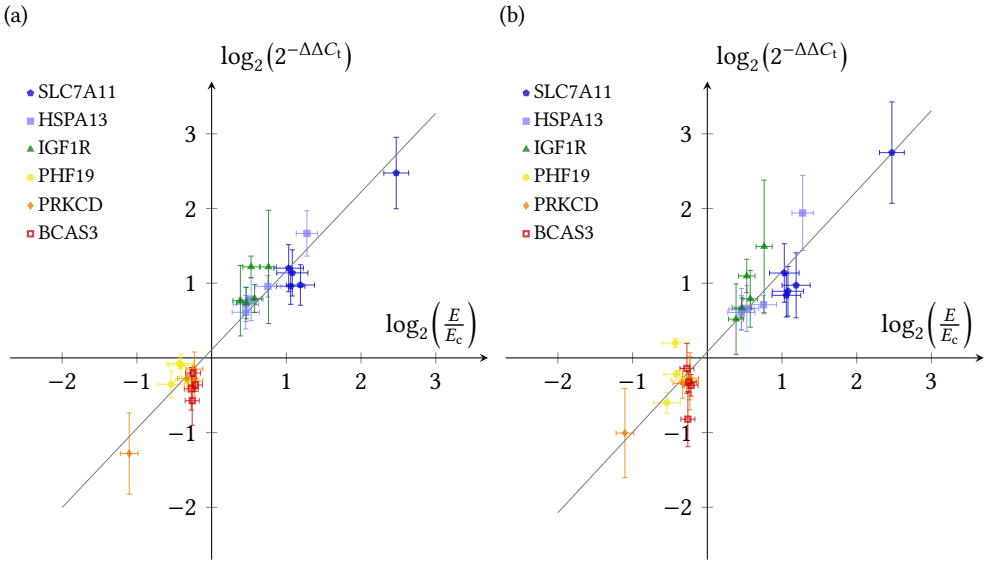

Figure 3.7: Correlation of gene expression levels obtained by NGS and RT-qPCR. The $\log_2(2^{-\Delta\Delta C_t})$ fold change based on the RT-qPCR results was plotted against the $\log_2\left(\frac{E}{E_c}\right)$ fold change based on the NGS results for the ligands E2, BPA, BPB, BPZ, and 4MeBPA (dots) with (a) *GAPDH* and (b) *HSP90AB1* as reference gene, respectively. A linear regression was calculated with Origin 7.5. The fit is shown in grey with (a) a slope of 1.06, incept of 0.11, R=0.96 and (b) slope of 1.08, intercept of 0.08, and R=0.94.

3.3.5 Microscale Thermophoresis

MST experiments were performed to verify the *in silico* predicted binding of the bisphenolic compounds and E2 as positive control to ERα *in vitro*. At least 11 concentrations were measured for each sample and the normalized fluorescence plotted against the concentration (Figure 3.8). A fit was performed according to the law of mass action

and the dissociation constant K_d calculated for all samples (Table 3.7). For each ligand, a concentration dependent effect on the detected fluorescence signal of the protein was measured, confirming the binding of all bisphenolic compounds and E2 to ERα *in vitro*.

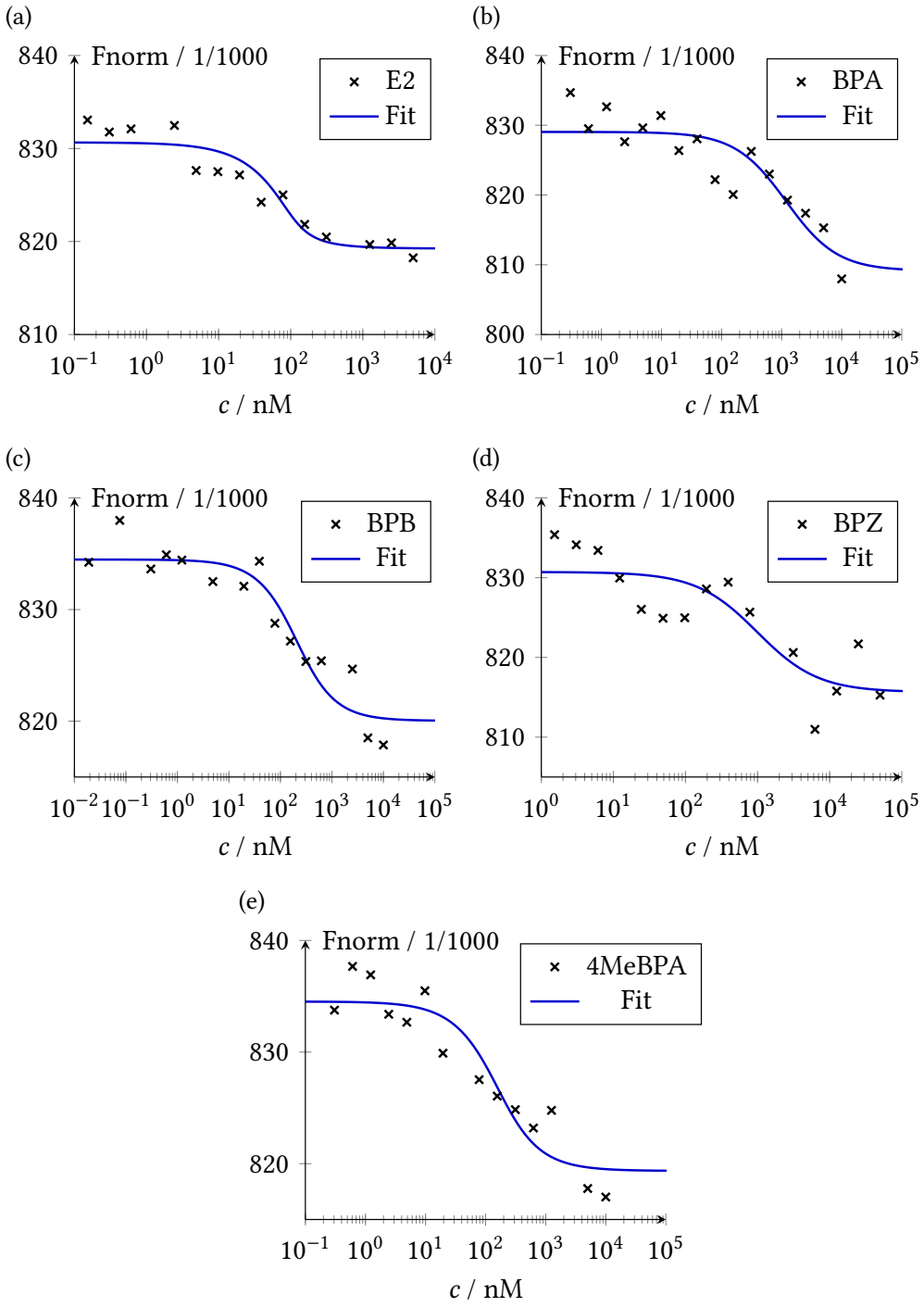

Figure 3.8: Analysis of the MST-experiments. The MST was performed with 95% LED and 20% MST power. Fluorescently labeled ERα was used as target with (a) E2, (b) BPA, (c) BPB, (d) BPZ, and (e) 4MeBPA as ligand, respectively. A fit was performed according to the law of mass action (blue).

3.3.6 Cytotoxicity

The cytotoxic effect of the bisphenolic compounds and E2 was analyzed with resazurin reduction assay in *ESR1*-overexpressing HEK293 cells (Figure 3.11). We generated ERα overexpressing HEK293 cells to investigate the effect of the bisphenolic compounds on non-breast cancer cells with high ERα expression. The IC_{50} of the bisphenolic compounds was mostly of the same order of magnitude as the IC_{50} of E2 towards HEK-ESR1 cells (Table 3.7). However, 4MeBPA was detected to affect the cells most with only half the IC_{50} of E2. Therefore, the increased gene expression profile induced by 4MeBPA might emerge from its higher cell toxicity. The following experiments were conducted based on the lowest IC_{50} to avoid toxic effects. All compounds have a cytotoxic effect against HEK-ESR1 cells.

3.3.7 ER transcription factor activation

After confirming the binding of the bisphenolic compounds to ERα *in vitro*, the activation of the transcription factor was analyzed with the ER transcription factor activation assay (Abcam) in *ESR1*-overexpressing HEK293 cells. The HEK-ESR1 cells were treated for 4 h or 8 h with 25 µm of the respective compound (Figure 3.9). The strongest activation of the ERα was observed with the cells treated with E2, followed by 4MeBPA. BPA shows a similar, but weaker activation. BPZ seemed to inhibit the activation of the receptor, as the activation was measured lower than with the control cells. For BPB the results differed dependent on the incubation time. In all cases, the ERα activation measured in the cells treated with E2 is greater than in the cells treated with the bisphenolic compounds. 4MeBPA had the strongest activation potential, whereas BPZ reduced the activation of ERα. We can confirm an effect of all bisphenol ligands on the activation of ERα.

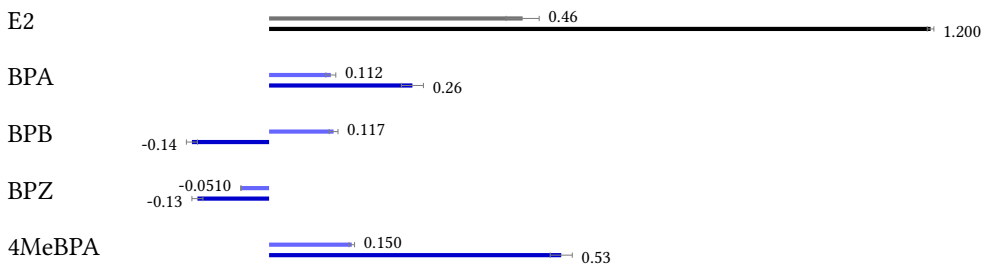

Figure 3.9: ER transcription factor assay. Activation of estrogen receptor was measured after 4 h and 8 h incubation time of HEK-ESR1 cells with 25 µM of the respective ligand. The difference optical density measured after 4 h is shown in the upper line and after 8 h in the lower line.

3.3.8 Cell cycle analysis

In order to evaluate a proliferative effect of the ligands through the estrogen receptor, cell cycle analysis was performed using flow cytometry. HEK-ESR1 cells were treated for 4 h and 8 h with 25 µM or 50 µM of the respective ligand. The amount of PI uptake was measured and the analyzed cells gated into four the four cell cycle phases: sub G1, G1/G0, S, and G2/M phase. The percentage of each cell cycle population is listed in Table 3.8. Treatment of HEK-ESR1 cells with E2, BPB and 4MeBPA resulted in an increased G2/M phase population, compared to the DMSO control (Figure 3.10). The results in MCF-7 cells are comparable to those in HEK-ESR1 cells (Figure 3.13, Table 3.9). Especially 4MeBPA seems to affect the cell cycle towards G2/M phase, indicating a proliferative effect on HEK-ESR1 and MCF-7 cells. Further research is required to understand the influence of 4MeBPA on the cell cycle. Cell cycle analysis revealed a proliferative effect of the bisphenols BPB and 4MeBPA.

Table 3.7: Molecular structure of the analyzed ligands and comparison of the inhibitory constant predicted *in silico* $K_{i,pred}$ with the dissociation constant K_d calculated by MST *in vitro*. The inhibitory constant IC_{50} was calculated based on the cytotoxicity assay.

Structure	Identifier	$K_{i,pred}$ / nM	K_d / nM	IC_{50} / µM
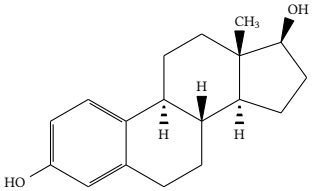	17-β-Estradiol E2 CAS 50-28-2	112.98	14.9 ± 2.1	68 ± 11
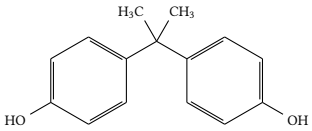	Bisphenol A BPA CAS 80-05-7	1350	1140 ± 150	168 ± 10
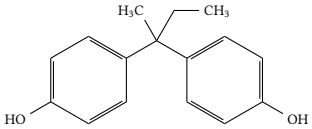	Bisphenol B BPB CAS 77-40-7	999.36	154 ± 18	108 ± 12
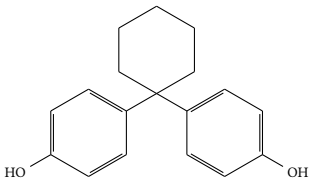	Bisphenol Z BPZ CAS 843-55-0	140.46	939 ± 198	87 ± 13
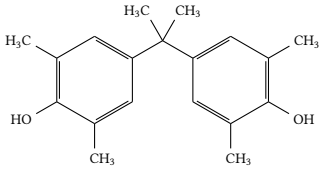	Tetramethyl bisphenol A 4MeBPA CAS 5613-46-7	167.29	103 ± 13	28.3 ± 4.3

Table 3.8: Cell cycle analysis was performed with the cell lines HEK-ESR1. Cells were treated with DMSO as control, E2, or the bisphenol compounds at a concentration of 25 µM or 50 µM for 4 h or 8 h, respectively. The percentage of cells in relation to the cell cycle phases is given.

HEK-ESR1	Phase	DMSO	E2	BPA	BPB	BPZ	4MeBPA
	sub G1 / %	1.2	1.6	1.3	1.3	1.5	1.5
4 h	G1/G0 / %	55.0	40.9	55.6	52.6	53.1	38.5
25 µM	S / %	22.5	22.9	23.4	22.3	22.8	27.0
	G2/M / %	20.0	33.6	18.9	22.4	21.5	31.8
	sub G1 / %	1.3	1.8	1.3	2.0	1.5	2.1
4 h	G1/G0 / %	56.5	39.7	55.5	47.4	56.4	47.4
50 µM	S / %	22.6	23.9	23.5	24.4	23.7	24.1
	G2/M / %	18.8	33.3	18.9	25.0	17.7	25.3
	sub G1 / %	1.1	4.9	1.4	1.9	1.4	3.7
8 h	G1/G0 / %	54.9	19.5	53.8	52.4	54.6	19.7
25 µM	S / %	23.2	33.7	24.2	23.5	22.7	26.5
	G2/M / %	19.3	40.6	19.5	21.3	20.1	48.3
	sub G1 / %	1.2	4.7	1.5	4.3	1.7	5.9
8 h	G1/G0 / %	56.2	22.9	55.0	41.8	59.6	31.1
50 µM	S / %	22.7	22.2	22.2	24.0	20.3	28.8
	G2/M / %	18.6	47.5	20.0	28.2	17.4	32.9

(a) E2

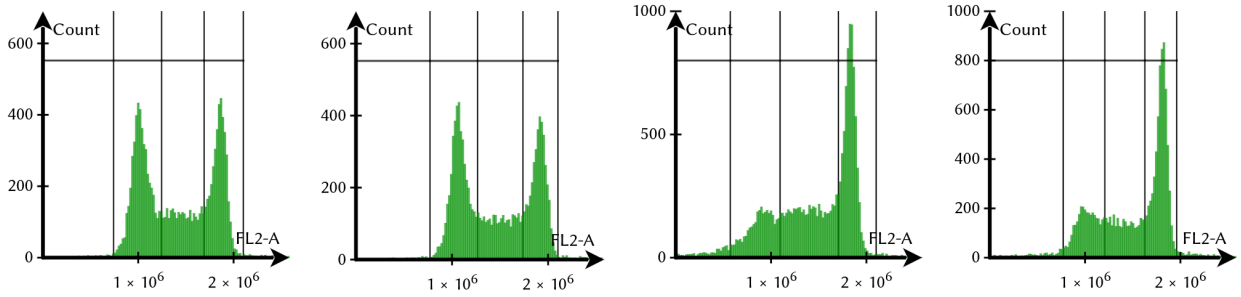

(b) BPA

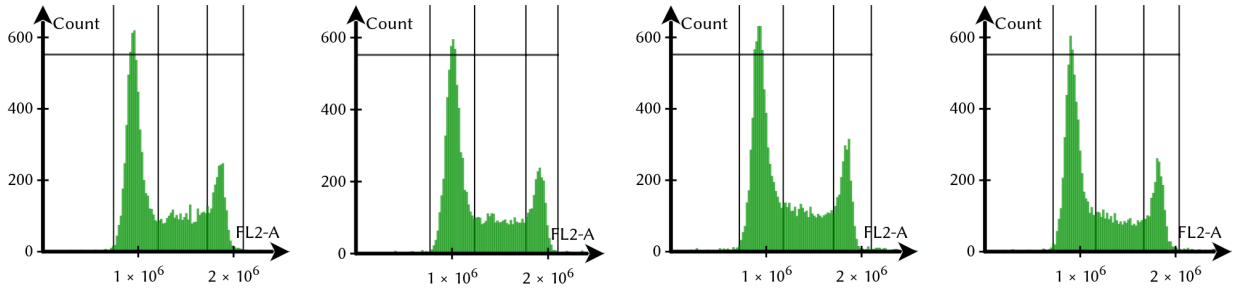

(c) BPB

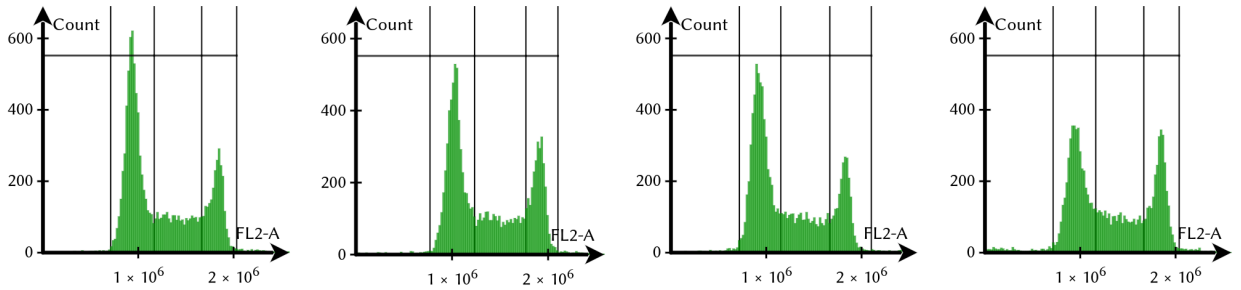

(d) BPZ

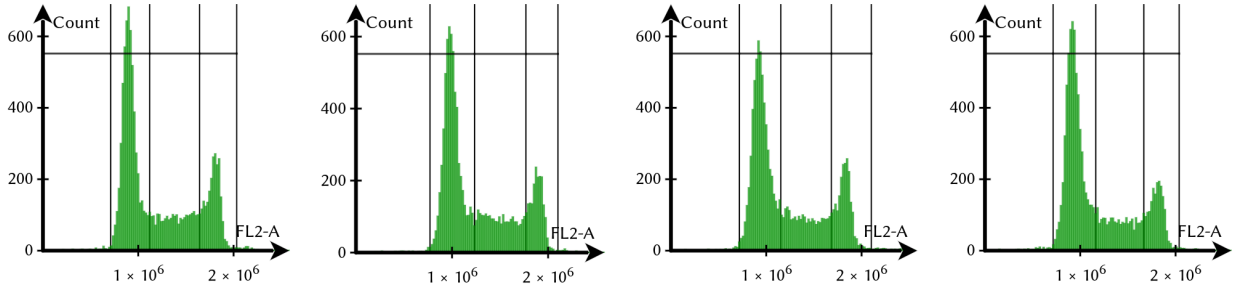

(e) 4MeBPA

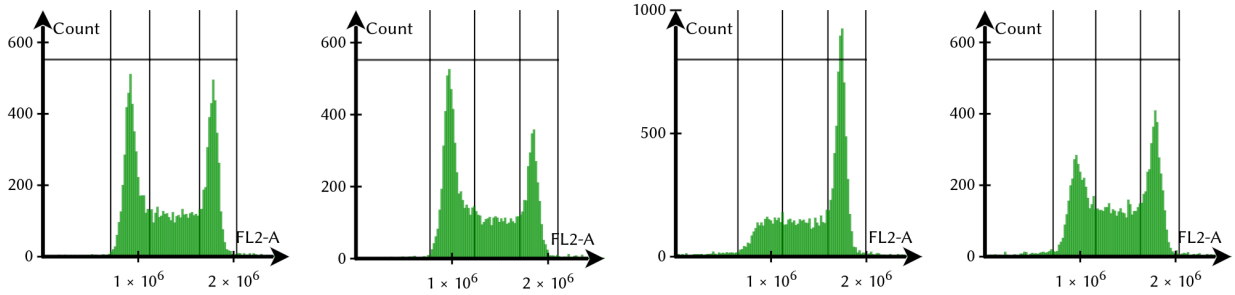

Figure 3.10: Cell Cycle Analysis. HEK-ESR1 cells were treated with (a) E2, (b) BPA, (c) BPB, (d) BPZ and (e) 4MeBPA. Each analysis was performed under four conditions: 4 h and 25 µM, 4 h and 50 µM, 8 h and 25 µM, 8 h and 50 µM (from left to right).

3.4 Discussion

In the present study, we evaluated the effect of the four bisphenolic compounds BPA, BPB, BPZ, 4MeBPA and E2 towards ERα. We found altered gene expression profiles in MCF-7 cells mediated by ERα activation upon exposure to these bisphenolics and observed their interaction with ERα.

Molecular docking was used to analyze the binding affinity of the bisphenolic compounds to ERα. The experiment revealed the lowest binding energy for all ligands was achieved while positioning the ligands in the same binding pocket as the natural ligand E2. The interacting amino acids of ERα with E2 match to those described in the literature [56, 59, 60]. Although all ligands bind to the same site of ERα, a different outcome in the molecular activation of target genes can be expected. The chemical similarity of the ligands guided them to the same binding site, but their differences were the reason for different molecular effects of the ligand-bound ERα in the cell. Small changes in the molecular structure of the bound ligand shifted the three-dimensional structure of the protein [61]. Especially, the AF-2 domain was directly influenced by the overall structure of the bound ligand offering slightly different binding sites for further downstream co-activator molecules, altering gene expression by the transcription factor [56]. Based on the molecular docking results, we conclude that all tested bisphenolic compounds bound to ERα-LBD *in silico*.

NGS was applied to analyze effects of the compounds on the gene expression. The sequencing revealed several differentially expressed genes in MCF-7 cells after treatment with BPA, BPB, BPZ, 4MeBPA, and E2. Upstream target analysis with IPA resulted in *ESR1* as possible target of all compounds. *TP53* was proposed as possible upstream target for all compounds, including E2, as well. As ERα is a protein involved in proliferation, ERα mediated actions are known to activate p53, in order to control the proliferation of the cells [62]. The finding of *ESR1* and *TP53* as possible upstream regulator therefore supports the estrogenic potential of the analyzed ligands.

As all bisphenol ligands and E2 were found to induce *ESR1*-mediated signaling in the cell, we first focused on the differentially expressed genes induced by all compounds. We found that all bisphenol ligands induced the *ESR1*-mediated upregulation of transcription factor genes such as the AP-1 transcription factor subunits *FOSL2* and *JUN*. FOSL2 is associated with increased invasive potential in breast cancer cells [63, 64]. After dimerization with JUN, the transcription factor AP-1 is known to regulate several proteases, relevant for migration and invasion [63]. The overexpressed transcription factor RUNX2 regulates osteoblast differentiation and was associated with bone metastasis in breast cancer [65, 66]. The expression of the transcriptional coregulator PHF19 was negatively influenced by BPA, BPB, 4MeBPA and E2. PHF19 belongs to the polycomb group proteins, which are transcriptional repressors relevant for embryonic development, proliferation and cancer [67, 68]. Besides further transcription factors, the breast carcinoma amplified sequence 3 (*BCAS3*) is a known direct target

of ESR1 and was downregulated with E2, BPA, BPB, and 4MeBPA. BCAS3 is described as transcriptional coactivator for ERα signaling, often found overexpressed in breast cancers [69, 70]. The progesterone receptor (*PGR*) was upregulated by all bisphenolic compounds and is directly regulated by ERα. The PGR status is used, together with ERα and HER2, as a prognostic marker for breast cancer, indicating good response to hormonal treatment if expressed [71, 72]. Upregulation of DNA-damage inducible transcript 4 (*DDIT4*) and immediate early response 3 (*IER3*) indicate activation of apoptotic systems due to bisphenol treatment [73, 74]. Further cytoplasmic-related genes are the microsome-associated heat shock protein 13 (HSPA13/ *HSPA13*), whose function is not clear yet [75]. The protein kinase C δ type (PKC δ / *PRKCD*) is associated with translocalization of ERα from the cytosol to the nucleus [76].

Three amino acid transporters from the solute carrier family 7 *SLC7A11*, *SLC7A2*, *SLC7A5* were upregulated in all samples. SLC members increase the nutritional supply and maintain the redox homeostasis in the cells [77–79]. Another membrane-associated gene is the adenosine A1 receptor (*ADORA1*), which is a direct target and regulator of ERα promoting proliferation [80]. The cadherin EGF LAG seven-pass G-type receptor 2 (CELSR2/ *CELSR2*) is involved in cell adhesion [81, 82]. Insulin like growth factor 1 receptor (*IGF1R*) was upregulated with all ligands. Activation of the IGF system is associated with cell growth, invasion, metastasis, angiogenesis and resistance to apoptosis [83–85]. IGF1R is expressed in breast cancers and correlated to ERα and PGR expression [86]. Stanniocalcin 2 (*STC2*) encodes a secreted glycoprotein, upregulated in ERα positive breast cancers and associated with tumor growth [87, 88].

In summary, all these genes indicate a strong regulation by *ESR1* signaling. We can therefore conclude that BPA, BPB, BPZ, and 4MeBPA activated ERα which altered gene expression promoting cell growth, invasion, migration, apoptosis and cancer development.

3.4.1 Specific gene expression by BPA

Besides genes differentially expressed by all ligands, BPA regulated an individual set of genes apart from the others. Among them is the interleukin 1 receptor associated kinase 1 binding protein 1 (*IRAK1BP1*) gene, relevant for the immune system. IRAK1BP1 has an inhibitory role in inflammation by effecting NF-κB. It increased the IL-10 production and promoted lipopolysaccharide tolerance [89, 90]. The non-coding small nuclear 7SK RNA (*RN7SK*) inactivates the positive elongation factor b, thereby negatively regulates the RNA polymerase II [91, 92]. Another target of *RNA7SK* is the transcriptional and chromatin regulator HMGA1. The interaction of RNA7SK and HMGA1 is relevant for differentiation and proliferation [92]. Furthermore, *RNA7SK* is involved in neuronal differentiation [93]. *RPPH1*, the ribonuclease P RNA component H1, is a long non-coding RNA and part of an endoribonuclease cleaving tRNA precursor molecules [94]. *RPPH1* was upregulated in breast cancer tissue and cell lines

and enhanced cell proliferation [94, 95]. Zhang and Tang (2017) discovered a target relationship between RPPH1 and the micro RNA miR-122, involving upregulation of miR-122 target genes like IGF-1R [94]. Furthermore, RPPH1 was upregulated in gastric cancer as well [96]. The orphan G protein coupled receptor (GPR27/ *GPR27*) was identified as a positive regulator of insulin production [97]. The chimeric translin-associated factor X - disrupted in schizophrenia 1 *TSNAX-DISC1* was expressed in endometrial cancer [98]. The dysregulation of TSNAX alters progesterone actions, implying an association with cancer [98].

3.4.2 Specific gene expression by BPB

The melanoma-associated antigen D4 (MAGED4/ *MAGED4*) was identified as a tumor-specific antigen for non-small cell lung cancer [99]. It was found in renal cell carcinoma [100] and esophageal squamous cell carcinoma [101]. Tumor necrosis factor ligand superfamily member 4 (*TNFSF4*) encodes Ox40 ligand, a cytokine of the TNF family [102]. Ox40 ligand affected atherosclerosis in mice and polymorphism were associated with increased risk of myocardial infarctions in human [102]. Mucin 2 (*MUC2*) encodes a human secretory mucin protein. Its major function is to protect the epithelial surface and the gut lumen [103]. MUC2 is expressed in mucinous breast cancer and may prevent tumor invasion [104]. The expression of MUC2 is associated with aggressive tumor behavior [105, 106].

3.4.3 Specific gene expression by BPZ

The transcription factor myocyte enhancer factor 2B (*MEF2B*) is a key regulator of Bcl-6, thereby affecting cell cycle, DNA damage repair and apoptosis [107]. The calcium voltage-gated channel auxiliary subunit $\beta 2$ (*CACNB2*) encodes a cytosolic subunit of calcium channels. The proper regulation of intracellular calcium levels is most important for the cardiovascular system. Dysregulation of the *CACNB2* gene are associated with cardiovascular diseases and mental disorders [108]. Overexpression of CACNB2 in HEK293 cells lead to increased cell proliferation and upregulation of the Ras-MAPK pathway [109]. Small Cajal body-specific RNA 2 (*SCARNA2*) is a long noncoding RNA and was found expressed in colorectal cancer [110]. Overexpression is correlated with a bad prognosis in colorectal cancer after surgery. *SCARNA2* binds competitively to miR-342-3p and thereby promotes chemoresistance by upregulation of the epidermal growth factor receptor and B-cell lymphoma 2 [110]. The PTPRF interacting protein $\alpha 4$ (*PPFIA4*) gene encodes the protein liprin-$\alpha 1$ which is frequently amplified in breast cancer and is associated with poor prognosis [111]. Liprin-$\alpha 1$ is required for the migration and invasion of breast cancer cells. The overexpression of *PPFIA4* enhanced the degradation of the extracellular matrix [112].

3.4.4 Specific gene expression by 4MeBPA

The inhibin subunit βE (*INHBE*) gene was significantly upregulated. Inhibin βE is a growth factor of the TGF-β-family and involved in the regulation of liver cell growth and differentiation [113]. Recently, Inhibin βE was suggested to be an insulin resistance-associated hepatokine and might therefore be relevant for diabetes [113]. *LGR6*, leucine rich repeat containing G protein-coupled receptor 6, is a stem cell-specific receptor [114]. LGR6 is upregulated in several cancer and correlated to act by Wnt signaling [114]. It is further associated in the progression of gastric cancer through the PI3K/Akt/mTOR pathway [115]. Overexpression of the family with sequence similarity 129 member A (FAM129A) inhibits apoptosis and induces migration and proliferation in cancer [116]. The branched chain amino acid transaminase 1 (*BCAT1*) gene is overexpressed in several cancers and induces cell proliferation, migration, invasion and cell cycle arrest [117–119]. Kelch domain containing 7B (*KLHDC7B*) is overexpressed in breast cancer cells [120, 121]. *KLHDC7B* was identified as epigenetic marker in breast cancer cells and tissue [121]. It is associated with gene modulation in the interferon signaling pathway during breast tumorigenesis [120].

3.4.5 Verification of ERα binding, activation, and proliferative effects

The binding of the bisphenolic compounds to ERα was verified *in silico*. The RNA sequencing resulted in *ESR1* as upstream regulator and several differentially expressed genes regulated by *ESR1*, which further supports the estrogenic effect of the compounds. We applied MST to confirm the binding of the bisphenolic compounds *in vitro* and used an ER transcription factor activation assay and cell cycle analysis to test for ERα-mediated effects in the cell.

The MST experiment enabled the calculation of dissociation constants of the bisphenolic compounds and ERα. In all cases, the K_d of the bisphenols were higher than for E2, indicating that the bisphenolic compounds bound less strong to ERα than the natural ligand E2. However, binding of all compounds to E2 could be confirmed *in vitro* by MST. We analyzed the activation of ERα in HEK-ESR1 cells after two timepoints. BPA and 4MeBPA activated ERα in a time-dependent manner. E2 showed the highest activation, followed by 4MeBPA. BPB seemed to inhibit ERα after 8 h but not after 4 h. BPZ reduced the ERα activity with increasing time. We could confirm the activation of ERα by BPA, BPB, and 4MeBPA and propose an inhibitory effect of BPZ on the ERα activity.

Furthermore, we performed cell cycle analysis with two timepoints and two concentrations in HEK-ESR1 and MCF-7 cells. E2 and 4MeBPA induced the strongest proliferative effect, followed by BPB. Treatment with BPA and BPZ did not influence the cell cycle. Therefore, we verified a proliferative effect of 4MeBPA and BPB in ERα expressing cells.

The results confirm the expected binding of the bisphenolic compounds to ERα in *in vitro* and indicate ERα-mediated effects in the cells, with varying intensity. Therefore, we demonstrate the interaction of the compounds with ERα, mediating endocrine effects in HEK-ESR1 and MCF-7 cells.

3.4.6 Environmental concentrations of bisphenolic compounds

Whereas the endocrine effect of bisphenolic compounds can clearly be demonstrated, the question regarding actual uptake concentrations and effects is still unanswered. BPA is found ubiquitous in the environment with concentrations in the soil from 0.55 to 147 $\mu g\,kg^{-1}$ (dry weight), in sediments from < 0.24 to 492 $\mu g\,kg^{-1}$ (dry weight), and in groundwater and surface water from 0.001 to 20 $mg\,m^{-3}$ [122].

Studies in food revealed concentrations ranging from 0.1 to 790 $\mu g\,kg^{-1}$ (fresh weight) and < 0.00073 to 0.86 $mg\,m^{-3}$ in drinking water. In marine animals the BPA concentrations varies between 0.33 and 213.1 $\mu g\,kg^{-1}$ (fresh weight) [122]. Corrales et al. (2015) report concentrations in fish within a range of 0.2 to 13 000 $\mu g\,kg^{-1}$ [123].

Based on the available data, the United States Environment Protection Agency (USEPA) constitute a reference dose for oral exposure of BPA at 50 $\mu g\,kg^{-1}\,d^{-1}$ [123]. The European Food Safety Authority established a temporary Tolerable Daily Intake of BPA of 4 $\mu g\,kg^{-1}\,d^{-1}$ in 2015 [124]. The daily dietary BPA intake was estimated between 0.02 and 0.081 $\mu g\,kg^{-1}\,d^{-1}$ for adults and 0.22 to 0.33 $\mu g\,kg^{-1}\,d^{-1}$ for infants [122, 123].

BPA is excreted in the urine, but levels measured in tissues revealed concentrations of BPA in the brain with up to 2.36 $ng\,g^{-1}$, in the liver from 0.9 to 2.77 $ng\,g^{-1}$, and in the adipose tissue from 1.12 to 12.28 $ng\,g^{-1}$ [123]. However, the degree of accumulation potency and excretion is still fairly uncertain.

The concentrations of bisphenol analogues in the environment are similar to those observed solely for BPA [40]. However, TDI values are generally not available due to few data [40]. In order to make a statement regarding the accumulation of bisphenol compounds in the human body and the intensity of the molecular effects, further research needs to be conducted regarding uptake concentrations, accumulation, and excretion rates.

3.5 Conclusion

With this study, we verified the binding of BPA, BPB, BPZ, and 4MeBPA to ERα *in silico*, *in vitro* and confirmed the activation of the receptor with BPA, BPB and 4MeBPA. Furthermore, BPB and 4MeBPA revealed a proliferative potential on ERα positive cells. NGS gave insights into the molecular effects of these compounds mediated by ERα. We found 14 upregulated genes (*ADORA1*, *DDIT4*, *CELSR2*, *FOSL2*, *JUN*, *HSPA13*, *IER3*, *IGF1R*, *PGR*, *RUNX2*, *SLC7A11*, *SLC7A2*, *SLC7A5*, *STC2*) and three downregulated genes

(*BCAS3*, *PHF19*, *PRKCD*) in almost all samples associated with cell growth, invasion, migration, apoptosis and cancer development. Furthermore, each ligand induced a specific gene expressing, indicating side effects. BPA, BPB, BPZ, and 4MeBPA should therefore be regarded as endocrine disrupting chemicals. To better understand how plasticizers and other xenobiotics impact on both our exposome and human health is highly relevant from the perspective of life sciences as well as from an ethical and societal perspective and should be regarded as one of the major interdisciplinary challenges of our time.

3.6 Acknowledgement

This work was supported by the *Deutsche Forschungsgemeinschaft* (GRK 2015/2). The authors gratefully acknowledge the computing time granted on the supercomputer Mogon at Johannes Gutenberg University Mainz (hpc.uni-mainz.de). Cell sorting support by the IMB Flow Cytometry Core Facility is gratefully acknowledged.

3.7 Supplementary material

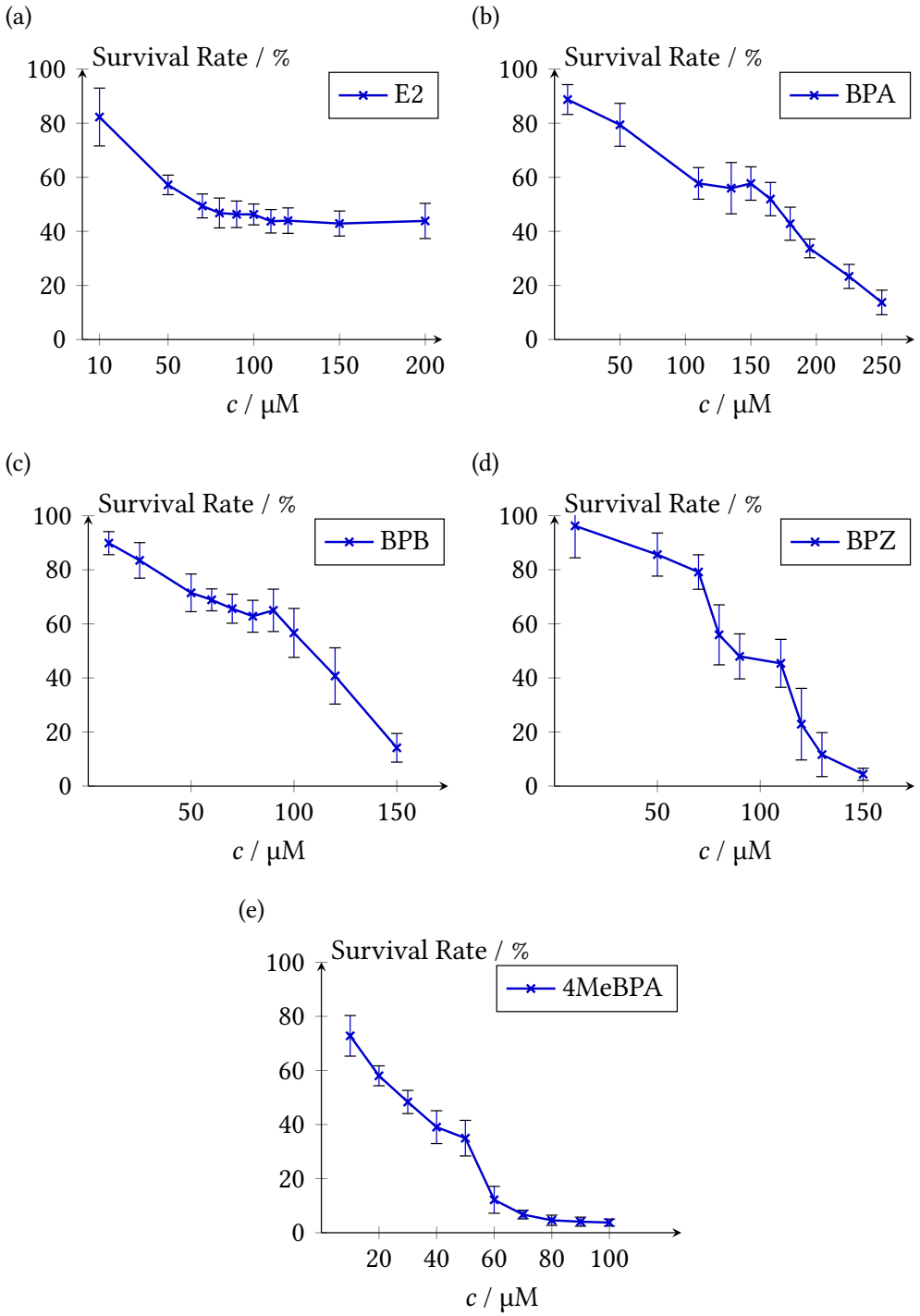

Figure 3.11: Analysis of the cytotoxicity assay. The survival rate was measured for (a) E2, (b) BPA, (c) BPB, (d) BPZ, and (e) 4MeBPA respectively and represented as mean ± SD.

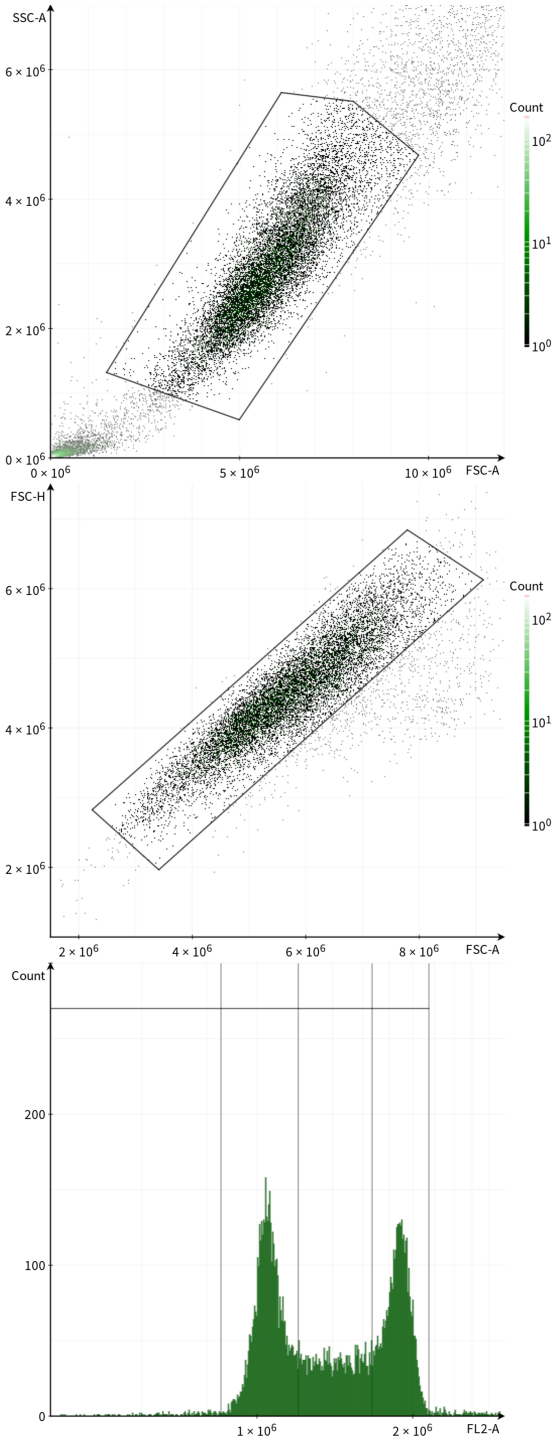

Figure 3.12: Gating in the cell cycle experiments. HEK-ESR1 cells were treated with E2 for 4 h at 25 µM. (Top) The major cell population was selected. (Middle) Aggregates and doublets were removed. (Bottom) The selected cells were gated into four groups based on their PI content detected by the FL2-A detector.

Table 3.9: Cell cycle analysis was performed with the cell line MCF-7. Cells were treated with DMSO as control, E2, or the bisphenol compounds at a concentration of 25 µM or 50 µM for 4 h or 8 h, respectively. The percentage of cells in relation to the cell cycle phases is given.

Treatment	Phase	DMSO	E2	BPA	BPB	BPZ	4MeBPA
	sub G1 / %	1.9	0.9	0.5	1.4	0.6	2.0
4 h	G1/G0 / %	46.9	34.2	48.0	49.8	47.1	34.6
25 µM	S / %	26.0	25.2	24.0	25.9	25.9	26.8
	G2/M / %	24.8	39.5	27.2	22.8	26.1	35.9
	sub G1 / %	0.6	0.7	0.5	1.3	1.1	1.7
4 h	G1/G0 / %	46.3	32.8	45.5	42.9	48.8	40.1
50 µM	S / %	26.3	24.4	26.3	26.2	26.0	24.3
	G2/M / %	26.4	41.6	27.1	29.3	23.4	33.3
	sub G1 / %	1.6	1.1	1.0	1.4	0.9	2.8
8 h	G1/G0 / %	46.2	24.2	48.8	47.4	48.6	26.5
25 µM	S / %	26.6	25.9	22.9	22.9	24.0	24.5
	G2/M / %	25.1	48.3	27.0	28.2	26.3	45.7
	sub G1 / %	0.6	1.2	0.9	1.1	1.0	2.2
8 h	G1/G0 / %	45.2	23.5	46.2	40.4	46.2	29.0
50 µM	S / %	26.6	26.3	27.0	25.3	22.2	23.3
	G2/M / %	27.0	48.8	25.3	32.6	29.9	44.5

(a) E2

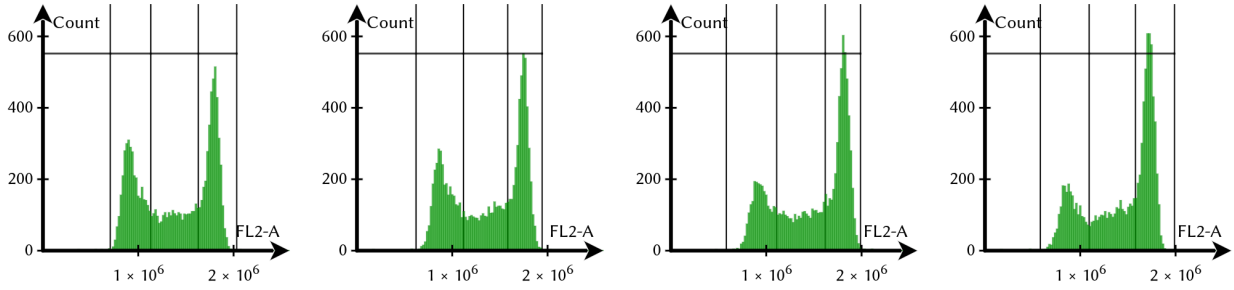

(b) BPA

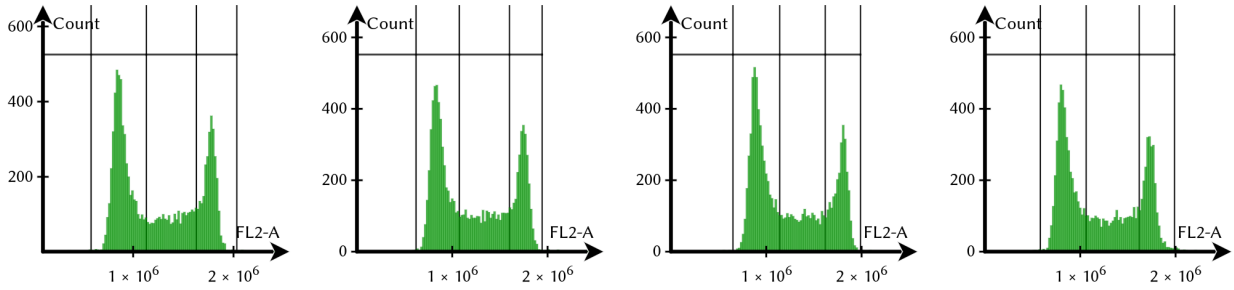

(c) BPB

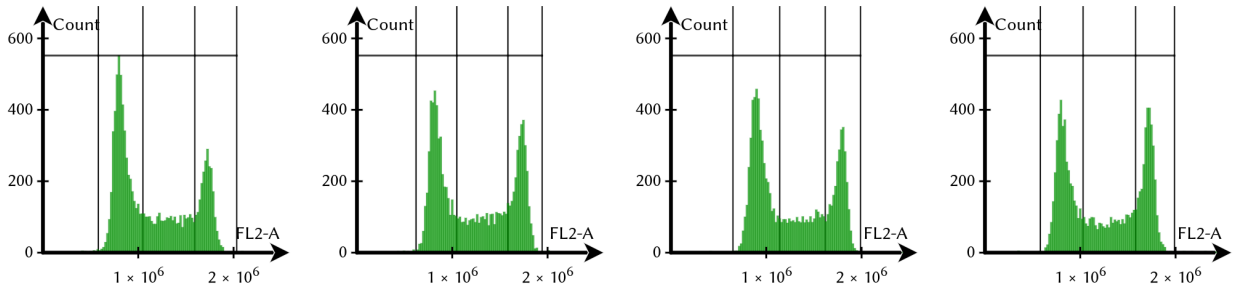

(d) BPZ

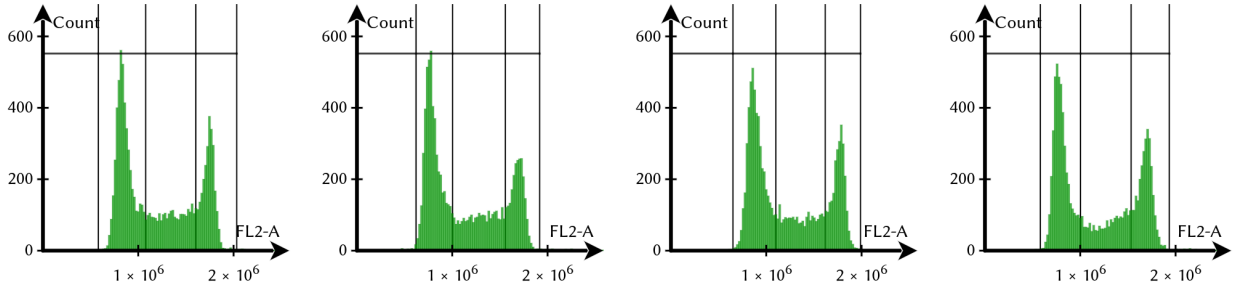

(e) 4MeBPA

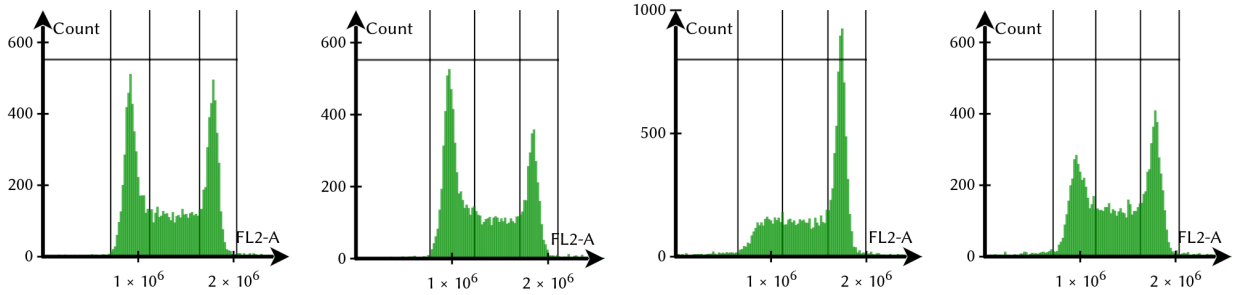

Figure 3.13: Cell Cycle Analysis. MCF-7 cells were treated with (a) E2, (b) BPA, (c) BPB, (d) BPZ and (e) 4MeBPA. Each analysis was performed under four conditions: 4 h and 25 µM, 4 h and 50 µM, 8 h and 25 µM, 8 h and 50 µM (from left to right).

4 Butyl octyl phthalate interacts with estrogen receptor α in MCF-7 breast cancer cells promoting cancer development

Chapter 4 is based on the manuscript "Butyl octyl phthalate interacts with estrogen receptor α in MCF-7 breast cancer cells promoting cancer development" by M. Böckers, N. W. Paul and T. Efferth, which is in preparation. I performed and analyzed the experiments, prepared the figures and wrote the manuscript with contributions from all authors. The RNA sequencing experiment was performed by StarSEQ GmbH, Mainz, Germany. The manuscript is reproduced verbatim. Minor modifications were made for consistency within this thesis, such as combining the abbreviations and the method section from all manuscripts into a single chapter, respectively.

4.1 Abstract

The environmental pollution with microplastic and especially the leaching of plasticizers is increasingly regarded with concern. The uptake of microplastic by marine animals might bring the plasticizers into the food chain, which might affect the human health. Phthalate compounds are discussed to act as endocrine disruptors. Here, we analyzed the effect of the three phthalates benzyl butyl phthalate (BBP), butyl cyclohexyl phthalate (BCP) and butyl octyl phthalate (BOP) towards the human breast cancer cell line MCF-7. We applied molecular docking, microscale thermophoresis, and cell cycle analysis with MCF-7 cells, and measured estrogen receptor α (ERα) activation on *ESR1*-overexpressing HEK293 cells. BBP, BCP and BOP bound *in silico* and *in vitro* to ERα and activated the receptor. BBP and BOP further influenced the cell cycle progression. In addition, we applied next-generation sequencing and found 15 differentially expressed genes after treatment of MCF-7 cells with BOP: *CYP1A1*, *DDIT4*, *KLHL24*, *SLC7A11*, *CEACAM5*, *STC2*, *SLC7A5*, and *IER3* were upregulated, and *FKBP4*, *TFAP2C*, *CDK1*, *CCNA2*, *PGR*, *SFPQ*, and *ADORA1* were downregulated. The gene expression pattern was associated with interference in the cell cycle, increased tumorigenesis, proliferation, metastasis and poorer survival in cancer cells. Our results revealed an endocrine disruptive potential of BOP on MCF-7 breast cancer cells and showed the interaction of BBP, BCP, and BOP with ERα *in vitro*.

4.2 Introduction

The consequences of microplastic on human health becomes an increasingly relevant research topic [125–128]. During the production of plastic, phthalates are often added to enhance the material properties [129]. However, the added phthalate compounds are not directly involved in the covalent polymerization, but remain weakly attached to the polymer chains [130]. This may cause leaching of phthalates from the plastic [131, 132]. Microplastic ingestion might lead to the incorporation of phthalates into marine animals, and subsequently human beings.

Among the phthalates, benzyl butyl phthalate (BBP) is one of to the most widely used and studied compounds [129]. BBP is used as plasticizer in PVC, consumer end products, medical devices and others [133–135]. Due to its toxic and endocrine disrupting properties, usage of BBP became restricted and was considered as water pollutant [133, 134, 136]. While BBP is well studied, other phthalate compounds such as butyl cyclohexyl phthalate (BCP), and butyl octyl phthalate (BOP) require further risk assessment. First studies revealed cyto- and genotoxic effects induced by BCP [131, 137].

Phthalates were found with adverse health effects in animal studies, especially related to reproductive and developmental effects [15]. It is therefore suspected that the added phthalate compounds should be considered as endocrine disrupting chemicals (EDC) [134, 138, 139]. EDCs mimic hormones and induce hormonal effects in the cells, mediated by nuclear receptors such as the estrogen receptor (ER) [140, 141]. ERs exist in two isoforms: ERα (*ESR1*) and ERβ (*ESR2*), with ERα being most important for development and reproduction [53]. The receptor binds its natural ligand 17-β-estradiol (E2) in the ligand binding domain (LBD) [54]. Subsequent three-dimensional change of the protein induces dimerization of the receptor and translocation to the nucleus, where ERα binds to the DNA and functions as transcription factor [54]. ERα is mainly associated with development, reproduction, proliferation effects [52, 57].

In this study, we used RNA sequencing to reveal the effect of phthalate exposure on the gene expression in MCF-7 cells. We demonstrated that BCP, BBP, and BOP all bind and activate ERα and that BOP induced differential expression of 15 genes regulated by *ESR1*, indicating a possible endocrine disrupting effect in MCF-7 breast cancer cells *in vitro*.

4.3 Results

4.3.1 Molecular Docking

We performed molecular docking analysis to investigate the *in silico* binding of the phthalates to the ERα-LBD (Table 4.1). *In silico* binding of the phthalate compounds to ERα-LBD indicated higher binding energies to the protein, compared to the natural ligand E2. The phthalate compounds share 9 amino acids of ERα-LBD to which they all

bind: Leu346, Thr347, Ala350, Glu353, Leu387, Leu391, Phe404, Leu525, Leu540. Four amino acids are also shared with E2 as ligand: Leu346, Glu353, Phe404, and Leu525. The binding position calculated with the lowest energy is visualized in Figure 4.1. BBP, BCP, and BOP bound to ERα-LBD *in silico*.

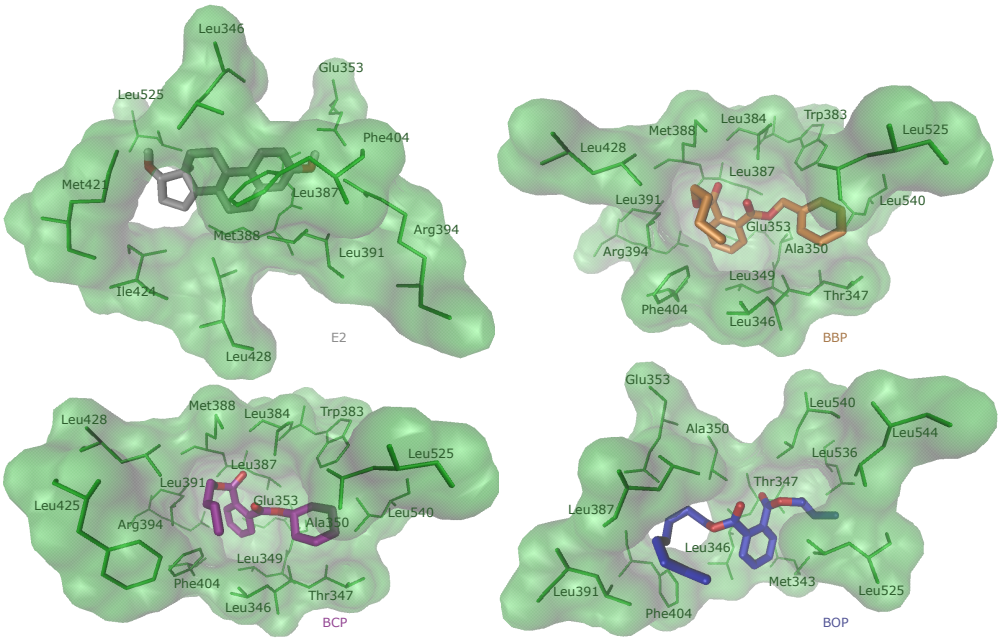

Figure 4.1: Visualization of the molecular docking result. The lowest binding energy position of the ligands E2 (grey), BBP (orange), BCP (purple), and BOP (blue) in ERα-LBD are shown. Each ligand is displayed with the interacting amino acids of ERα-LBD.

Table 4.1: Result of molecular docking. For each ligand, the lowest and mean binding energy and the predicted inhibitory constant $K_{i,pred}$ are given. The torsdof parameter Td indicates the torsional degree of freedom of each ligand. The amino acids of ERα-LBD involved in hydrophobic interactions and hydrogen bonds (H-bonds) are listed.

	lowest binding energy / kcal mol^{-1}	mean binding energy / kcal mol^{-1}	$K_{i,pred}$ / nM	Td	No. of cluster	Runs in 1st cluster	Amino acids involved in hydrophobic interactions	Amino acids involved in H-bonds
E2	−9.48	−9.45	112.95	2	1	250/250	Leu346 Leu387 Met388 Leu391 Phe404 Met421 Ile424 Leu428 Leu525	Glu353 Arg394
BBP	−7.80	−7.60	1930	9	12	29/250	Leu346 Thr347 Leu349 Ala350 Glu353 Trp383 Leu384 Leu387 Met388 Leu391 Arg394 Phe404 Leu428 Leu525 Leu540	-
BCP	−8.09	−7.63	1170	8	10	121/250	Leu346 Thr347 Leu349 Ala350 Glu353 Trp383 Leu384 Leu387 Met388 Leu391 Arg394 Phe404 Phe425 Leu428 Leu525 Leu540	-
BOP	−7.43	−6.80	3590	14	13	7/250	Met343 Leu346 Thr347 Ala350 Glu353 Leu387 Leu391 Phe404 Leu525 Leu536 Leu540 Leu544	-

4.3.2 Microscale Thermophoresis

Microscale thermophoresis (MST) was used to investigate the binding capability of the phthalate ligands and E2 to ERα *in vitro*. For all ligands the detected fluorescent signal decreased with increasing concentration, indicating binding of all ligands to ERα (Figure 4.2). The calculated dissociation constant of BCP was higher than of the other ligands (Table 4.2), indicating a lower binding capability to the protein. The *in vitro* binding to ERα was confirmed for all ligands.

4.3.3 Cytotoxicity

The cytotoxic effect of the phthalates was analyzed with the resazurin reduction assay. All three phthalate compounds did not reduce the survival rate of the cells in the measured concentration range below 60% (Figure 4.9). The IC_{50} of E2 in HEK-ESR1 cells was measured as (68 ± 11) µM (Chapter 3). For the following experiments, concentrations were chosen below the IC_{50} of E2, to avoid any cytotoxic effects in the cells.

4.3.4 ER transcription factor activation assay

As the binding of BBP, BCP, and BOP to ERα was verified *in silico* and *in vitro*, the activation of the receptor was measured with the ER transcription factor activation assay in ERα overexpressing HEK-ESR1 cells. A time-dependent activation of ERα was found for all ligands (Figure 4.3). While BBP induced the strongest activation after 4 h, the activation after treatment with BOP was strongest after 8 h. However, the natural ligand E2 was the most active compound at both time points. All phthalates activated the estrogen receptor *in vitro*.

4.3.5 Cell cycle analysis

Cell cycle analysis was performed to search for possible proliferative effects of the phthalate compounds in MCF-7 (Figure 6.8) and HEK-ESR1 (Figure 4.8) cells. The cells were treated with the compounds in two different concentrations and time points. An increase in the G2/M population was detected for BBP in HEK-ESR1 and BOP in MCF-7 cells (Table 6.5). Treatment with BCP did not influence the cell cycle distribution of both cell lines. BBP and BOP interfered with the cell cycle in HEK-ESR1 and MCF-7 cells.

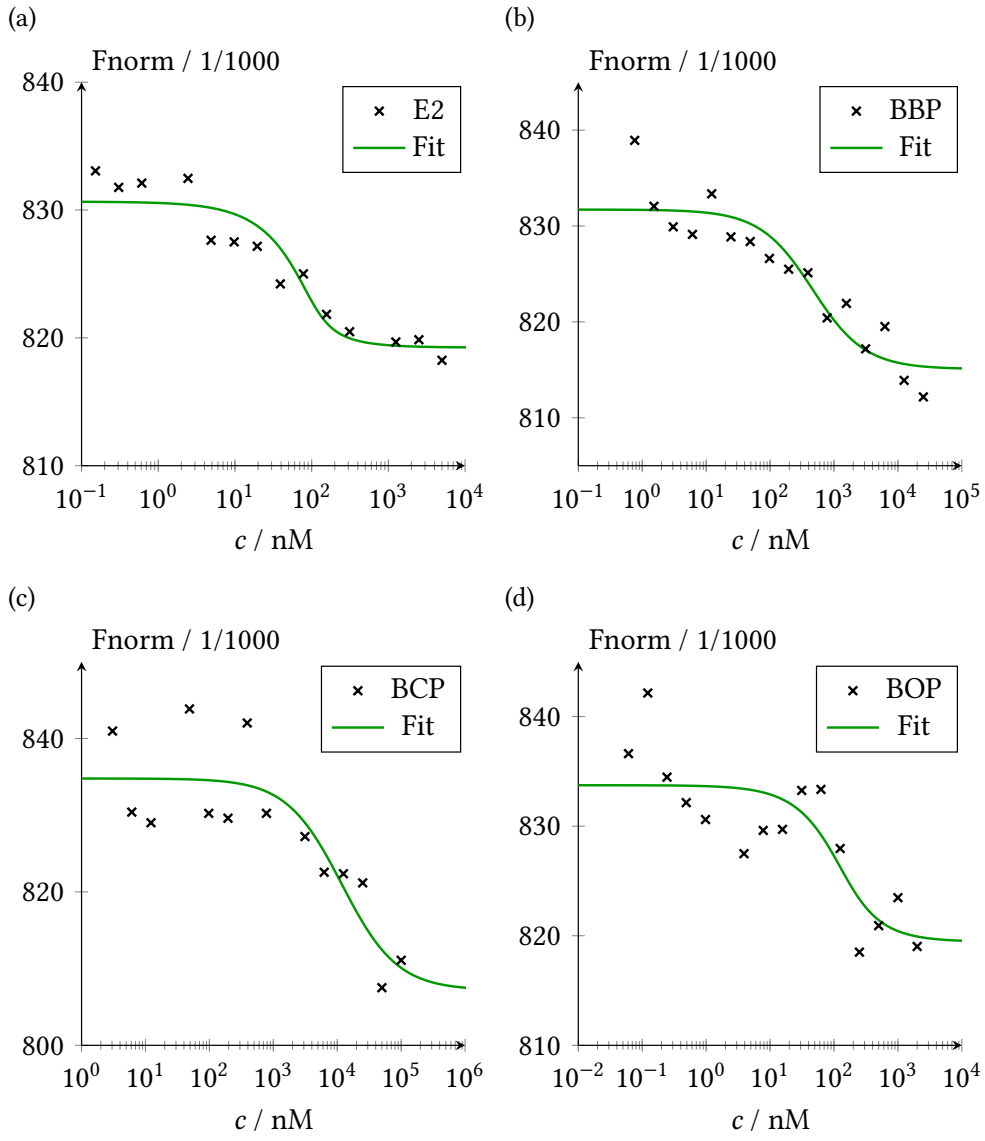

Figure 4.2: Analysis of the MST-experiments. The MST was performed with 95% LED and 20% MST power. Fluorescently labeled ERα was used as target with (a) E2, (b) BBP, (c) BCP, and (d) BOP as ligand, respectively. A fit was performed according to the law of mass action (green).

Table 4.2: Molecular structure of the analyzed ligands and comparison of the inhibitory constant predicted *in silico* ($K_{i,pred}$) with the dissociation constant calculated by MST *in vitro* (K_d).

Structure	Name	$K_{i,pred}$ / nM	K_d / nM
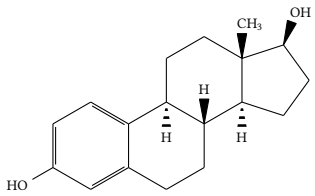	17-β-Estradiol E2 CAS 50-28-2	112.98	14.9 ± 2.1
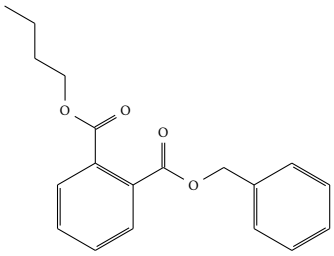	Benzylbutylphthalate BBP CAS 85-68-7	1930	412 ± 54
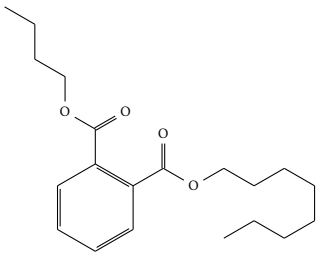	Butyloctylphthalate BOP CAS 84-78-6	3590	66 ± 16
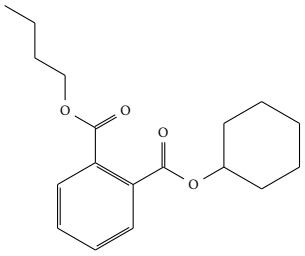	Butylcyclohexylphthalate BCP CAS 84-64-0	1170	11 800 ± 1800

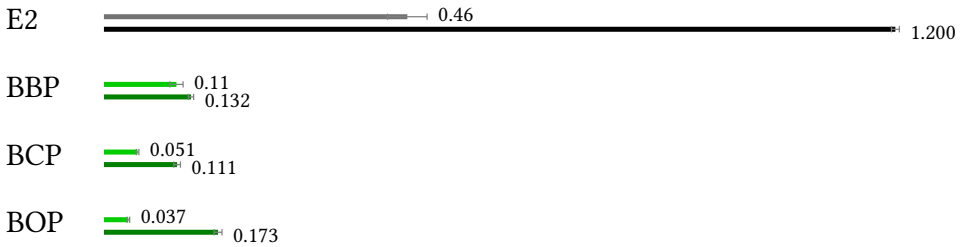

Figure 4.3: ER transcription factor assay. Activation of estrogen receptor was measured after 4 h and 8 h incubation time of HEK-ESR1 cells with 25 µM of the respective ligand. The difference optical density measured after 4 h is shown in the upper line and after 8 h in the lower line.

Table 4.3: Cell cycle analysis. HEK-ESR1 and MCF-7 cells were treated with 25 µM or 50 µM of BBP, BCP, or BOP and incubated for 4 h or 8 h, respectively. DMSO was used as control.

		HEK-ESR1				MCF-7			
Treatment	Phase	DMSO	BBP	BCP	BOP	DMSO	BBP	BCP	BOP
	sub G1 / %	0.4	0.2	0.6	0.5	0.2	0.2	0.2	0.3
4 h	G1/G0 / %	54.3	50.5	54.3	52.2	46.7	45.8	43.2	43.2
25 µM	S / %	23.4	24.4	22.5	22.1	24.4	25.6	25.9	25.6
	G2/M / %	21.9	24.4	22.5	25.1	28.4	28.2	30.6	30.7
	sub G1 / %	0.2	0.7	0.6	0.4	0.0	0.2	0.2	0.0
4 h	G1/G0 / %	56.1	51.0	54.5	52.4	47.2	42.9	42.9	42.0
50 µM	S / %	23.7	23.2	26.7	26.2	24.0	27.1	26.2	25.7
	G2/M / %	20.0	24.8	18.2	20.8	28.8	29.9	30.6	32.2
	sub G1 / %	0.1	0.2	0.3	0.1	0.1	0.1	0.5	0.2
8 h	G1/G0 / %	54.3	54.3	51.8	51.1	48.6	50.5	48.8	47.1
25 µM	S / %	23.6	21.3	26.2	26.8	26.3	25.2	24.4	25.1
	G2/M / %	21.5	24.0	21.6	22.0	25.0	24.2	26.3	27.5
	sub G1 / %	0.1	0.6	0.3	0.7	0.1	0.1	0.1	1.0
8 h	G1/G0 / %	55.3	52.8	54.0	53.1	45.9	51.6	48.7	40.4
50 µM	S / %	23.2	21.9	25.2	27.2	24.7	22.5	22.6	26.3
	G2/M / %	20.9	24.6	20.4	18.9	29.3	25.8	28.5	31.9

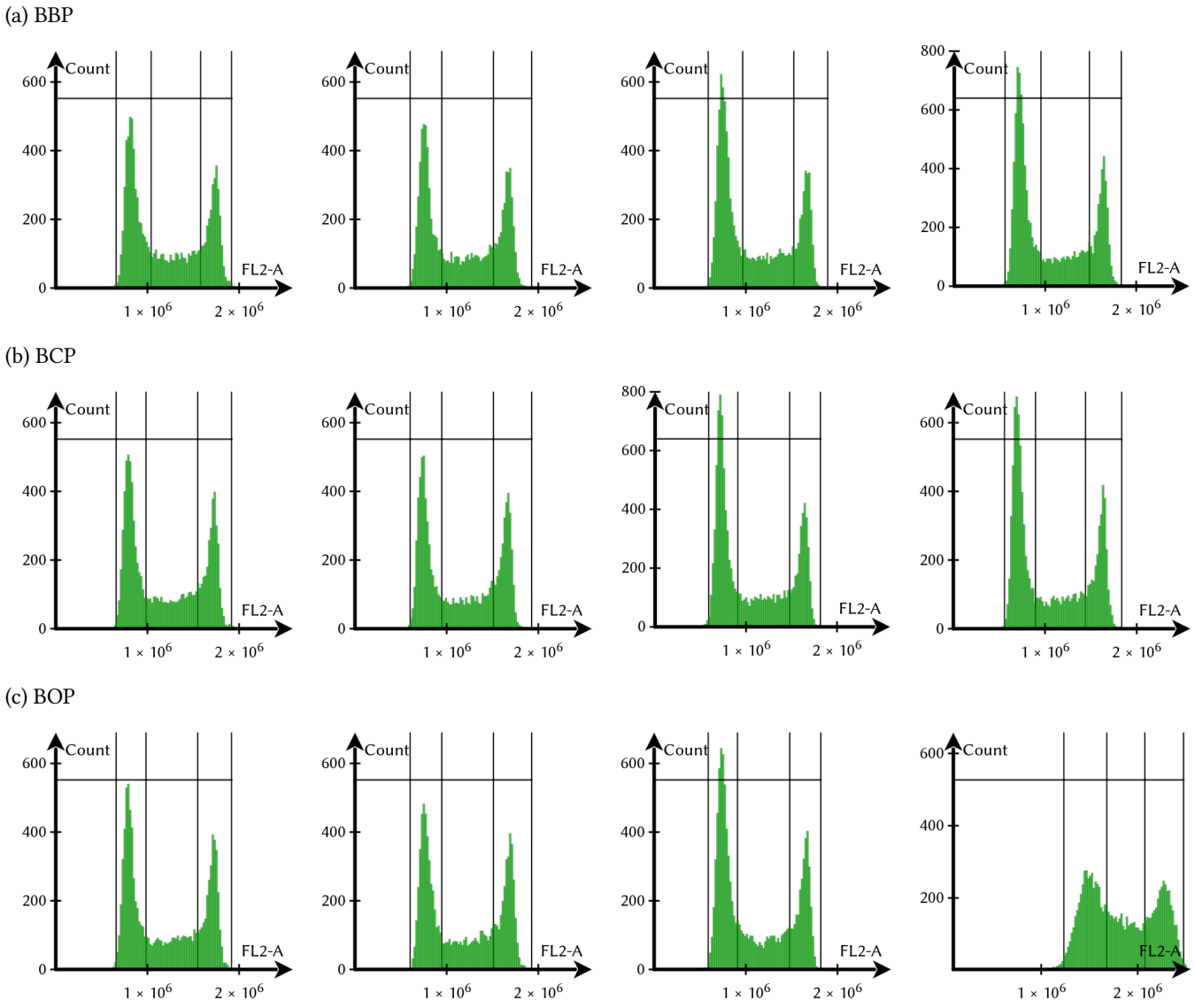

Figure 4.4: Cell Cycle Analysis. MCF-7 cells were treated with (a) BBP, (b) BCP, and (c) BOP. Each analysis was performed under four conditions: 4 h with 25 µM and 50 µM, 8 h with 25 µM and 50 µM (from left to right).

4.3.6 RNA sequencing

In order to analyze the molecular effects induced by the phthalates, we performed RNA sequencing. As BOP was measured with the lowest K_d, the highest ER activation after 8 h, and a proliferative effect in MCF-7 cells, the gene expression after BOP treatment was analyzed by NGS. Upstream target analysis by IPA identified *ESR1* as the top most likely upstream regulator of the gene expression pattern. A total of 15 differentially expressed genes regulated by ERα were found (Figure 4.5). *CYP1A1*, *DDIT4*, *KLHL24*, *SLC7A11*, *CEACAM5*, *STC2*, *SLC7A5*, and *IER3* were upregulated and *FKBP4*, *TFAP2C*, *CDK1*, *CCNA2*, *PGR*, *SFPQ*, and *ADORA1* were downregulated after treatment of MCF-7 cells with BOP. Besides genes regulated by *ESR1*, several other genes were found differentially expressed after treatment with BOP. Genes expressed with a fold change of at least (-)1 and unrelated to *ESR1* regulation are listed in Table 4.4. RNA sequencing identified several differentially expressed genes induced by BOP in MCF-7 cells.

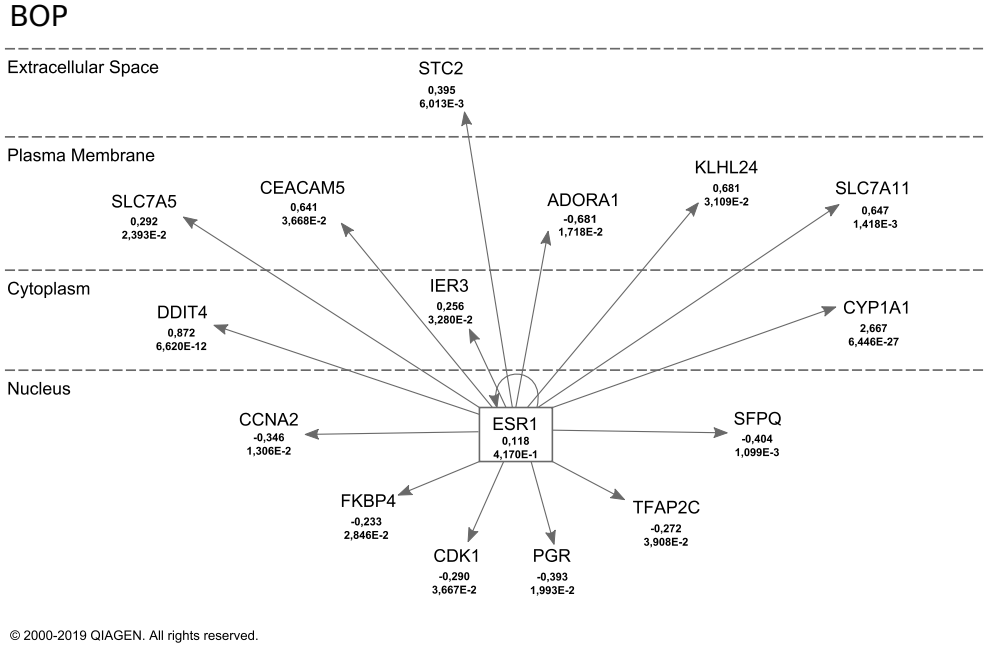

Figure 4.5: Upstream analysis with Ingenuity Pathway Analysis software. Differentially expressed genes induced by BOP and in connection with *ESR1* regulation are shown. For each gene the fold change and the *p*-value are given. The figure was modified based on the IPA Path Designer.

Table 4.4: Specific gene expression induced by BOP. For each gene the fold change $\log_2\left(\frac{E_{\mathrm{BOP}}}{E_{\mathrm{c}}}\right)$ with corresponding standard error $\Delta\log_2\left(\frac{E_{\mathrm{BOP}}}{E_{\mathrm{c}}}\right)$ and p-value are listed. ID refers to the name of the gene, E to the expression induced by the respective ligand, and E_c to the expression under control conditions. p-values indicate the comparison with the DMSO-control.

ID	$\log_2\left(\frac{E_{\mathrm{BOP}}}{E_{\mathrm{c}}}\right)$	$\Delta\log_2\left(\frac{E_{\mathrm{BOP}}}{E_{\mathrm{c}}}\right)$	p	Entrez Gene Name
MAGED4	8.439	1.547	$4.93 \cdot 10^{-8}$	MAGE family member D4B
FSBP	5.990	1.917	$1.78 \cdot 10^{-3}$	fibrinogen silencer binding protein
TRIM39-RPP21	5.782	1.989	$3.65 \cdot 10^{-3}$	TRIM39-RPP21 readthrough
U2AF1L5	5.597	1.693	$9.45 \cdot 10^{-4}$	U2 small nuclear RNA auxiliary factor 1
JMJD7-PLA2G4B	5.105	2.533	$4.38 \cdot 10^{-2}$	JMJD7-PLA2G4B readthrough
TIAF1	2.947	1.485	$4.72 \cdot 10^{-2}$	TGFB1-induced anti-apoptotic factor 1
MMP19	2.310	0.905	$1.07 \cdot 10^{-2}$	matrix metallopeptidase 19
LOC102724093	1.909	0.879	$2.98 \cdot 10^{-2}$	golgin subfamily A member 6-like protein 4
IRAK1BP1	1.623	0.813	$4.59 \cdot 10^{-2}$	interleukin 1 receptor associated kinase 1 binding protein 1
FAHD2CP	1.400	0.711	$4.90 \cdot 10^{-2}$	fumarylacetoacetate hydrolase domain containing 2C, pseudogene
WDR97	1.253	0.631	$4.70 \cdot 10^{-2}$	WD repeat domain 97
ZNF460	1.252	0.600	$3.68 \cdot 10^{-2}$	zinc finger protein 460
GPRASP2	1.169	0.391	$2.81 \cdot 10^{-3}$	G protein-coupled receptor associated sorting protein 2
GUCA1B	1.112	0.562	$4.80 \cdot 10^{-2}$	guanylate cyclase activator 1B
LACE1	−1.032	0.481	$3.20 \cdot 10^{-2}$	AFG1 like ATPase
TEX14	−1.245	0.472	$8.26 \cdot 10^{-3}$	testis expressed 14, intercellular bridge forming factor
KCNQ2	−1.542	0.768	$4.48 \cdot 10^{-2}$	potassium voltage-gated channel subfamily Q member 2
SENP3-EIF4A1	−2.148	1.081	$4.69 \cdot 10^{-2}$	SENP3-EIF4A1 readthrough (NMD candidate)
FAM72C	−3.872	1.286	$2.61 \cdot 10^{-3}$	family with sequence similarity 72 member D
CD36	−4.538	2.049	$2.68 \cdot 10^{-2}$	CD36 molecule

4.3.7 RT-qPCR

RT-qPCR was used to confirm the gene expression of selected genes measured by NGS. *GAPDH* was used as reference gene. The log2 fold change expression of the RT-qPCR experiment was plotted against the log2 fold change expression of the NGS experiment (Figure 4.6). A linear fit was performed with a calculated R value of 0.90. The induced gene expression was confirmed.

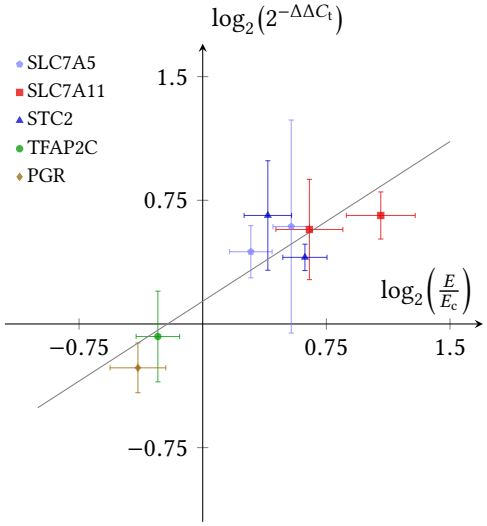

Figure 4.6: Correlation of gene expression levels obtained by NGS and RT-qPCR. The fold change based on the RT-qPCR results was plotted against the fold change based on the NGS results for the ligands E2 and BOP (dots). The was calculated with *GAPDH* as reference gene. A linear regression was calculated with Origin 7.5. The fit is shown in grey with a slope of 0.65 and an intercept of 0.14 and an R value of 0.90.

4.4 Discussion

In this study, we analyzed the interaction of the three phthalate compounds BBP, BCP, and BOP on ERα and the molecular effects of BOP on the gene expression in MCF-7 cells.

4.4.1 Verification of ERα binding, activation, and proliferative effects

The molecular docking results indicate binding of BBP, BCP, and BOP to ERα-LBD *in silico*. The calculated binding energy was higher compared to E2, indicating weaker binding. Whereas E2 is a rather rigid ligand, the phthalate compounds have far more

freely rotatable bonds, resulting in more possibilities of the ligands to be placed in the binding pocket, which may not all be covered during the molecular docking process. The torsional degree of freedom is represented by the torsdof parameter which further correlates with the amount of identified ligand cluster. Whereas all docking runs of E2 resulted in one cluster with a maximum difference between the single runs of 2.0 Å, the dockings with the phthalate ligands resulted in several clusters. Due to their higher flexibility, the molecular docking simulations of the phthalate compounds need to be considered more carefully. Nevertheless, binding to the protein *in silico* can be confirmed. The *in vitro* binding of all ligands to ERα was confirmed by MST. The dissociation constant indicated that BOP bound most stably to ERα, followed by BBP. BCP bound less stable to the receptor. The activation of the receptor was measured for all ligands. Treatment with BOP for 8 h resulted in the strongest activation, apart from E2. E2 is known to induce proliferative effects in cells [142]. The proliferative effect of the three phthalate compounds on MCF-7 and HEK-ESR1 cells was measured by analyzing the cell cycle distribution. For BBP and BOP a proliferative effect was found, indicating an endocrine disrupting potential of both ligands. In summary, BBP, BCP, and BOP bound *in silico* and *in vitro* to ERα and were able to activate the receptor. BBP and BOP further show proliferative effects.

4.4.2 Gene expression by BOP

BOP induced differential expression of 15 genes in MCF-7 cells. The transcription factor AP-2γ (*TFAP2C*) was negatively affected by BOP-treatment. TFAP2C was found to be expressed in breast cancer cells and has a role in tumor progression [143, 144]. This transcription factor further downregulates the expression of p21, a cell cycle inhibitor [145]. Other cell cycle associated genes were downregulated as well, such as the cyclin-dependent kinase 1 (*CDK1*) and cyclin A2 (*CCNA2*). The gene expression pattern indicated BOP-mediated cell cycle disturbances in breast cancer cells. The splicing factor proline and glutamine rich (*SFPQ*) is involved in transcription and pre-mRNA splicing [146] and was downregulated after BOP-treatment. Downregulation of *SFPQ* was associated with shorter overall survival in colorectal cancer patients [147]. In mice, SFPQ acted as tumor suppressor by regulating cell proliferation and tumorigenesis [148]. The immunophilin FK506-binding protein (*FKBP4*) is usually elevated expressed in ERα positive breast cancers [149, 150], but was downregulated in our analysis. FKBP4 is associated with steroid receptors in general, altering the receptor activity [149]. One steroid receptor was downregulated as well: the progesterone receptor (PGR). PGR is associated with breast cancer progression and used, besides ERα and HER2, as prognostic marker [151]. A negative PGR status correlates with a poorer survival [152].

Some genes coding for cytoplasmic proteins were upregulated after treatment with BOP. The DNA damage-inducible transcript 4 (*DDIT4*) is activated by cellular stress

and a known inhibitor of the mammalian target of rapamycin (mTOR). Elevated *DDIT4* expression promotes tumorigenesis and correlates with poorer survival in several cancer types [153–155]. The immediate early response 3 (*IER3*) gene is activated upon cellular stress [156] and was upregulated after BOP-treatment. IER3 is involved in apoptosis and cell cycle arrest and was identified as potential tumor suppressor in cervical carcinoma [157]. Further upregulated was the gene *CYP1A1*, coding for the cytochrome P450 family 1A1 enzyme. CYP1A1 metabolizes xenobiotics, such as polycyclic aromatic hydrocarbons, to epoxides and thereby contributing to the toxicity and carcinogenicity of these xenobiotics [158, 159].

Two members of the solute carrier family 7, *SLC7A5* and *SLC7A11*, were both upregulated upon BOP-treatment. SLC7 are important membrane transporters for amino acid supply, especially required for fast growing tumor cell ensuring steadily supply with nutrients [160]. Especially *SLC7A5* and *SLC7A11* are overexpressed in breast cancer and associated with worse therapy progress [161]. The adenosine A1 receptor (*ADORA1*) is a target of E2-activated ERα and regulates the transcription of ERα, favoring proliferation [80]. In contrast, treatment with BOP reduced the mRNA expression level of *ADORA1*, indicating an altered gene transcription. The carcinoembryonic antigen related cell adhesion molecule 5 (*CEACAM5*) is a cell adhesive protein and expressed in several cancer, such as gastrointestinal and breast cancer [162]. *CEACAM5* is used as a biomarker for prognosis in colorectal cancer [162, 163]. Its overexpression after treatment with the phthalate compound might result in an increased metastatic potential. The kelch like family member 24 (*KLHL24*) gene encodes the substrate receptor for a ubiquitin ligase [164]. Mutations in the *KLHL24* gene are discussed in relation to skin diseases [165]. *KLHL24* was overexpressed in MCF-7 cells after treatment with BOP. Finally, the glycoprotein stanniocalcin 2 (*STC2*) was overexpressed as well. The glycoprotein is involved in the homeostasis of calcium and phosphate [87]. *STC2* was reported to be upregulated in E2-treated MCF-7 cells [166], breast cancer [167] and is associated with proliferation in cancer [88, 168]. Besides genes regulated by *ESR1*, treatment with BOP also induced differential expression of *ESR1*-independent genes, indicating further side effects in the cells.

In summary, treatment with BOP induced differential expression of several *ESR1*-regulated genes. The gene expression pattern is associated with interference in the cell cycle, increased tumorigenesis, proliferation, metastasis and poorer survival in cancer cells.

4.5 Conclusion

In this study we demonstrated that all tested phthalate compounds bound to ERα *in silico* and *in vitro*. BBP, BCP, and BOP all activated the receptor although less strongly compared to the natural ligand E2. BBP and BOP influenced the cell cycle distribution in HEK-ESR1 and MCF-7 cells, respectively. RNA sequencing revealed differen-

tially expression of 15 genes in relation to *ESR1*-regulation: *CYP1A1*, *DDIT4*, *KLHL24*, *SLC7A11*, *CEACAM5*, *STC2*, *SLC7A5*, *IER3*, *FKBP4*, *TFAP2C*, *CDK1*, *CCNA2*, *PGR*, *SFPQ*, and *ADORA1* in MCF-7 cells. The identified gene expression pattern indicated an influence of BOP on the cell cycle, tumorigenesis, proliferation, metastasis and poorer survival in cancer. The results indicated an endocrine effect of BOP on MCF-7 cells mediated by ERα.

4.6 Acknowledgement

This work was supported by the *Deutsche Forschungsgemeinschaft* (GRK 2015/2). The authors gratefully acknowledge the computing time granted on the supercomputer Mogon at Johannes Gutenberg University Mainz (hpc.uni-mainz.de). Cell sorting support by the IMB Flow Cytometry Core Facility is gratefully acknowledged.

4.7 Supplementary material

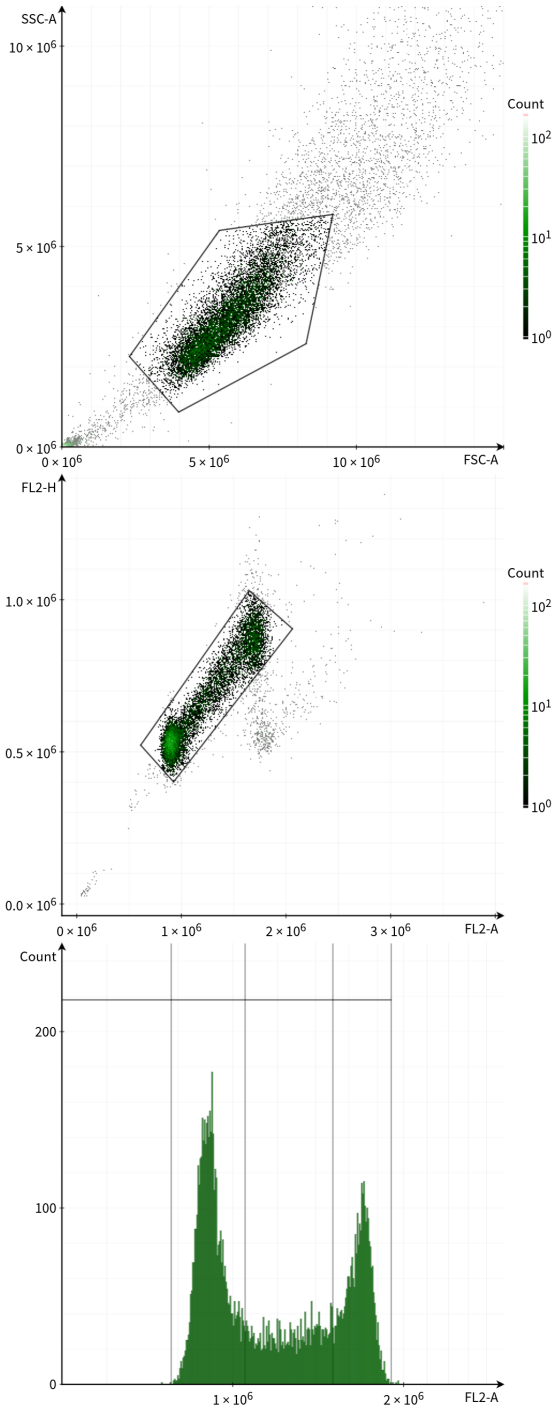

Figure 4.7: Gating in the cell cycle experiments. MCF-7 cells were treated with DMSO for 4 h at 50 µM. (Top) The major cell population was selected. (Middle) Aggregates and doublets were removed. (Bottom) The selected cells were gated into four groups based on their PI content detected by the FL2-A detector.

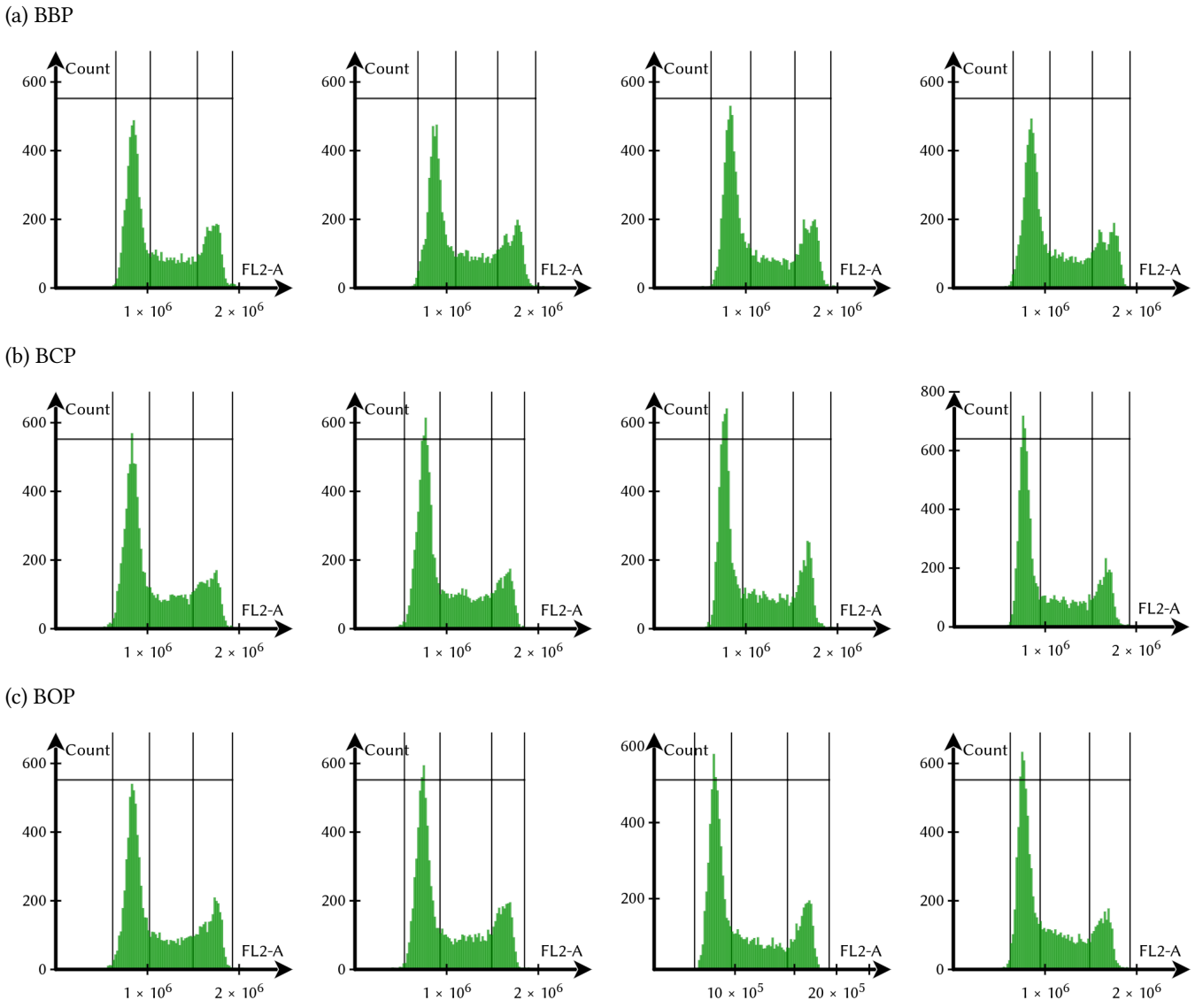

Figure 4.8: Cell Cycle Analysis. HEK-ESR1 cells were treated with (a) BBP, (b) BCP, and (c) BOP. Each analysis was performed under four conditions: 4 h with 25 µM and 50 µM, 8 h with 25 µM and 50 µM (from left to right).

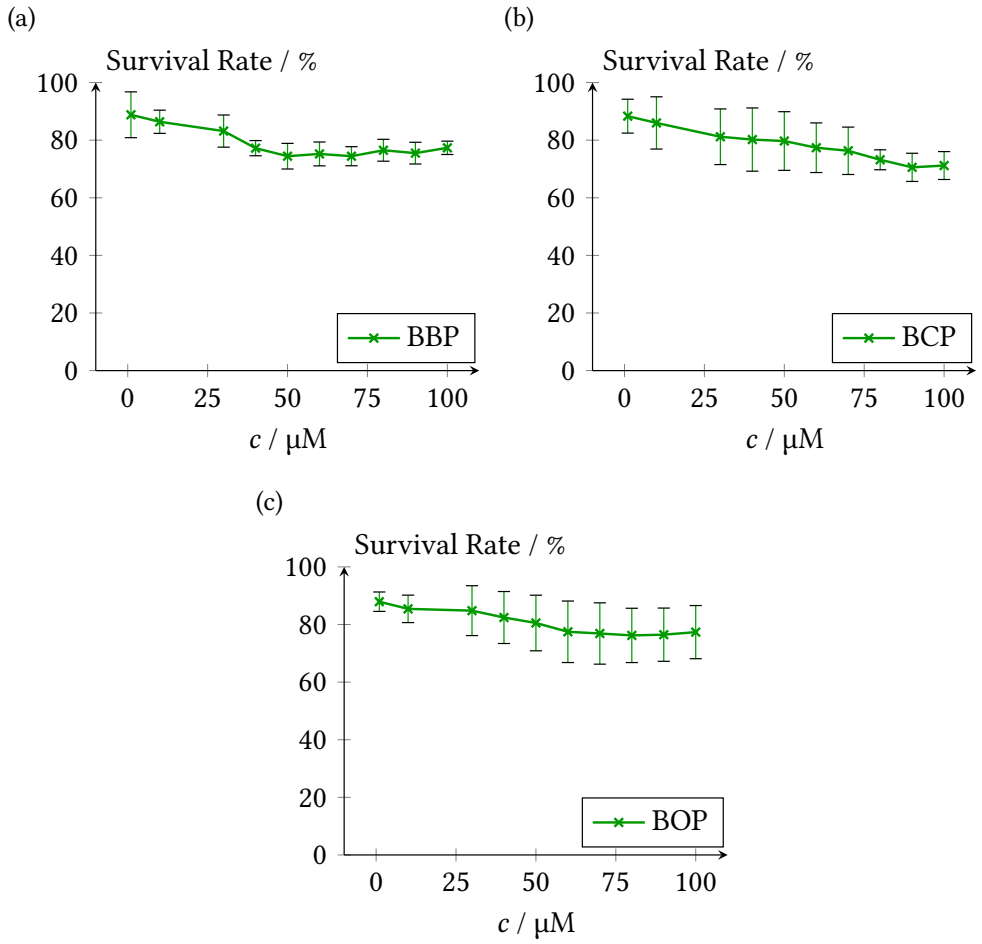

Figure 4.9: Analysis of the cytotoxicity assay. The survival rate was measured for (a) BBP, (b) BCP, and (c) BOP, respectively and represented as mean ± SD.

5 Organophosphate ester tri-*o*-cresyl phosphate interacts with estrogen receptor α in MCF-7 breast cancer cells promoting cancer growth

Chapter 5 is based on the article "Organophosphate ester tri-*o*-cresyl phosphate interacts with estrogen receptor α in MCF-7 breast cancer cells promoting cancer growth" by M. Böckers, N. W. Paul and T. Efferth, which is published in *Toxicology and Applied Pharmacology* [169]. I performed and analyzed the experiments, prepared the figures and wrote the article with contributions from all authors. The RNA sequencing experiment was performed by StarSEQ GmbH, Mainz, Germany. The article is reproduced verbatim. Minor modifications were made for consistency within this thesis, such as combining the abbreviations and the method section from all manuscripts into a single chapter, respectively. Additionally, I moved figure 5.5 from the supplementary material into the main text.

5.1 Abstract

Plastic in the ocean degrades to microplastic, thereby enhancing the leaching of incorporated plasticizers due to the increased particle surface. The uptake of microplastic-derived plasticizers by marine animals and the subsequent entry in the food chain raises concerns for adverse health effects in human beings. Frequently used plasticizers as the organophosphate ester tri-*o*-cresyl phosphate (TOCP) are known to affect the male reproductive system. However, the overall endocrine potential of TOCP and the underlying molecular mechanisms remain elusive as yet. In this study, we investigated the molecular effects of TOCP on estrogen receptor α (ERα)-transfected HEK-ESR1 cells and the human breast cancer cell line MCF-7. Applying virtual screening and molecular docking, we identified TOCP as potent ligand of ERα *in silico*. Microscale thermophoresis confirmed the binding in *vitro* with similar intensity as the natural ligand 17-β-estradiol. To identify the molecular mechanisms of TOCP-mediated effects, we used next-generation sequencing to analyze the gene expression pattern of TOCP-treated MCF-7 cells. RNA sequencing revealed 22 differently ex-

pressed genes associated with *ESR1* as upstream regulator: *CYP1A1*, *SLC7A11*, *RUNX2*, *DDIT4*, *STC2*, *KLHL24*, *CCNG2*, *CEACAM5*, *SLC7A2*, *MAP1B*, *SLC7A5*, *IGF1R*, *CD55*, *FOSL2*, *VEGFA*, and *HSPA13* were upregulated and *PRKCD*, *CCNE1*, *CEBPA*, *SFPQ*, *TNFAIP2*, *KRT19* were downregulated. The affected genes promote tumor growth by increasing angiogenesis and nutritional supply, favor invasion and metastasis, and interfere with the cell cycle. Based on the gene expression pattern, we conclude TOCP to mediate endocrine effects on MCF-7 cells by interacting with ERα.

5.2 Introduction

The consequences of plastic in the ocean are increasingly discussed as a threat to the environment [170–172]. The plastic degrades into smaller particles, so-called microplastic, with a size below 5 mm [173]. As a consequence, the increased surface of the microplastic facilitates leaching of the incorporated plasticizers. The plasticizers enter the food chain through uptake by marine animals [174]. Potential adverse health effects on the human body are currently under investigation and are controversially discussed [16, 126].

Prominent examples of plasticizers are bisphenol compounds, such as BPA, or phthalates [175, 176]. They are widely added during the production of plastic to improve the characteristics of the material [177]. In addition, organophosphate esters, such as tri-cresyl phosphate (TCP), represent another group of frequently used additives [178]. TCP is widely used as plasticizer, flame retardant, lubricant and jet oil additive [179, 180]. Among the three isomers of TCP, tri-*o*-cresyl phosphate (TOCP) is the most toxic compound.

TOCP exerts neurotoxic effects [181–183] and induces organophosphate-induced delayed neuropathy (OPIDN) [184, 185]. TOCP was further reported to cause liver toxicity [186] and reproductive toxicity. Especially the male reproductive system was affected by TOCP with a reduced sperm motility, number, and autophagy of spermatogonial stem cells in rat [187–192]. Little is known about TOCP-induced female reproductive toxicity. Yang et al. (2019) reported toxic effects of TOCP on the placenta in mice [193] and Hu et al. (2019) discovered ovarian failure in mice [194]. The endocrine potential of TOCP and the underlying molecular mechanisms are not yet understood.

Investigations on microplastic and plasticizers revealed an impairment of growth, reproduction, and fertility in sea animals [8, 10, 195]. Therefore, endocrine effects of the microplastic-released compounds are highly likely. Most relevant for reproductive functions is the hormone 17-β-estradiol (E2), mediating growth, differentiation and development by interacting with the nuclear transcription factor estrogen receptor α (ERα/*ESR1*) [52]. ERα is mainly expressed in the breast, ovary, uterus, kidney, and bone [52]. In its inactivated state, the receptor is located in the cytosol. Binding of a ligand

in the ligand binding domain (LBD) triggers dimerization and translocation of the receptor to the nucleus, where it functions as transcription factor [54]. Interference with ERα by xenoestrogens, such as plasticizers, could therefore modulate the receptor effects and disrupt the endocrine system.

In this study, we investigated the effect of the organophosphate TOCP on human ERα *in silico* and *in vitro*. RNA sequencing identified molecular effects of TOCP on the human breast cancer cell line MCF-7, revealing endocrine dysregulation favoring tumorigenesis.

5.3 Results

5.3.1 Molecular Docking

From a chemical library of 1800 substances, we identified TOCP among the top 50 compounds binding to ERα-LBD by virtual screening. Molecular docking of TOCP to the whole ERα-LBD resulted in the same lowest energy position as docking with E2 (Figure 5.1). The lowest binding energy of TOCP was smaller than of E2, indicating a stronger binding to the protein (Table 5.1). Both compounds interacted with the amino acids: Leu346, Glu353, Leu387, Leu391, Arg394, Phe404, Met421, Ile424, Leu428, and Leu525. All 250 runs with E2 resulted in the same cluster, while for TOCP 92% of the runs resulted in the same lowest binding position. This effect was probably caused by the higher torsdof parameter of TOCP, demonstrating more free rotatable bonds, which increased the possible binding positions and therefore resulted in a more diverse outcome. Molecular docking demonstrated binding of TOCP with a higher affinity as E2 to ERα-LBD *in silico*.

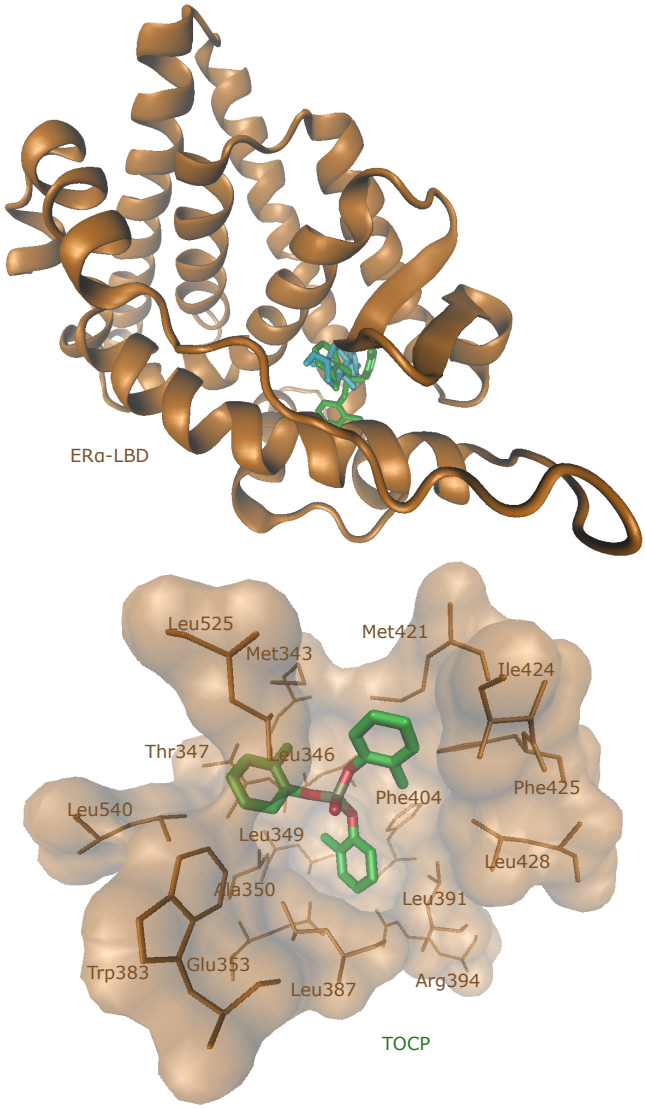

Figure 5.1: Visualization of the molecular docking result. E2 (blue) and TOCP (green) bind to the same binding pocket of ERα-LBD. The lowest binding energy position of TOCP in the ERα-LBD is displayed with the interacting amino acids of ERα-LBD.

Table 5.1: Result of molecular docking. For each ligand, the lowest and mean binding energy and the predicted inhibitory constant $K_{i,pred}$ are given. The torsdof parameter Td indicates the torsional degree of freedom of each ligand. The amino acids of ERα-LBD involved in hydrophobic interactions and hydrogen bonds (H-bonds) are listed.

	lowest binding energy / kcal mol^{-1}	mean binding energy / kcal mol^{-1}	$K_{i,pred}$ / nM	Td	No. of cluster	Runs in 1st cluster	Amino acids involved in hydrophobic interactions	Amino acids involved in H-bonds
E2	−9.48	−9.45	112.95	2	1	250/250	Leu346 Leu387 Met388 Leu391 Phe404 Met421 Ile424 Leu428 Leu525	Glu353 Arg394
TOCP	−10.05	−9.82	42.85	6	3	231/250	Met343 Leu346 Thr347 Leu349 Ala350 Glu353 Trp383 Leu387 Leu391 Arg394 Phe404 Met421 Ile424 Phe425 Leu428 Leu525 Leu540	-

5.3.2 RNA sequencing

RNA sequencing revealed 47 differentially regulated genes associated with a known regulation by ESR1 as upstream regulator after treatment of MCF-7 cells with TOCP (Figure 5.2). Among them, 22 genes were expressed with a fold change of at least 0.5 or -0.5: *CYP1A1*, *SLC7A11*, *RUNX2*, *DDIT4*, *STC2*, *KLHL24*, *CCNG2*, *CEACAM5*, *SLC7A2*, *MAP1B*, *SLC7A5*, *IGF1R*, *CD55*, *FOSL2*, *VEGFA*, and *HSPA13* were upregulated and *PRKCD*, *CCNE1*, *CEBPA*, *SFPQ*, *TNFAIP2*, and *KRT19* were downregulated after TOCP treatment. The corresponding gene expression induced by E2 is listed in Table 5.4. In addition, several genes unrelated to *ESR1* as upstream regulator were differentially expressed (Table 5.2).

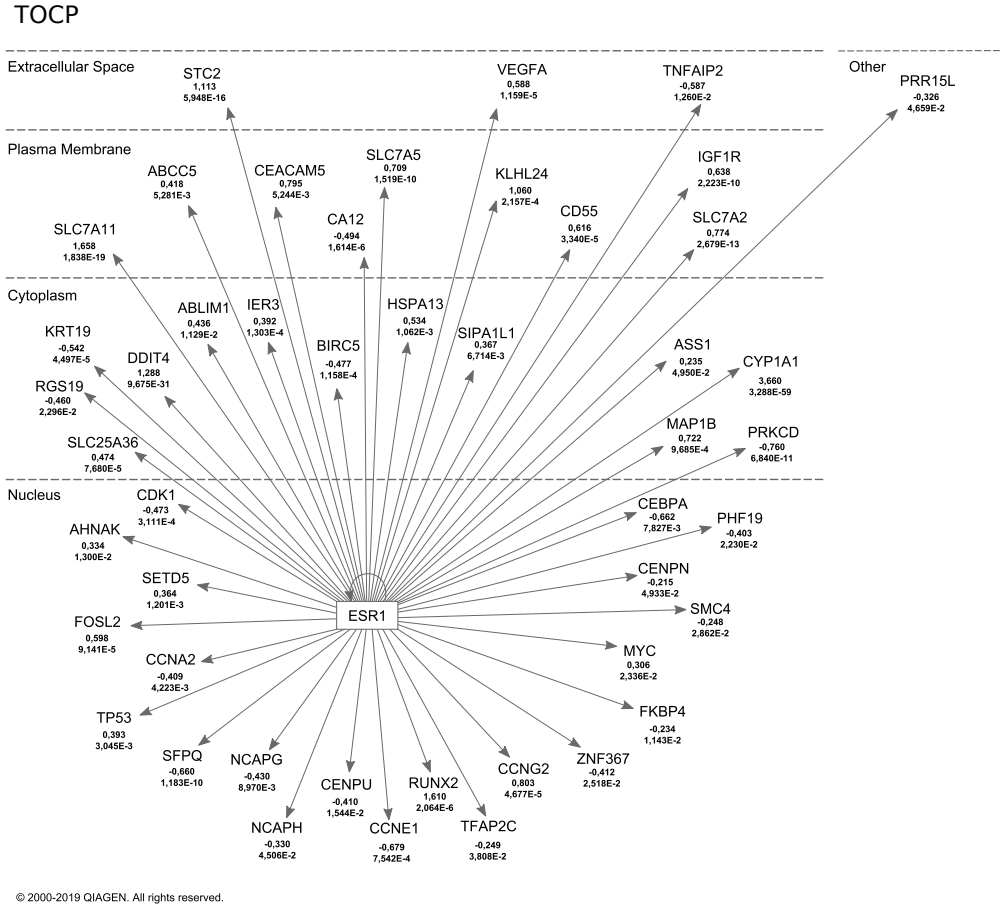

Figure 5.2: Upstream analysis with Ingenuity Pathway Analysis software. Differentially expressed genes induced by TOCP and associated with regulation by *ESR1* are shown. For each gene the fold change and the p-value are given. Figure was modified based on the IPA Path Designer.

Table 5.2: Specific gene expression induced by TOCP. For each gene the fold change $\log_2\left(\frac{E_{\text{TOCP}}}{E_c}\right)$ with corresponding standard error $\Delta \log_2\left(\frac{E_{\text{TOCP}}}{E_c}\right)$ and p-value are listed. ID refers to the name of the gene, E to the expression induced by the respective ligand, and E_c to the expression under control conditions. p-values indicate the comparison with the DMSO-control.

ID	$\log_2\left(\frac{E_{\text{TOCP}}}{E_c}\right)$	$\Delta \log_2\left(\frac{E_{\text{TOCP}}}{E_c}\right)$	p	Entrez Gene Name
MAGED4	7.784	1.591	$9.87 \cdot 10^{-7}$	MAGE family member D4B
INO80B-WBP1	5.374	2.146	$1.23 \cdot 10^{-2}$	INO80B-WBP1 readthrough (NMD candidate)
LOC101928673	5.099	2.219	$2.16 \cdot 10^{-2}$	uncharacterized LOC101928673
TBC1D3K	3.473	1.337	$9.38 \cdot 10^{-3}$	TBC1 domain family member 3F
BEST1	3.038	1.040	$3.48 \cdot 10^{-3}$	bestrophin 1
CACNB2	2.950	1.034	$4.32 \cdot 10^{-3}$	calcium voltage-gated channel auxiliary subunit beta 2
SCN4A	2.918	1.224	$1.71 \cdot 10^{-2}$	sodium voltage-gated channel alpha subunit 4
LOC401261	2.671	1.282	$3.72 \cdot 10^{-2}$	uncharacterized LOC401261
LOC107986167	2.551	1.208	$3.46 \cdot 10^{-2}$	uncharacterized LOC107986167
LOC102723985	2.547	1.294	$4.90 \cdot 10^{-2}$	uncharacterized LOC102723985
ANKRD31	2.230	0.931	$1.66 \cdot 10^{-2}$	ankyrin repeat domain 31
MMP19	1.988	0.934	$3.32 \cdot 10^{-2}$	matrix metallopeptidase 19
LEKR1	1.967	0.871	$2.39 \cdot 10^{-2}$	leucine, glutamate and lysine rich 1
LOC107987398	1.927	0.935	$3.94 \cdot 10^{-2}$	putative uncharacterized protein FLJ44672
DDIT3	1.802	0.284	$2.20 \cdot 10^{-10}$	DNA damage inducible transcript 3
ZFP2	1.760	0.897	$4.98 \cdot 10^{-2}$	ZFP2 zinc finger protein
SLC43A1	1.751	0.527	$8.98 \cdot 10^{-4}$	solute carrier family 43 member 1
NCR3LG1	1.710	0.744	$2.15 \cdot 10^{-2}$	natural killer cell cytotoxicity receptor 3 ligand 1
RNF150	1.705	0.680	$1.22 \cdot 10^{-2}$	ring finger protein 150
RASD1	1.682	0.632	$7.84 \cdot 10^{-3}$	ras related dexamethasone induced 1
LOC105376781	1.656	0.419	$7.85 \cdot 10^{-5}$	uncharacterized LOC105376781
IRAK1BP1	1.627	0.807	$4.38 \cdot 10^{-2}$	interleukin 1 receptor associated kinase 1 binding protein 1
FAM157B	1.600	0.661	$1.55 \cdot 10^{-2}$	family with sequence similarity 157 member A
FSCN2	1.552	0.790	$4.93 \cdot 10^{-2}$	fascin actin-bundling protein 2, retinal
WDR97	1.548	0.599	$9.69 \cdot 10^{-3}$	WD repeat domain 97
MALAT1	1.520	0.308	$7.95 \cdot 10^{-7}$	metastasis associated lung adenocarcinoma transcript 1
LOC105378936	1.511	0.408	$2.13 \cdot 10^{-4}$	uncharacterized LOC105378936
LOC105379407	−1.538	0.538	$4.27 \cdot 10^{-3}$	chondroitin sulfate proteoglycan 4 pseudogene 3 Y-linked
WNT4	−1.557	0.777	$4.50 \cdot 10^{-2}$	Wnt family member 4
MAFA	−1.575	0.469	$7.74 \cdot 10^{-4}$	MAF bZIP transcription factor A
TMEM238	−1.698	0.419	$5.03 \cdot 10^{-5}$	transmembrane protein 238
LOC107986035	−2.278	0.762	$2.81 \cdot 10^{-3}$	basic proline-rich protein-like
CHST1	−2.365	1.132	$3.66 \cdot 10^{-2}$	carbohydrate sulfotransferase 1
LMO1	−2.612	1.069	$1.46 \cdot 10^{-2}$	LIM domain only 1
KDR	−2.754	1.031	$7.59 \cdot 10^{-3}$	kinase insert domain receptor
AKR1D1	−4.928	2.472	$4.62 \cdot 10^{-2}$	aldo-keto reductase family 1 member D1
PHOSPHO2-KLHL23	−6.844	1.778	$1.18 \cdot 10^{-4}$	kelch like family member 23
SPANXA1	−7.434	1.672	$8.72 \cdot 10^{-6}$	SPANX family member C

5.3.3 RT-qPCR

The expression of 6 differentially expressed genes was confirmed by RT-qPCR. Fold changes of the RT-qPCR experiment were plotted against the fold changes measured by RNA sequencing (Figure 5.3). The observed expression trends of both experiments matched each other with an R value of 0.91. The fold change values can be taken from table 5.5.

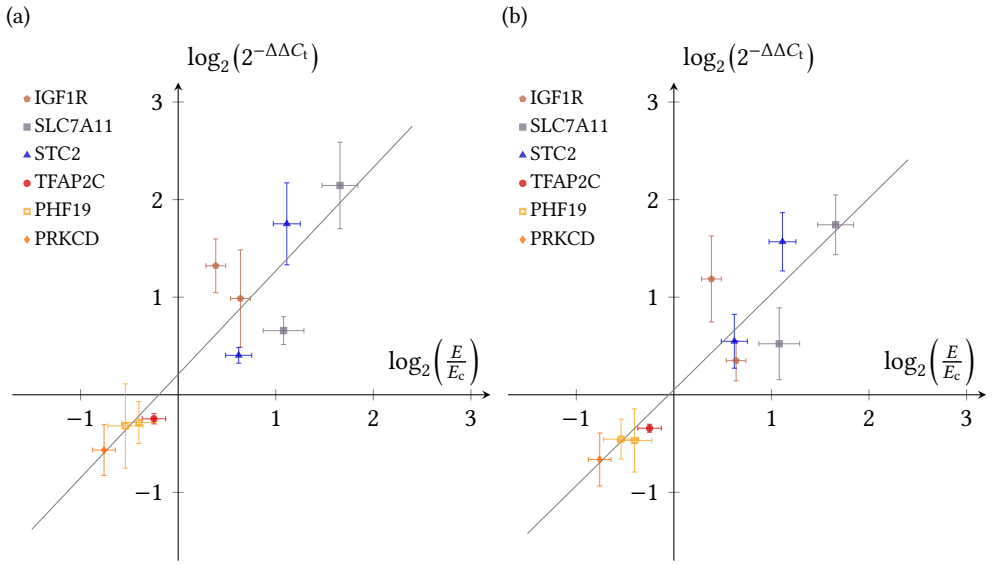

Figure 5.3: Correlation of gene expression levels obtained by NGS and RT-qPCR. The fold change based on the RT-qPCR results was plotted against the fold change based on the NGS results for the ligands E2 and TOCP (dots). The was calculated with (a) *GAPDH* and (b) *HSP90AB1* as reference gene, respectively. A linear regression was calculated with Origin 7.5. The fit is shown in grey with (a) slope of 1.06, intercept of 0.21, R value of 0.91 and (b) slope of 0.98, intercept of 0.05, R value of 0.91.

5.3.4 Microscale Thermophoresis

Microscale thermophoresis experiments resulted in a concentration-dependent fluorescence for both ligands (Figure 5.4). Therefore, E2 and TOCP bound to ERα *in vitro*. The calculated dissociation constants of the natural ligand E2 and TOCP were similar to each other (Table 5.3).

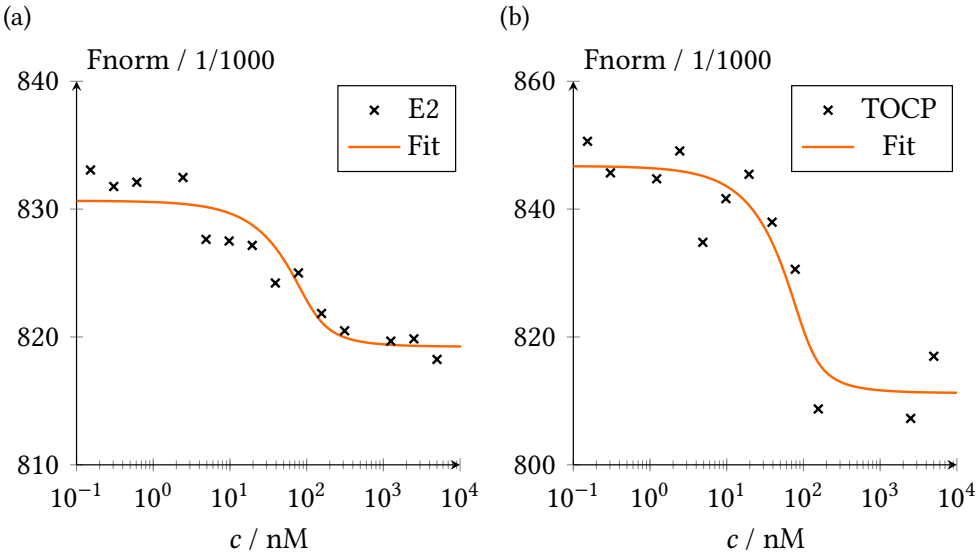

Figure 5.4: Analysis of the MST-experiments. The MST was performed with 95% LED and 20% MST power. Fluorescently labeled ERα was used as target with (a) E2, and (b) TOCP as ligand, respectively. A fit was performed according to the law of mass action (orange).

Table 5.3: Molecular structure of the analyzed ligands and comparison of the inhibitory constant predicted *in silico* ($K_{i,pred}$) with the dissociation constant calculated by MST *in vitro* (K_d).

Structure	Name	$K_{i,pred}$ / nM	K_d / nM
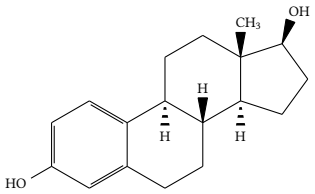	17-β-Estradiol E2 CAS 50-28-2	112.98	14.9 ± 2.1
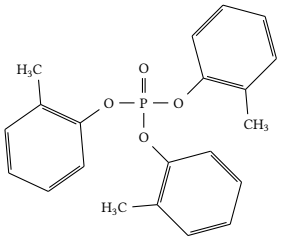	Tri-*o*-cresyl phosphate TOCP CAS 78-30-8	42.85	10.7 ± 1.6

5.3.5 Cytotoxicity

The cytotoxic effect of TOCP was investigated on HEK-ESR1 cells (Figure 5.8). The IC_{50} of TOCP (47.9 µM ± 2.1 µM) was measured smaller but of the same order of magnitude as E2 (68 µM ± 11 µM). For further experiments the half IC_{50} was used.

5.3.6 ER transcription factor activation

ER transcription factor activation assay was performed with E2 and TOCP in ERα-overexpressing HEK293 cells. Despite previous similar binding capabilities of E2 and TOCP *in silico* and *in vitro*, E2 activated the receptor 10 times stronger than TOCP after 4 h incubation time. After 8 h, the activation increased further for E2, while a negative effect was measured for TOCP (Figure 5.5).

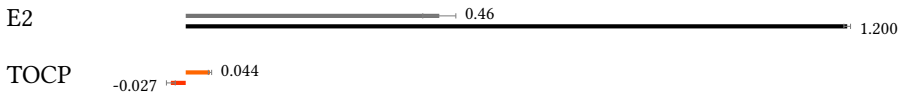

Figure 5.5: ER transcription factor assay. Activation of ERα was measured after 4 h and 8 h incubation time of HEK-ESR1 cells with 25 µM of the respective ligand. The difference optical density measured after 4 h is shown in the upper line and after 8 h in the lower line.

5.3.7 Cell cycle

The effect of TOCP on the cell cycle was measured with PI staining. In HEK-ESR1 and MCF-7 cells (Figure 5.7) a trend towards G2/M phase was detected. The effect was stronger on the HEK-ESR1 cell line (Table 5.6). TOCP induced proliferative effects on HEK-ESR1 and MCF-7 cells.

5.4 Discussion

In this study, we investigated the molecular effect of the organophosphate ester TOCP on human MCF-7 breast cancer cells and ERα-transfected HEK-ESR1 cells. Molecular docking demonstrated binding of TOCP to ERα-LBD with a higher affinity compared to the natural ligand E2. The amino acids involved in the binding matched those described in the literature [56, 60]. Therefore, the binding of TOCP to ERα-LBD was confirmed *in silico*. Wang et al. (2020) also found TOCP to be highly likely to bind to ERα [196].

5.4.1 Gene expression by TOCP

NGS revealed several differentially expressed genes induced by TOCP, associated with upstream regulation of ESR1. Some of those genes were only found differentially expressed after treatment with TOCP, but not with E2. Reasons are probably the altered three-dimensional structure of the ligand-bound ERα protein. The molecular structure of TOCP is less planar than E2, indicating different effects for the overall 3D-structure.

Among the upregulated genes was the runt-related transcription factor 2 (*RUNX2*). RUNX2 regulates the expression of bone matrix proteins [197] and was associated with breast cancer metastases in the bone [66]. Another transcription factor gene, *FOSL2*, was also expressed in increased amounts. FOSL2 is a subunit of the AP-1 transcription factor and increases invasion and migration in breast cancer cells, contributing to an aggressive phenotype [198]. The transcription factor CAAT enhancer binding protein α (*CEBPA*) was downregulated. CEBPA is associated with reduced cell growth and acts as tumor suppressor, especially in the differentiation of granulocytes [199, 200]. Two cyclins were differentially expressed after treatment with TOCP. Cyclin G2 (*CCNG2*) was upregulated, although E2-activated ERα is known to downregulate its expression [201]. Upregulation of cyclin G2 induced cell cycle arrest in breast cancer cells, indicating growth inhibition [202]. In contrast, cyclin E1 (*CCNE1*) was downregulated. Cyclin E1 plays a role in cell cycle progression and overexpression was associated with poorer survival and carcinogenesis in breast cancer and endometrial adenocarcinoma [203–205]. The splicing factor proline and glutamine rich (*SFPQ*) was downregulated in MCF-7 cells. In mice, SFPQ was identified as tumor suppressor by inhibiting tumorigenesis [148]. Reduced *SFPQ* levels were further associated with a shorter survival time in colorectal cancer patients [147].

The cytochrome P450 member gene *CYP1A1* was upregulated. CYP1A1 is known as phase I enzyme, metabolizing xenobiotics, such as polycyclic aromatic hydrocarbons, and thereby increasing their carcinogenicity [158, 159]. The DNA damage inducible transcript 4 (*DDIT4*) was upregulated as well. Upregulation of DDIT4 was correlated with worth outcome in solid tumors and acute myeloid leukemia [153, 155]. It further increased proliferation and tumorigenesis in gastric cancer cells and tissues [154]. The microtubule associated protein 1B (*MAP1B*) was upregulated. MAP1B is mainly required for axonal growth [206]. Two genes related to cytoplasmatic activity were downregulated: *KRT19* and *PRKCD*. Keratin 19 (*KRT19*) was elevated expressed in breast cancers and increased cell proliferation and invasion after knockdown [207]. Protein kinase C delta (*PRKCD*) is relevant for the transfer of activated ERα to the nucleus [76]. Its role in tumor development was controversially discussed [208, 209].

In addition, several genes coding for proteins located at the plasma membrane were differentially expressed after treatment with TOCP. The expression of three members of the solute carrier family were elevated: *SLC7A11*, *SLC7A2*, and *SLC7A5*. All

members are relevant for the nutritional supply of cells by transporting amino acids [79]. Increased expression of SLC members may promote tumor growth [78]. The expression of *CEACAM5*, coding for a cell adhesive protein, was increased. Same was observed in gastric cancer cells [162].The upregulated insulin like growth factor 1 (*IGF1R*) indicates increased proliferation and tumorigenic effects [85]. Crosstalk between the ERα and IGF pathway is well-known, confirming the estrogenic effect of TOCP [83]. *CD55* was overexpressed, as was reported for several cancer types [210]. The expression of *CD55* in the breast is still controversially discussed [210, 211].

Stanniocalcin 2 (*STC2*) is an estrogen-responsive gene that encodes a secreted glycoprotein, whose upregulation was associated with tumor dormancy in breast cancer [166, 212]. Overexpression of *STC2* was associated with increased cell proliferation in cervical cancer and promoted migration and invasion in ovarian cancer [88, 213]. The vascular endothelial growth factor A (*VEGFA*) is most relevant to promote angiogenesis in growing tumors [214]. *VEGFA* was upregulated after TOCP-treatment, favoring cancer progression. The expression of *ESR1*-unrelated genes demonstrates further side effects of TOCP in MCF-7 breast cancer cells.

In summary, the gene expression profile induced by TOCP is associated with increased tumor growth enhanced by promoting angiogenesis and nutritional supply. Further gene expression indicates enhanced invasive and metastatic potential of the breast cancer cells and an influence on the cell cycle. The observed gene expression profile supports an endocrine function of TOCP by interaction with ERα.

5.4.2 Verification of ERα binding, and proliferative effects

Molecular docking demonstrated binding of TOCP to ERα-LBD *in silico*. An interaction between TOCP and the estrogen receptor was further confirmed by the observed gene expression pattern in MCF-7 cells. We therefore investigated the binding *in vitro*, by applying MST, which confirmed the binding of TOCP to ERα *in vitro*. Although the ER transcription factor assay did not show a similar activation of TOCP compared to E2, flow cytometry showed a proliferative trend in HEK-ESR1 and MCF-7 cells. Further research is required to understand the influence of TOCP on the cell cycle.

5.5 Conclusion

In this study, we observed the binding of TOCP to ERα *in silico* and *in vitro* with similar intensity as E2. In addition, we demonstrated the differential expression of 47 genes associated with *ESR1*-regulation in MCF-7 cells compared to untreated cells. *CYP1A1*, *SLC7A11*, *RUNX2*, *DDIT4*, *STC2*, *KLHL24*, *CCNG2*, *CEACAM5*, *SLC7A2*, *MAP1B*, *SLC7A5*, *IGF1R*, *CD55*, *FOSL2*, *VEGFA*, and *HSPA13* were upregulated and *PRKCD*, *CCNE1*, *CEBPA*, *SFPQ*, *TNFAIP2*, and *KRT19* were downregulated after TOCP treatment with a fold

change of at least 0.5 or -0.5, respectively. The gene expression pattern is likely to promote tumor growth by upregulating angiogenesis and nutritional supply, further increases invasion and metastasis, and indicates disruptions in the cell cycle. Our results show an endocrine effect of TOCP on HEK-ESR1 and MCF-7 cells mediated by ERα.

5.6 Acknowledgement

This work was supported by the *Deutsche Forschungsgemeinschaft* (GRK 2015/2). The authors gratefully acknowledge the computing time granted on the supercomputer Mogon at Johannes Gutenberg University Mainz (hpc.uni-mainz.de). Cell sorting support by the IMB Flow Cytometry Core Facility is gratefully acknowledged.

5.7 Supplementary material

Table 5.4: Differentially expressed genes induced by E2 and TOCP associated with ESR1 regulation. For each gene the fold change $\log_2\left(\frac{E}{E_c}\right)$ with corresponding standard error $\Delta\log_2\left(\frac{E}{E_c}\right)$ and p-value are listed. ID refers to the name of the gene, E to the expression induced by the respective ligand, and E_c to the expression under control conditions.

Table 5.4: Comparative presentation of differentially expressed genes in relation to ESR1

ID	$\log_2\left(\frac{E_{E2}}{E_c}\right)$	$\Delta\log_2\left(\frac{E_{E2}}{E_c}\right)$	p_{E2}	$\log_2\left(\frac{E_{TOCP}}{E_c}\right)$	$\Delta\log_2\left(\frac{E_{TOCP}}{E_c}\right)$	p_{TOCP}
ABCC5				0.418	0.150	$5.28 \cdot 10^{-3}$
ABHD2	0.881	0.126	$2.61 \cdot 10^{-12}$			
ABLIM1				0.436	0.172	$1.13 \cdot 10^{-2}$
ACKR3	−1.122	0.412	$6.42 \cdot 10^{-3}$			
AHNAK	0.313	0.138	$2.32 \cdot 10^{-2}$	0.334	0.134	$1.30 \cdot 10^{-2}$
ASS1				0.235	0.120	$4.95 \cdot 10^{-2}$
BCAS3	−0.260	0.094	$6.01 \cdot 10^{-3}$			
BIRC5				−0.477	0.124	$1.16 \cdot 10^{-4}$
CA12				−0.494	0.103	$1.61 \cdot 10^{-6}$
CCNA2				−0.409	0.143	$4.22 \cdot 10^{-3}$
CCND1	0.223	0.113	$4.88 \cdot 10^{-2}$			
CCNE1				−0.679	0.202	$7.54 \cdot 10^{-4}$
CCNG2	−0.495	0.242	$4.03 \cdot 10^{-2}$	0.803	0.197	$4.68 \cdot 10^{-5}$
CD55				0.616	0.148	$3.34 \cdot 10^{-5}$
CDK1				−0.473	0.131	$3.11 \cdot 10^{-4}$
CEACAM5				0.795	0.285	$5.24 \cdot 10^{-3}$
CEBPA				−0.662	0.249	$7.83 \cdot 10^{-3}$
CELSR2	0.541	0.100	$5.82 \cdot 10^{-8}$			
CENPN				−0.215	0.110	$4.93 \cdot 10^{-2}$
CENPU				−0.410	0.169	$1.54 \cdot 10^{-2}$
CYP1A1				3.660	0.226	$3.29 \cdot 10^{-59}$
DDIT4	0.369	0.135	$6.32 \cdot 10^{-3}$	1.288	0.112	$9.67 \cdot 10^{-31}$
DDX21	0.338	0.105	$1.25 \cdot 10^{-3}$			
EDN1	1.206	0.419	$3.97 \cdot 10^{-3}$			
EFNA1	−0.442	0.170	$9.24 \cdot 10^{-3}$			
ESR1	−0.164	0.151	0.28			
FAM102A	0.505	0.097	$1.89 \cdot 10^{-7}$			
FKBP4				−0.234	0.092	$1.14 \cdot 10^{-2}$
FMN1	0.588	0.197	$2.78 \cdot 10^{-3}$			
FOSL2	0.459	0.157	$3.37 \cdot 10^{-3}$	0.598	0.153	$9.14 \cdot 10^{-5}$
GATA3	−0.304	0.118	$1.01 \cdot 10^{-2}$			
GREB1	0.681	0.345	$4.85 \cdot 10^{-2}$			
HSPA13	0.753	0.173	$1.32 \cdot 10^{-5}$	0.534	0.163	$1.06 \cdot 10^{-3}$
IER3	0.236	0.105	$2.50 \cdot 10^{-2}$	0.392	0.102	$1.30 \cdot 10^{-4}$
IGF1R	0.385	0.101	$1.40 \cdot 10^{-4}$	0.638	0.101	$2.22 \cdot 10^{-10}$
JUN	0.395	0.197	$4.43 \cdot 10^{-2}$			
KDM4B	0.558	0.184	$2.45 \cdot 10^{-3}$			
KLHL24				1.060	0.286	$2.16 \cdot 10^{-4}$
KRT19				−0.542	0.133	$4.50 \cdot 10^{-5}$
LDLR	0.438	0.125	$4.81 \cdot 10^{-4}$			
MAP1B				0.722	0.219	$9.69 \cdot 10^{-4}$
MYC				0.306	0.135	$2.34 \cdot 10^{-2}$
NCAPG				−0.430	0.164	$8.97 \cdot 10^{-3}$
NCAPH				−0.330	0.165	$4.51 \cdot 10^{-2}$

Table 5.4: Comparative presentation of differentially expressed genes in relation to ESR1

ID	$\log_2\left(\frac{E_{E2}}{E_c}\right)$	$\Delta\log_2\left(\frac{E_{E2}}{E_c}\right)$	p_{E2}	$\log_2\left(\frac{E_{TOCP}}{E_c}\right)$	$\Delta\log_2\left(\frac{E_{TOCP}}{E_c}\right)$	p_{TOCP}
PES1	0.239	0.110	$2.94 \cdot 10^{-2}$			
PHF19	−0.541	0.179	$2.45 \cdot 10^{-3}$	−0.403	0.176	$2.23 \cdot 10^{-2}$
PRKCD				−0.760	0.116	$6.84 \cdot 10^{-11}$
PRR15L				−0.326	0.164	$4.66 \cdot 10^{-2}$
PVR	0.479	0.183	$8.66 \cdot 10^{-3}$			
RARA	0.303	0.127	$1.69 \cdot 10^{-2}$			
RGS19				−0.460	0.202	$2.30 \cdot 10^{-2}$
RUNX2	0.749	0.365	$4.02 \cdot 10^{-2}$	1.610	0.339	$2.06 \cdot 10^{-6}$
SEMA3B	0.695	0.161	$1.62 \cdot 10^{-5}$			
SETD5				0.364	0.112	$1.20 \cdot 10^{-3}$
SFPQ				−0.660	0.103	$1.18 \cdot 10^{-10}$
SIAH2	0.324	0.128	$1.14 \cdot 10^{-2}$			
SIPA1L1				0.367	0.135	$6.71 \cdot 10^{-3}$
SLC25A36				0.474	0.120	$7.68 \cdot 10^{-5}$
SLC7A11	1.080	0.209	$2.43 \cdot 10^{-7}$	1.658	0.184	$1.84 \cdot 10^{-19}$
SLC7A2	0.426	0.111	$1.18 \cdot 10^{-4}$	0.774	0.106	$2.68 \cdot 10^{-13}$
SLC7A5	0.537	0.111	$1.41 \cdot 10^{-6}$	0.709	0.111	$1.52 \cdot 10^{-10}$
SMC4				−0.248	0.113	$2.86 \cdot 10^{-2}$
SNAI2	2.260	1.139	$4.73 \cdot 10^{-2}$			
STC2	0.620	0.134	$3.41 \cdot 10^{-6}$	1.113	0.138	$5.95 \cdot 10^{-16}$
TFAP2C				−0.249	0.120	$3.81 \cdot 10^{-2}$
TNFAIP2				−0.587	0.235	$1.26 \cdot 10^{-2}$
TP53				0.393	0.133	$3.04 \cdot 10^{-3}$
TSPAN9	−0.622	0.211	$3.17 \cdot 10^{-3}$			
VAV3	−0.880	0.257	$6.24 \cdot 10^{-4}$			
VEGFA				0.588	0.134	$1.16 \cdot 10^{-5}$
XBP1	0.227	0.089	$1.09 \cdot 10^{-2}$			
ZNF367				−0.412	0.184	$2.52 \cdot 10^{-2}$
ZNF703	0.284	0.135	$3.53 \cdot 10^{-2}$			

Table 5.5: Comparison of the log2 fold changes from the RT-qPCR and RNA sequencing experiments including standard error. For the RT-qPCR experiment, the values for *GAPDH* and *HSP90AB1* as reference gene are given separately.

		RT-qPCR *GAPDH*		RT-qPCR *HSP90AB1*		RNA seq	
Gene	Ligand	$\log_2\left(2^{-\Delta\Delta C_t}\right)$	$\Delta\log_2\left(2^{-\Delta\Delta C_t}\right)$	$\log_2\left(2^{-\Delta\Delta C_t}\right)$	$\Delta\log_2\left(2^{-\Delta\Delta C_t}\right)$	$\log_2\left(\frac{E}{E_c}\right)$	$\Delta\log_2\left(\frac{E}{E_c}\right)$
IGF1R	E2	1.322	± 0.275	1.187	± 0.441	0.385	± 0.101
	TOCP	0.987	± 0.498	0.350	± 0.207	0.638	± 0.101
PHF19	E2	−0.320	± 0.432	−0.455	± 0.204	−0.541	± 0.179
	TOCP	−0.284	± 0.214	−0.468	± 0.324	−0.403	± 0.176
PRKCD	E2	-	-	-	-	-	-
	TOCP	−0.567	± 0.260	−0.663	± 0.271	−0.760	± 0.116
SLC7A11	E2	0.658	± 0.143	0.523	± 0.368	1.080	± 0.209
	TOCP	2.145	± 0.443	1.742	± 0.306	1.658	± 0.184
STC2	E2	0.404	± 0.080	0.548	± 0.276	0.620	± 0.134
	TOCP	1.752	± 0.420	1.568	± 0.299	1.113	± 0.138
TFAP2C	E2	-	-	-	-	-	-
	TOCP	−0.246	± 0.052	−0.343	± 0.041	−0.249	± 0.120

Table 5.6: Cell cycle analysis. HEK-ESR1 and MCF-7 cells were treated with 25 µM or 50 µM of TOCP and incubated for 4 h or 8 h, respectively. DMSO was used as control.

		HEK-ESR1		MCF-7	
Treatment	Phase	DMSO	TOCP	DMSO	TOCP
	sub G1 / %	0.6	0.8	0.1	0.3
4 h	G1/G0 / %	54.4	50.1	47.6	42.7
25 µM	S / %	26.0	25.1	23.6	28.8
	G2/M / %	18.5	24.0	28.5	27.8
	sub G1 / %	0.8	0.6	0.1	0.0
4 h	G1/G0 / %	57.3	49.1	46.2	43.9
50 µM	S / %	21.6	28.0	24.2	27.3
	G2/M / %	19.9	22.0	29.4	28.7
	sub G1 / %	0.2	0.3	0.1	0.0
8 h	G1/G0 / %	50.7	50.9	50.0	47.9
25 µM	S / %	26.1	23.3	22.7	22.3
	G2/M / %	22.1	24.9	27.2	29.7
	sub G1 / %	0.1	0.5	0.0	0.0
8 h	G1/G0 / %	54.1	47.1	45.3	45.6
50 µM	S / %	24.7	28.9	24.1	23.2
	G2/M / %	20.8	22.4	30.5	31.0

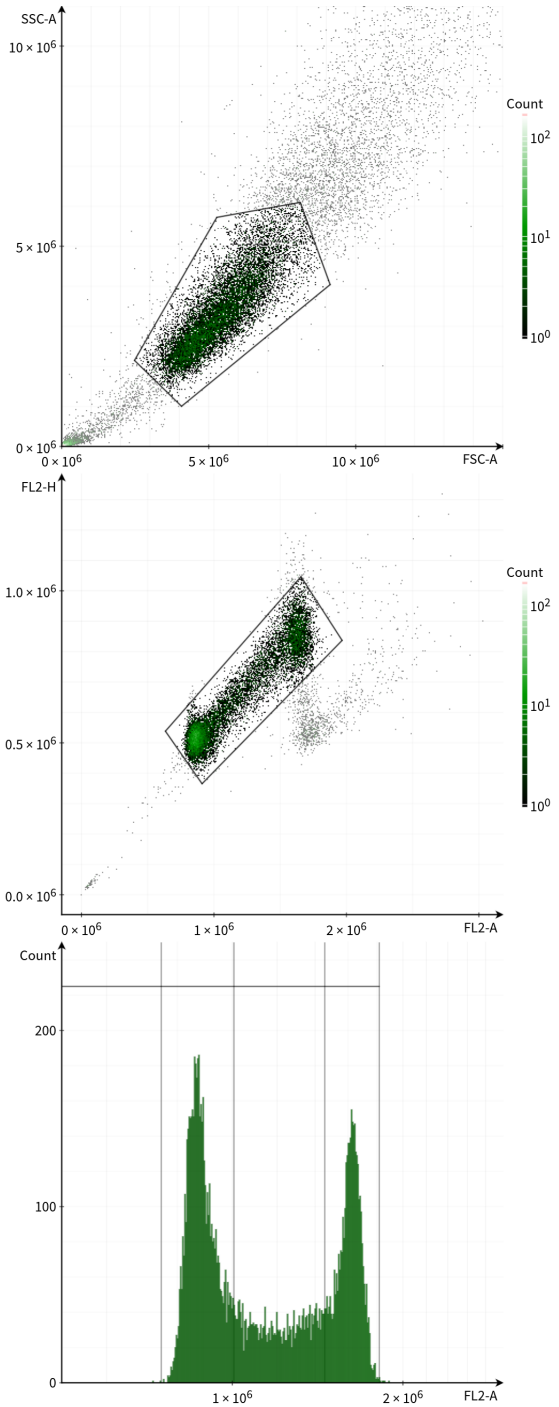

Figure 5.6: Gating in the cell cycle experiments. MCF-7 cells were treated with DMSO for 8 h at 50 µM. (Top) The major cell population was selected. (Middle) Aggregates and doublets were removed. (Bottom) The selected cells were gated into four groups based on their PI content detected by the FL2-A detector.

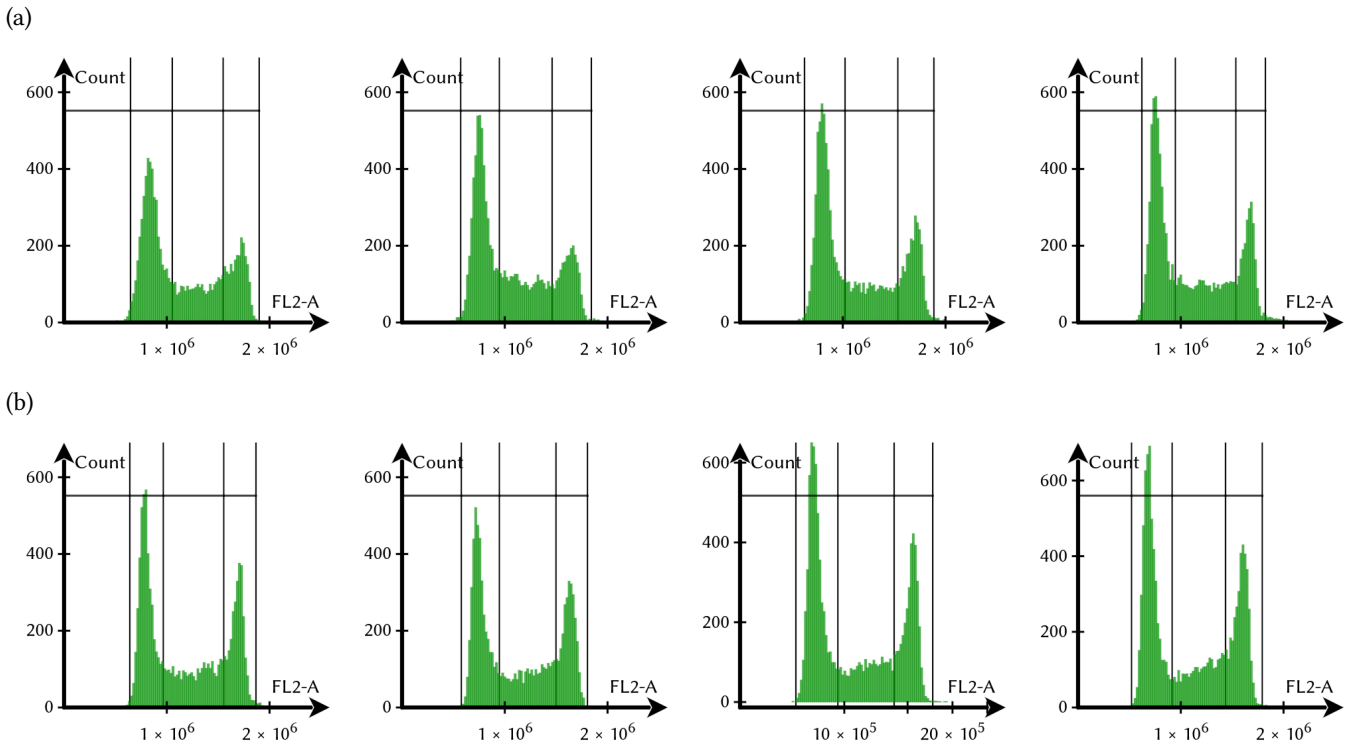

Figure 5.7: Cell cycle analysis. (a) HEK-ESR1 and (b) MCF-7 cells were treated with TOCP. Each analysis was performed under four conditions: 4 h with 25 µM and 50 µM, 8 h with 25 µM and 50 µM (from left to right).

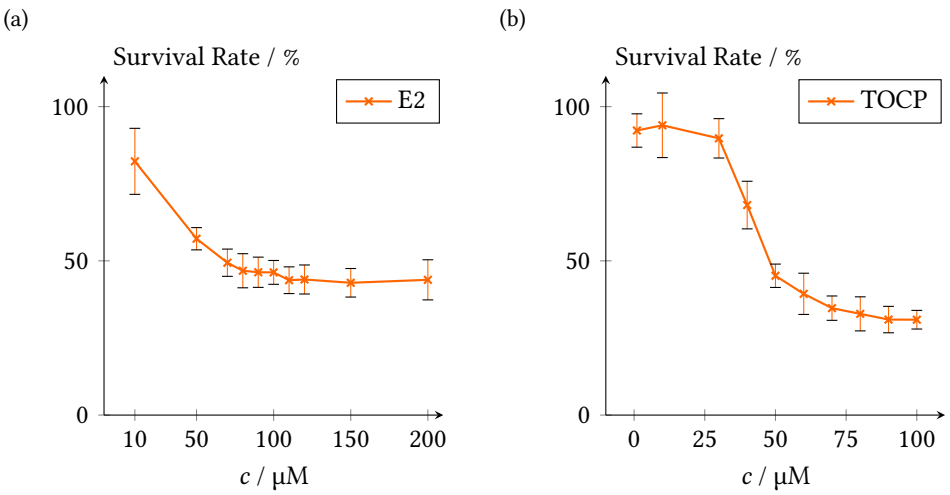

Figure 5.8: Resazurin-Assay. HEK293-ESR1 cells were incubated with different concentrations of (a) E2 and (b) TOCP for 72 h. Metabolisation of resazurin to resorufin was measured colorimetric. Each experiment was repeated three times.

6 Indeno[1,2,3-*cd*]pyrene and picene mediate actions *via* estrogen receptor α signaling pathway in *in vitro* cell systems, altering gene expression

Chapter 6 is based on the article "Indeno[1,2,3-*cd*]pyrene and picene mediate actions *via* estrogen receptor α signaling pathway in *in vitro* cell systems, altering gene expression" by M. Böckers, N. W. Paul and T. Efferth, which is published in *Toxicology and Applied Pharmacology* [215]. I performed and analyzed the experiments, prepared the figures and wrote the article with contributions from all authors. The RNA sequencing experiment was performed by StarSEQ GmbH, Mainz, Germany. The article is reproduced verbatim. Minor modifications were made for consistency within this thesis, such as combining the abbreviations and the method section from all manuscripts into a single chapter, respectively.

6.1 Abstract

Currently, the environmental impact of ubiquitous plastic debris triggered quite some public attention. However, the global impact of microplastic on human health is by and large either unknown or neglected. By looking at the underlying biochemical mechanisms leading to the global health threat microplastic was discovered to carry persistent organic pollutants, such as polycyclic aromatic hydrocarbons (PAH), to marine life. The effect of microplastic-ingestion in the human body remains unfortunately somewhat elusive as of yet. For this reason, we screened for compounds binding to the human estrogen receptor α (ERα) and identified the PAH compounds indeno[1,2,3-*cd*]pyrene (Indpy) and picene (Pice) with a high binding affinity. We applied next-generation sequencing to analyze the differentially expressed genes in MCF-7 cells after treatment with Indpy and Pice. We found 8 upregulated genes: *ABCC5*, *CCNG2*, *CYP1A1*, *DDIT4*, *IER3*, *RUNX2*, *STC2*, and *SLC7A5* and 14 downregulated genes: *ADORA1*, *CEBPB*, *CELSR2*, *CTSD*, *CXCL12*, *KRT19*, *PGR*, *PKIB*, *RARA*, *RET*, *SEMA3B*, *SIAH2*, *TFAP2C*, and *XBP1* induced by both ligands and associated with *ESR1*-regulation. The altered gene expression may influence cell proliferation and metas-

tasis, favoring cancer development with a poor response to therapy. In addition, we confirmed the binding of Indpy and Pice to ERα using molecular docking and microscale thermophoresis. ERα activation was measured with *ESR1*-overexpressing HEK293 (HEK-ESR1) cells and confirmed for Indpy. In conclusion, we showed an *ESR1*-mediated influence of the PAH compounds Indpy and Pice on the gene expression pattern of MCF-7 cells, possibly also promoting breast cancer development in patients.

6.2 Introduction

Plastic waste in the ocean breaks down into microplastic [6, 216] and thus becomes an increasing risk for the environment [5]. Microplastic is frequently ingested by fishes and other sea animals and can thereby enter the human food chain [23, 217, 218]. In addition, uptake of microplastic from food packaging material contributes to the microplastic load in humans [219–221].

Currently, three main threats from microplastic are discussed. First, microplastic particles carry persistent organic pollutants (POP) to marine life [222, 223]. Second, the release of plasticizers, such as bisphenol A, induces adverse health effects in marine animals [16, 224]. Third, microorganisms inhabit microplastic particles and are carried with the material to new habitats with unknown consequences [225–227].

The non-polar microplastics attract hydrophobic compounds present in the water, such as POP [228]. Most frequently detected POP are polycyclic aromatic hydrocarbons (PAH), polychlorinated biphenyls (PCB) and organochlorines (DDT, DDE) [229–233]. POP are considered toxic, endocrine disrupting and partly mutagenic and carcinogenic [229, 231]. The impact of microplastic mediated POP toxicity is still controversially discussed [234–236].

While PAH are also found in marine animals that have not been in contact with microplastic, the leaching of PAH from plastic particles into marine animals [237, 238] has to be considered as an additional distribution vector. Especially for PAH, the U.S. EPA classified 16 compounds as “priority pollutants”, including indeno(1,2,3-cd)pyrene [231, 239].

Despite preliminary findings, it is currently unclear, whether or how these toxins contribute to the endocrine effects observed in sea animals after ingestion. When looking at possible health impacts of plastic debris on human health, it seems plausible to hypothesize that due to the similar structure of the above-mentioned compounds compared to 17-β-estradiol (E2), an interaction with the human estrogen receptor might be possible. The estrogen receptor (ER) functions as a transcription factor in the nucleus [54]. ERs are activated by binding to E2, mediating cell growth, differentiation and development [48, 49]. Two ERs are identified: ERα (*ESR1*) and ERβ (*ESR2*) [54]. After binding of E2 in the ligand binding domain (LBD) the receptor homo- or

heterodimerizes and relocates to the nucleus [54]. Gene expression is mediated either directly by the receptor (targeting estrogen-responsive elements on the DNA), or indirectly (binding other transcription factors and thereby steering them to a specific gene) [58]. Further non-genomic actions in the cytosol are reported [240]. Ligands fitting in the LBD of ER can alter the gene expression by modifying the three-dimensional structure of the receptor. Thus, the question remains whether PAH bind in the LBD of ER and induce hormonal actions in the cells.

In this study, we investigated the molecular effect of the PAH indeno[1,2,3-cd]pyrene (Indpy) and picene (Pice) on the human estrogen receptor α by applying RNA sequencing, microscale thermophoresis, ER transcription factor assay, cell cycle analysis and molecular docking. We found that both compounds interacted with ERα and induced a gene expression associated with cancer development.

6.3 Results

6.3.1 RNA sequencing

We performed RNA sequencing to analyze the influence of Indpy and Pice on the gene expression in MCF-7 cells. RNA sequencing revealed differentially expressed genes related to *ESR1* as upstream regulator after treatment with Indpy (Figure 6.1) and Pice (Figure 6.2). 8 genes were upregulated after treatment of MCF-7 cells with both PAH compounds: *ABCC5*, *CCNG2*, *CYP1A1*, *DDIT4*, *IER3*, *RUNX2*, *STC2*, and *SLC7A5*. 14 genes were downregulated with both ligands: *ADORA1*, *CEBPB*, *CELSR2*, *CTSD*, *CXCL12*, *KRT19*, *PGR*, *PKIB*, *RARA*, *RET*, *SEMA3B*, *SIAH2*, *TFAP2C*, and *XBP1* . In addition, each ligand regulated the expression of several genes not related to *ESR1*. The most differentially expressed genes with a fold change of at least -2 to 2, are listed in Table 6.1 for Indpy and Table 6.2 for Pice. The experiment showed an influence on the gene expression in MCF-7 cells.

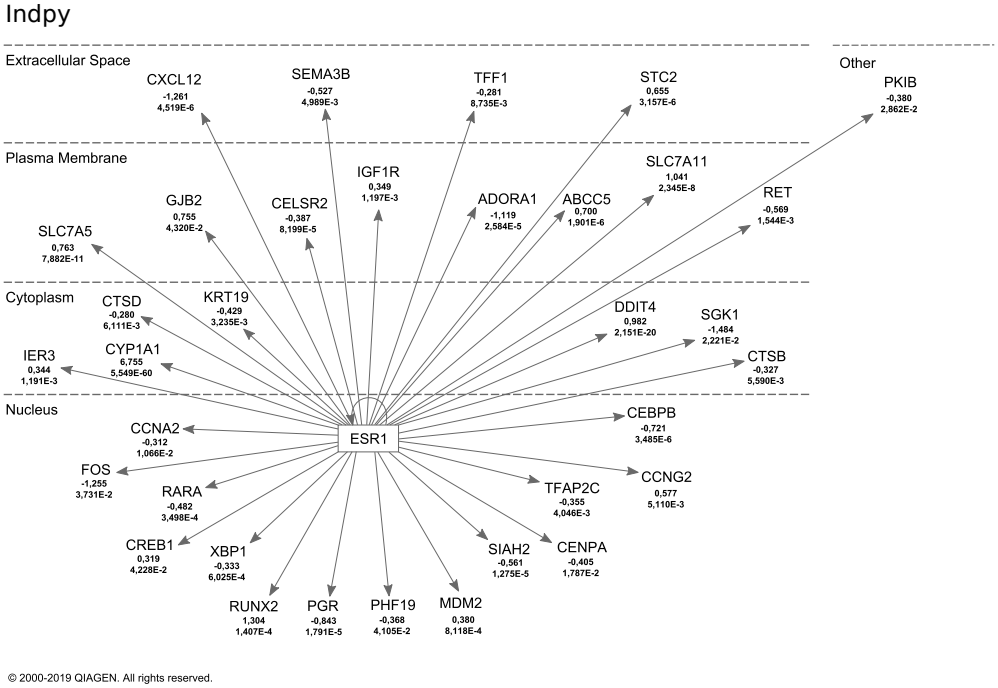

© 2000-2019 QIAGEN. All rights reserved.

Figure 6.1: Upstream analysis with Ingenuity Pathway Analysis software. Differentially expressed genes induced by Indpy in connection with ESR1 signaling are shown. For each gene the fold change and the p-value are given. The figure was modified based on the IPA Path Designer.

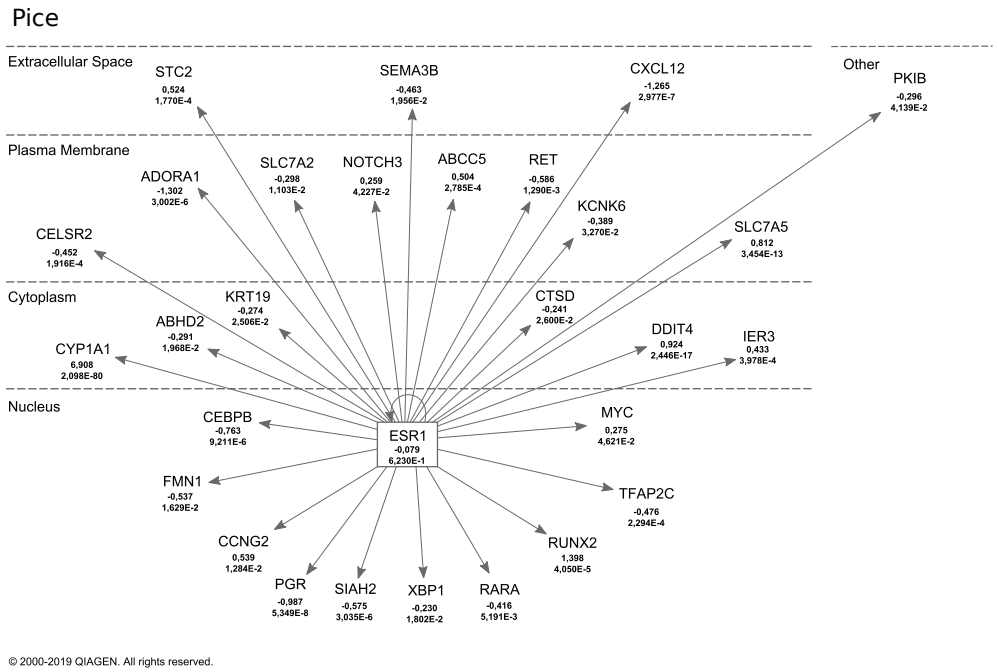

Figure 6.2: Upstream analysis with Ingenuity Pathway Analysis software. Differentially expressed genes induced by Pice in connection with ESR1 signaling are shown. For each gene the fold change and the p-value are given. The figure was modified based on the IPA Path Designer.

Table 6.1: Specific gene expression induced by Indpy. For each gene the fold change $\log_2\left(\frac{E_{\text{Indpy}}}{E_{\text{c}}}\right)$ with corresponding standard error $\Delta \log_2\left(\frac{E_{\text{Indpy}}}{E_{\text{c}}}\right)$ and p-value are listed. ID refers to the name of the gene, E to the expression induced by the respective ligand, and E_c to the expression under control conditions. p-values indicate the comparison with the DMSO-control.

ID	$\log_2\left(\frac{E_{\text{Indpy}}}{E_{\text{c}}}\right)$	$\Delta \log_2\left(\frac{E_{\text{Indpy}}}{E_{\text{c}}}\right)$	p	Entrez Gene Name
LOC107985872	6.398	1.792	$3.58 \cdot 10^{-4}$	uncharacterized LOC107985872
MEF2B	6.063	1.865	$1.15 \cdot 10^{-3}$	myocyte enhancer factor 2B
RNA18S5	5.844	1.936	$2.54 \cdot 10^{-3}$	RNA, 18S ribosomal 5
RPS10-NUDT3	4.937	2.278	$3.02 \cdot 10^{-2}$	RPS10-NUDT3 readthrough
TSPEAR	4.831	2.337	$3.88 \cdot 10^{-2}$	thrombospondin type laminin G domain and EAR repeats
FSBP	4.736	2.380	$4.66 \cdot 10^{-2}$	fibrinogen silencer binding protein
U2AF1L5	4.125	1.924	$3.20 \cdot 10^{-2}$	U2 small nuclear RNA auxiliary factor 1
AMER2	3.319	1.126	$3.21 \cdot 10^{-3}$	APC membrane recruitment protein 2
ALDH3A1	3.149	0.652	$1.36 \cdot 10^{-6}$	aldehyde dehydrogenase 3 family member A1
ATOH8	3.056	1.043	$3.40 \cdot 10^{-3}$	atonal bHLH transcription factor 8
LOC401261	2.597	1.279	$4.23 \cdot 10^{-2}$	uncharacterized LOC401261
ALDH1A3	2.517	0.357	$1.88 \cdot 10^{-12}$	aldehyde dehydrogenase 1 family member A3
LOC105374986	2.302	0.897	$1.03 \cdot 10^{-2}$	uncharacterized LOC105374986
HMOX1	2.284	0.288	$1.98 \cdot 10^{-15}$	heme oxygenase 1
IL17REL	2.254	0.632	$3.62 \cdot 10^{-4}$	interleukin 17 receptor E like
AHRR	2.202	0.280	$3.56 \cdot 10^{-15}$	aryl-hydrocarbon receptor repressor
LOC105369201	2.024	0.413	$9.60 \cdot 10^{-7}$	uncharacterized LOC105369201
LOC107986035	−2.840	0.788	$3.13 \cdot 10^{-4}$	basic proline-rich protein-like
TMEFF1	−2.991	1.492	$4.51 \cdot 10^{-2}$	transmembrane protein with EGF like and two follistatin like domains 1
RGPD3	−3.238	1.131	$4.18 \cdot 10^{-3}$	RANBP2-like and GRIP domain containing 5
LOC105371893	−4.445	2.034	$2.88 \cdot 10^{-2}$	uncharacterized LOC105371893
TBC1D3G	−5.771	2.145	$7.13 \cdot 10^{-3}$	TBC1 domain family member 3F
FAM226B	−6.466	1.927	$7.93 \cdot 10^{-4}$	family with sequence similarity 226 member B
PHOSPHO2-KLHL23	−7.038	1.767	$6.80 \cdot 10^{-5}$	kelch like family member 23

Table 6.2: Specific gene expression induced by Pice. For each gene the fold change $\log_2\left(\frac{E_{\text{Pice}}}{E_{\text{c}}}\right)$ with corresponding standard error $\Delta \log_2\left(\frac{E_{\text{Pice}}}{E_{\text{c}}}\right)$ and p-value are listed. ID refers to the name of the gene, E to the expression induced by the respective ligand, and E_c to the expression under control conditions. p-values indicate the comparison with the DMSO-control.

Table 6.2: Specific gene expression by Pice.

ID	$\log_2\left(\frac{E_{\text{Pice}}}{E_{\text{c}}}\right)$	$\Delta \log_2\left(\frac{E_{\text{Pice}}}{E_{\text{c}}}\right)$	p	Entrez Gene Name
GDF1	9.155	1.505	$1.19 \cdot 10^{-9}$	growth differentiation factor 1
RNA18S5	9.066	1.534	$3.47 \cdot 10^{-9}$	RNA, 18S ribosomal 5
SNORD3B-2	8.765	1.545	$1.40 \cdot 10^{-8}$	small nucleolar RNA, C/D box 3B-2
RNU4-2	8.286	1.556	$9.99 \cdot 10^{-8}$	RNA, U4 small nuclear 2
MAGED4	7.749	1.630	$2.00 \cdot 10^{-6}$	MAGE family member D4B
RNU4-1	7.582	1.609	$2.44 \cdot 10^{-6}$	RNA, U4 small nuclear 1
SNORA73A	6.579	1.565	$2.61 \cdot 10^{-5}$	small nucleolar RNA, H/ACA box 73A

Table 6.2: Specific gene expression by Pice.

ID	$\log_2\left(\frac{E_{\text{Pice}}}{E_{\text{c}}}\right)$	$\Delta\log_2\left(\frac{E_{\text{Pice}}}{E_{\text{c}}}\right)$	p	Entrez Gene Name
RNVU1-7	6.242	1.138	$4.17 \cdot 10^{-8}$	RNA, variant U1 small nuclear 7
HIST1H4B	6.002	1.909	$1.67 \cdot 10^{-3}$	histone cluster 1 H4 family member b
CNTNAP3	5.893	1.928	$2.24 \cdot 10^{-3}$	contactin associated protein like 3
HIST1H2AH	5.774	1.965	$3.30 \cdot 10^{-3}$	histone cluster 1 H2A family member h
SCARNA10	5.719	2.019	$4.63 \cdot 10^{-3}$	small Cajal body-specific RNA 10
SNORD3A	5.647	0.648	$2.88 \cdot 10^{-18}$	small nucleolar RNA, C/D box 3A
LOC107985872	5.629	2.023	$5.41 \cdot 10^{-3}$	uncharacterized LOC107985872
SCARNA13	5.613	2.050	$6.17 \cdot 10^{-3}$	small Cajal body-specific RNA 13
HIST1H2BI	5.592	2.031	$5.90 \cdot 10^{-3}$	histone cluster 1 H2B family member i
CYP1B1-AS1	5.083	2.227	$2.25 \cdot 10^{-2}$	CYP1B1 antisense RNA 1
LOC101929066	4.986	1.951	$1.06 \cdot 10^{-2}$	uncharacterized LOC101929066
RN7SK	4.975	0.561	$7.33 \cdot 10^{-19}$	RNA, 7SK small nuclear
RPPH1	4.960	0.503	$5.91 \cdot 10^{-23}$	ribonuclease P RNA component H1
SCARNA16	4.863	2.335	$3.72 \cdot 10^{-2}$	small Cajal body-specific RNA 16
SNORA73B	4.800	2.407	$4.61 \cdot 10^{-2}$	small nucleolar RNA, H/ACA box 73B
TRIM39-RPP21	4.798	2.408	$4.63 \cdot 10^{-2}$	TRIM39-RPP21 readthrough
TSPEAR	4.759	2.385	$4.60 \cdot 10^{-2}$	thrombospondin type laminin G domain and EAR repeats
U2AF1L5	4.399	1.952	$2.42 \cdot 10^{-2}$	U2 small nuclear RNA auxiliary factor 1
HIST1H1E	4.390	1.384	$1.51 \cdot 10^{-3}$	histone cluster 1 H1 family member e
RMRP	4.383	0.692	$2.37 \cdot 10^{-10}$	RNA component of mitochondrial RNA processing endoribonuclease
SCARNA2	4.305	0.821	$1.56 \cdot 10^{-7}$	small Cajal body-specific RNA 2
RNA28S5	4.026	0.210	$6.28 \cdot 10^{-82}$	RNA, 28S ribosomal 5
RN7SL1	3.870	0.440	$1.35 \cdot 10^{-18}$	RNA, 7SL, cytoplasmic 1
RN7SL2	3.817	0.479	$1.70 \cdot 10^{-15}$	RNA, 7SL, cytoplasmic 2
AMER2	3.388	1.122	$2.54 \cdot 10^{-3}$	APC membrane recruitment protein 2
HIST1H3F	3.265	1.604	$4.17 \cdot 10^{-2}$	histone cluster 1 H3 family member f
HIST1H1B	3.038	0.986	$2.06 \cdot 10^{-3}$	histone cluster 1 H1 family member b
ATOH8	2.932	1.073	$6.31 \cdot 10^{-3}$	atonal bHLH transcription factor 8
LOC647070	2.789	1.219	$2.21 \cdot 10^{-2}$	uncharacterized LOC647070
ALDH1A3	2.787	0.326	$1.21 \cdot 10^{-17}$	aldehyde dehydrogenase 1 family member A3
LOC105374986	2.747	0.817	$7.71 \cdot 10^{-4}$	uncharacterized LOC105374986
ALDH3A1	2.669	0.731	$2.59 \cdot 10^{-4}$	aldehyde dehydrogenase 3 family member A1
HIST1H1D	2.624	1.317	$4.62 \cdot 10^{-2}$	histone cluster 1 H1 family member d
HIST1H4E	2.602	1.122	$2.04 \cdot 10^{-2}$	histone cluster 1 H4 family member e
AHRR	2.468	0.276	$4.36 \cdot 10^{-19}$	aryl-hydrocarbon receptor repressor
IL17REL	2.374	0.621	$1.33 \cdot 10^{-4}$	interleukin 17 receptor E like
RNA45S5	2.333	0.340	$6.29 \cdot 10^{-12}$	RNA, 45S pre-ribosomal 5
LOC102724093	2.233	0.835	$7.49 \cdot 10^{-3}$	golgin subfamily A member 6-like protein 4
BPIFA4P	2.048	1.036	$4.80 \cdot 10^{-2}$	BPI fold containing family A member 4, pseudogene
SLC34A3	2.044	1.017	$4.44 \cdot 10^{-2}$	solute carrier family 34 member 3
LOC105369201	2.038	0.379	$7.38 \cdot 10^{-8}$	uncharacterized LOC105369201
FAM47E	−2.125	0.917	$2.05 \cdot 10^{-2}$	family with sequence similarity 47 member E
WNT4	−2.313	0.856	$6.91 \cdot 10^{-3}$	Wnt family member 4
RGPD6	−2.620	0.417	$3.20 \cdot 10^{-10}$	RANBP2-like and GRIP domain containing 5
LRRC37A6P	−3.219	1.532	$3.57 \cdot 10^{-2}$	leucine rich repeat containing 37 member A6, pseudogene
LOC107986035	−3.628	0.978	$2.08 \cdot 10^{-4}$	basic proline-rich protein-like
DEPDC1-AS1	−4.935	2.391	$3.90 \cdot 10^{-2}$	DEPDC1 antisense RNA 1

Table 6.2: Specific gene expression by Pice.

ID	$\log_2\left(\frac{E_{\text{Pice}}}{E_{\text{c}}}\right)$	$\Delta\log_2\left(\frac{E_{\text{Pice}}}{E_{\text{c}}}\right)$	p	Entrez Gene Name
PHOSPHO2-KLHL23	−6.697	1.777	$1.65 \cdot 10^{-4}$	kelch like family member 23

6.3.2 RT-qPCR

The gene expression measured with RNA sequencing was verified with RT-qPCR. Five differentially expressed genes were selected for verification (Figure 6.3). As RNA sequencing did not reveal altered expression of *GAPDH* and *HSP90AB1*, both genes were used as reference genes for the RT-qPCR experiments. The log2 fold change of the RT-qPCR experiment was plotted against the log2 fold change of the NGS data. A linear regression was performed for both reference genes, resulting in an RNA value of $R = 0.96$, each. The gene expression of RT-qPCR supported the RNA sequencing result.

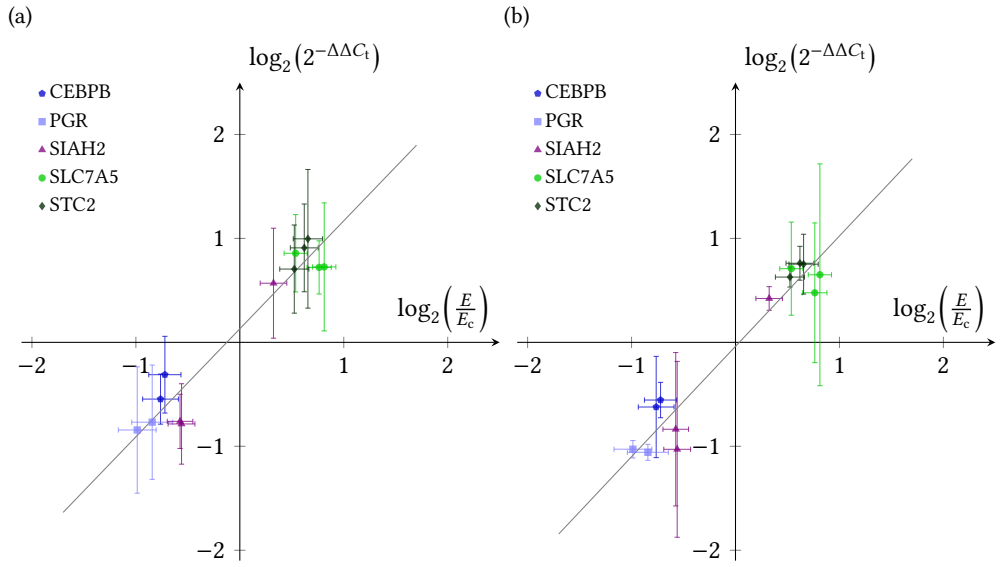

Figure 6.3: Correlation of gene expression levels obtained by NGS and RT-qPCR. The fold change based on the RT-qPCR results was plotted against the fold change based on the NGS results for the ligands E2, Indpy and Pice (dots). The was calculated with (a) GAPDH and (b) HSP90AB1 as reference gene, respectively. A linear regression was calculated with Origin 7.5. The fit is shown in grey with (a) a slope of 1.04, intercept of 0.13, R=0.96 and (b) a slope of 1.06, intercept of -0.04, R=0.96.

6.3.3 Microscale Thermophoresis

Indpy, Pice, and the natural ligand E2 were analyzed for their *in vitro* binding to ERα with MST. At least 13 different ligand concentrations were measured, each. For all compounds a concentration dependent fluorescence signal was overserved (Figure 6.4). A linear fit based on the law of mass action was used to calculate the dissociation constant K_d. The K_d for Indpy and Pice with ERα was of the same order of magnitude

as the K_d for E2 (Table 6.3). MST confirms the binding of Indpy and Pice to ERα *in vitro*.

Table 6.3: Molecular structure of the analyzed ligands and comparison of the inhibitory constant predicted *in silico* $K_{i,pred}$ with the dissociation constant calculated by MST *in vitro* K_d.

Structure	Name	$K_{i,pred}$ / nM	K_d / nM
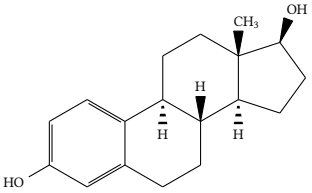	17-β-Estradiol E2 CAS 50-28-2	112.98	14.9 ± 2.1
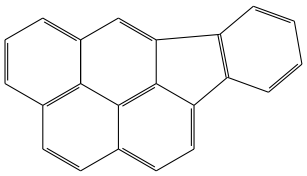	Indeno[1,2,3-cd]pyrene Indpy CAS 193-39-5	65.96	8.0 ± 1.2
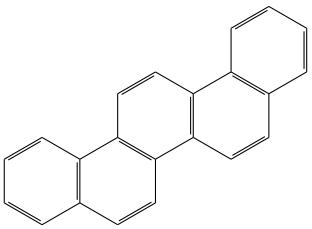	Picene Pice CAS 213-46-7	40.21	13.8 ± 3.8

6.3.4 ER-TF-Activation Assay

We used the ER transcription factor assay to prove, whether Indpy and Pice also activated the receptor. The assay was performed with *ESR1*-overexpressing HEK-ESR1 cells, which were used to detect a stronger signal. E2 was used as control and showed the strongest activation of ERα (Figure 6.5). Indpy induced a time-dependent activation of ERα, whereas Pice seemed to inhibit the activation of ERα with increasing time. Indpy activated ERα, although less prominent than E2, while Pice reduced the activation of the receptor.

6.3.5 Cell cycle analysis

One mechanism of action of ERα is proliferation. We therefore investigated the cell cycle distribution after treatment of HEK-ESR1 and MCF-7 (Figure 6.8) cells with Indpy

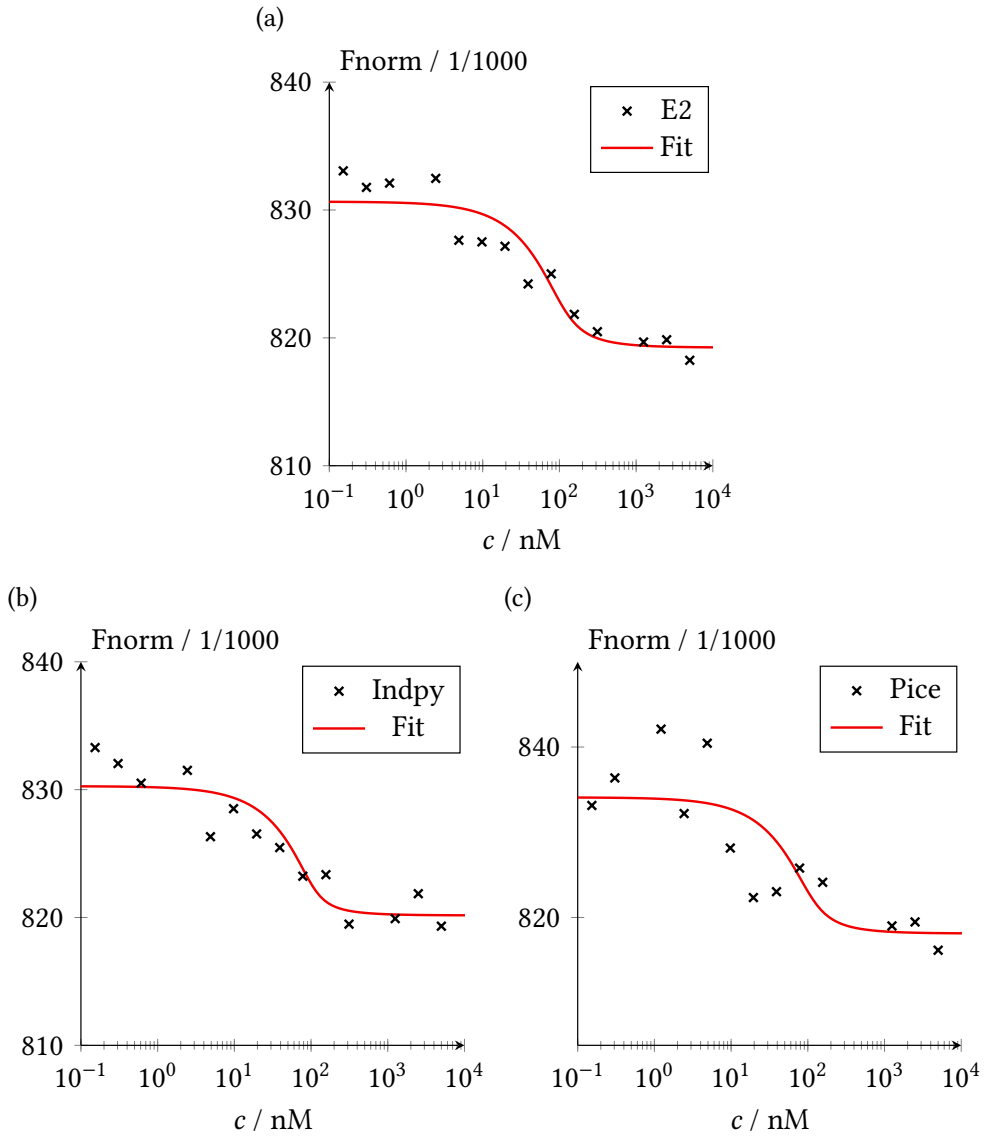

Figure 6.4: Analysis of the MST-experiments. The MST was performed with 95% LED and 20% MST power. Fluorescently labeled ERα was used as target with (a) E2, (b) Indpy, and (c) Pice as ligand, respectively. A fit was performed according to the law of mass action (red).

Figure 6.5: ER transcription factor assay. Activation of estrogen receptor was measured after 4 h and 8 h incubation time of HEK-ESR1 cells with 0.5 µM of the respective ligand. The difference optical density measured after 4 h is shown in the upper line and after 8 h in the lower line.

and Pice using two time points and two concentrations, each. In all cases, no clear effect on the cell cycle distribution was measured (Table 6.5).

6.3.6 Molecular Docking

Molecular docking was performed to analyze the binding potential of both PAH compounds to the estrogen receptor. Molecular docking of Indpy and Pice to the entire ERα-LBD showed that both compounds bound to the same binding pocket of ERα-LBD as E2 *in silico* (Figure 6.6, upper left). The lowest binding energy of the compounds to ERα-LBD was even lower than that of E2, indicating a stronger binding to the receptor (Table 6.4). The Lamarckian algorithm resulted 250 times in the same outcome, indicating a low deviation of the calculation. All compounds interacted with the amino acids Leu391, Arg394, Phe404, Met421, Ile424, and Leu525. The lowest binding energy position of each ligand in ERα-LBD is presented in Figure 6.6. Indpy and Pice bind to ERα-LBD *in silico*.

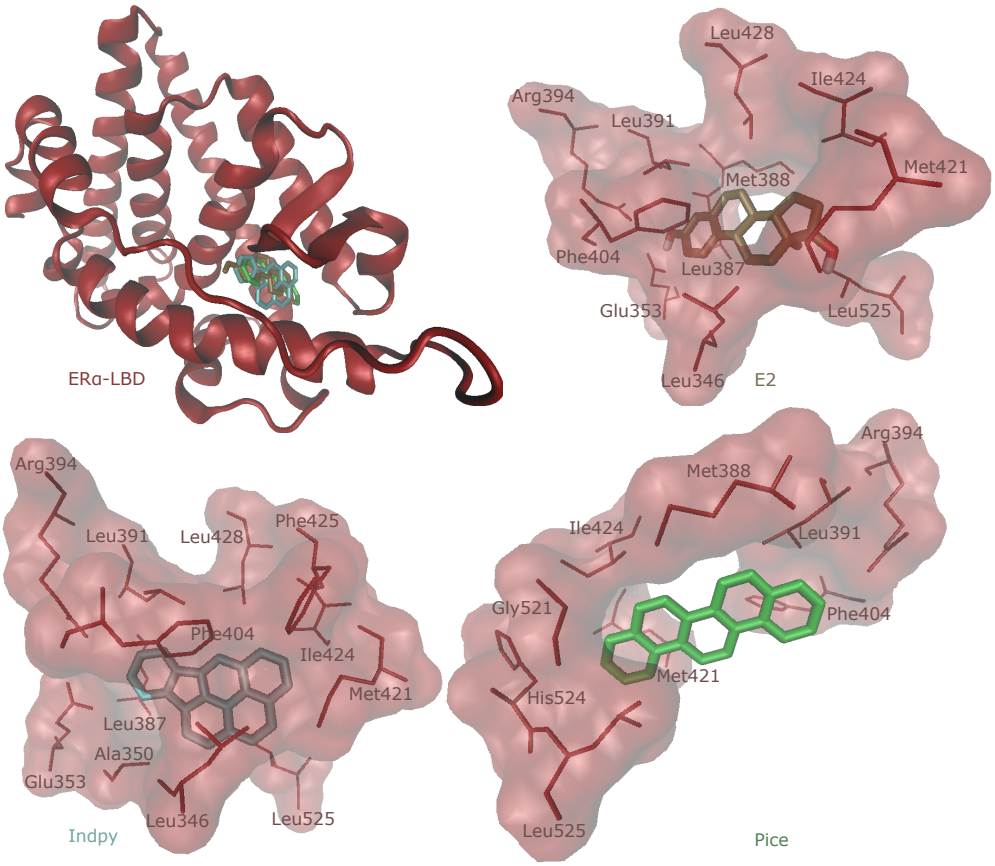

Figure 6.6: Visualization of the molecular docking result. The upper left image shows the result of the blind docking, with all ligands binding in the same pocket of ERα-LBD. The others images show the result of the defined docking for the ligands E2 (ochre), Indpy (grey), and Pice (green), respectively. Each ligand is displayed with the interacting amino acids of ERα-LBD.

Table 6.4: Result of molecular docking. For each ligand, the lowest and mean binding energy and the predicted inhibitory constant $K_{i,pred}$ are given. The torsdof parameter Td indicates the torsional degree of freedom of each ligand. The amino acids of ERα-LBD involved in hydrophobic interactions and hydrogen bonds (H-bonds) are listed.

	lowest binding energy / kcal mol^{-1}	mean binding energy / kcal mol^{-1}	$K_{i,pred}$ / nM	Td	Runs in 1st cluster	Amino acids involved in hydrophobic interactions	Amino acids involved in H-bonds
E2	−9.48	−9.45	112.95	2	250/250	Leu346 Leu387 Met388 Leu391 Phe404 Met421 Ile424 Leu428 Leu525	Glu353 Arg394
Indpy	−9.80	−9.80	65.96	0	250/250	Leu346 Ala350 Glu353 Leu387 Leu391 Arg394 Phe404 Met421 Ile424 Phe425 Leu428 Leu525	-
Pice	−10.09	−10.09	40.21	0	250/250	Met388 Leu391 Arg394 Phe404 Met421 Ile424 Gly521 His524 Leu525	-

6.4 Discussion

In this study, we analyzed the molecular effects of the PAHs Indpy and Pice on MCF-7 cells. RNA sequencing revealed several differentially expressed genes regulated by *ESR1*. Most prominently, *CYP1A1* was overexpressed with both ligands. *CYP1A1* codes for the cytochrome P450 family 1 member A1 (CYP1A1), which is involved in phase 1 metabolism of xenobiotics. Its upregulation was frequently reported after treatment with PAH [238, 241, 242]. CYP1A1 metabolizes PAH to epoxides, catalyzing the carcinogenic effects of PAH. CYP1A1 was upregulated after treatment with Indpy and Pice, probably leading to carcinogenic effects in the cells. The aryl-hydrocarbon receptor repressor (AhRR) is a known inhibitor of CYP1A1 [243] and was overexpressed after treatment with Indpy and Pice (Tables 3 and 4), confirming the activation of the cytochrome P450-mediated metabolism by Indpy and Pice.

Treatment with the PAH compounds further altered the expression of several genes coding for proteins, which function in the nucleus. *CCNG2* encodes the protein cyclin G2. While E2-bound ER is known to repress *CCNG2* expression, treatment with Indpy and Pice led to an upregulation of *CCNG2* [244]. Ahmed et al. (2012) identified *CCNG2* as target of the aryl-hydrocarbon receptor, which might explain the opposite expression status [244]. *CCNG2* overexpression was associated with cell cycle arrest [202]. *RUNX2* is a transcriptions factor involved in osteogenesis and bone metastases in breast cancer [65, 66] and was overexpressed with both PAH compounds. Other transcription factors were found to be downregulated with both compounds: *CEBPB*, *RARA*, *TFAP2C*, and *XBP1*. The CAAT enhancer binding protein β (*CEBPB*) was associated with proliferation and differentiation [199]. The retinoic acid receptor α (RARα/*RARA*) has antiproliferative effects [245, 246]. Hua et al. (2009) found similar binding regions of RARα and ERα on the DNA, with antagonizing effects [245]. Thereby, downregulation of *RARA* by PAH might enhance ERα-mediated proliferative effects. The transcription factor AP-2γ (*TFAP2C*) was strongly involved in ER gene expression by directly and indirectly interfering with ER expression [247]. Overexpression of *TFAP2C* was correlated with worse response to anti-hormone therapy [248]. The X-box binding protein 1 (*XBP1*) plays a major role in the unfolded protein response and is induced by hypoxia and relevant for tumor growth [249, 250]. Apart from transcription factors, the progesterone receptor (*PGR*) was found to be downregulated with both ligands. PGR is a hormone activated receptor with proliferative effects [71]. PGR status, together with ER and HER2, is important for treatment strategies in breast cancer. While ER and PGR positive tumors respond to hormone therapy, the outcome for ER positive but PGR negative tumors are worse [72]. The siah E3 ubiquitin protein ligase 2 (*SIAH2*) was downregulated after treatment with both PAH compounds. SIAH2 is involved in protein ubiquitination and hypoxia [251, 252]. Its downregulation was associated with resistance to endocrine therapy [253].

A number of genes coding for cytosolic proteins were found differentially expressed

after treatment with Indpy and Pice. The DNA-damage inducible transcript 4 (DDIT4) and the immediate early response 3 (IER3) genes were overexpressed, indicating involvement of apoptosis [73, 74]. Two direct targets of *ESR1* were downregulated after treatment with both compounds: cathepsin D (*CTSD*) and keratin 19 (*KRT19*). *CTSD* encodes an aspartyl protease which is usually highly expressed in breast cancer and associated with poor prognosis [254–256]. *KRT19* is negatively involved in invasion by interacting with the NOTCH signaling pathway [207].

Genes coding for plasma-membrane localized proteins were differentially expressed as well. The multidrug resistance-associated protein 5 (MRP5/*ABCC5*) was overexpressed after treatment with Indpy and Pice. MRP5 belongs to the family of ABC-transporters, responsible for drug efflux [257]. The solute carrier family 7 member *SLC7A5* was upregulated as well. SLC7A5 transports amino acids into the cell, providing nutritional supply [79]. The transporter plays a role in breast cancer and is associated with poor prognosis [258]. Other receptors were downregulated by the PAH compounds, like the adenosine A1 receptor (*ADORA1*), who is a direct target of ERα and usually upregulated in breast cancer promoting proliferation [80]. The transmembrane receptor cadherin EGF LAG seven-pass G-type receptor 2 (*CELSR2*) is involved in cell-cell adhesion and receptor-ligand interactions [81, 82]. The proto-oncogene *RET* encodes for a tyrosine kinase involved in proliferation, differentiation and migration [259, 260]. *RET* is often expressed in breast cancer, promoting migration [259].

The secreted glycoprotein Stanniocalcin 2 (*STC2*) was upregulated after treatment with Indpy and Pice. *STC2* is relevant for cell metabolism [87] and is often upregulated in cancers, correlating with cell proliferation [88]. The gene *CXCL12* codes for a cytokine, relevant for the migration of stem cells, therefore playing a critical role in metastasis [261]. *CXCL12* was downregulated after treatment with PAH. The semaphorin 3B (*SEMA3B*) gene was downregulated in both samples, too. SEMA3B can induce apoptosis and was therefore considered as tumor suppressor [262, 263]. The cAMP-dependent protein kinase inhibitor β gene (*PKIB*) was downregulated after treatment with both compounds. The protein regulates the PKA pathway and was associated with triple negative breast cancer [264, 265].

Treatment of MCF-7 cells with the PAH compounds Indpy and Pice revealed several differentially expressed genes. Indpy and Pice alter the gene expression mediated by *ESR1*, interfering in cell proliferation and metastasis. The observed effects favor cancer development with a poor response to therapy. *CELSR2*, *RARA*, *SEMA3B*, *SIAH2*, and *XBP1* were downregulated and *CCNG2* was upregulated by the PAH compounds, although E2-activated *ESR1* is known to cause the opposite effect. This indicates that Indpy and Pice are not that much E2 analogues, promoting ER action, but rather ligands interfering with the gene expression profile of ER. This may result in diverse gene transcription, complicating cancer treatment.

6.4.1 Specific gene expression by Indpy and Pice

Besides *ESR1*-mediated gene expression, several non-*ESR1* related genes were found to be differentially expressed by Indpy and Pice. Among them, the myocyte enhancer factor 2B (*MEF2B*) was overexpressed by Indpy. Ying et al. identified MEF2B as a regulator of the oncogene Bcl-6 [107]. APC membrane recruitment protein 2 (*AMER2*) was overexpressed by both compounds. AMER2 was identified as inhibitor of the Wnt signaling pathway, interfering with the gene expression [266]. Treatment with Indpy and Pice further resulted in the upregulation of two genes coding for aldehyde dehydrogenases (ALDH): *ALDH3A1* and *ALDH1A3*. ALDH convert aldehyde to carboxylic acid groups [267]. *ALDH3A1* expression is associated with cancer development and it was upregulated by PAH [268, 269].

Especially Pice activated more genes independent from *ESR1* regulation, compared to Indpy, indicating further modes of action of Pice in MCF-7 cells. The growth differentiation factor 1 (*GDF1*) was most upregulated after Pice-treatment. GDF-1 is a ligand of TGF-β, involved in development and differentiation [270, 271]. In addition, several members of the histone cluster families H1-H4 were upregulated after treatment with Pice. Being crucial for DNA organization, the upregulation of histone genes might interfere with gene regulation [272, 273]. Harris et al. reported an increase of histone mRNA during cell cycle progression, indicating cell proliferation as possible cause of the upregulation [274].

Indpy and Pice both influence the gene expression apart from *ESR1*-regulated genes. Taken together, the gene expression influences cell proliferation and metastasis, promoting cancer development.

6.4.2 Analysis of ERα binding, activation, and proliferative effects mediated by PAH compounds

The upstream target analysis of the RNA sequencing data revealed *ESR1* as top upstream regulator. In order to investigate the binding of Indpy and Pice to ERα *in vitro*, we performed microscale thermophoresis experiments. The calculated dissociation constants of both PAH compounds are similar to E2, indicating comparable binding properties. Although binding of Indpy and Pice to ERα is similar to the natural ligand E2, the ER activation is less prominent with Indpy and seems to be reduced by Pice. Both PAH compounds seem to result in different ERα actions than E2, which can also be seen in the RNA sequencing data as some genes were unexpectedly regulated. Nevertheless, both PAH compounds interfered in *ESR1*-related gene expression as upstream regulator. The actions of a ligand-activated ER depend on its three-dimensional structure, which is mainly caused by the ligand structure [61]. The differences of the analyzed structures are likely to result in a modified behavior of ERα. In addition, we did not find any effects of the PAH compounds on the cell cycle distribution, indicating different modes of action. We performed molecular docking with both compounds

and E2 as control to the ERα-LBD. Both PAH compounds were calculated with a lower binding energy towards the protein than E2, indicating binding to ERα-LBD *in silico*. The amino acids interacting in the binding match those described in the literature [56, 59]. The results of the molecular docking experiment match the observed *in vitro* binding of Indpy and Pice to ERα.

6.5 Conclusion

Treatment of MCF-7 cells with Indpy and Pice revealed several differentially expressed genes with *ESR1* identified as upstream regulator. *ABCC5*, *CCNG2*, *CYP1A1*, *DDIT4*, *IER3*, *RUNX2*, *STC2*, and *SLC7A5* were upregulated, and *ADORA1*, *CEBPB*, *CELSR2*, *CTSD*, *CXCL12*, *KRT19*, *PGR*, *PKIB*, *RARA*, *RET*, *SEMA3B*, *SIAH2*, *TFAP2C*, and *XBP1* were downregulated after treatment with both ligands. The gene expression pattern is likely to influence cell proliferation and metastasis, favoring cancer development with poor response to therapy. Each ligand further activated non-*ESR1* regulated genes, indicating further molecular actions in the cells apart from ERα. We further confirmed the binding of Indpy and Pice to ERα *in silico* and *in vitro*. Indpy and Pice did not alter the cell cycle of MCF-7 or HEK-ESR1 cells, and only Indpy showed a positive signal in ER activation assay, suggesting different mode of PAH-induced ERα actions in the cells, compared to E2. In the light of the latent threat to human health brought about by plastic compounds migrating from the environment into (human) food chains and the human body, we strongly believe in the necessity to foster interdisciplinary research at the interfaces of biology, biochemistry, pharmacology, biomedicine and those disciplines working on ethical and social concepts for the responsible use of resources and the protection of biodiversity and human health.

6.6 Acknowledgement

This work was supported by the *Deutsche Forschungsgemeinschaft* (GRK 2015/2). The authors gratefully acknowledge the computing time granted on the supercomputer Mogon at Johannes Gutenberg University Mainz (hpc.uni-mainz.de). Cell sorting support by the IMB Flow Cytometry Core Facility is gratefully acknowledged.

6.7 Supplementary material

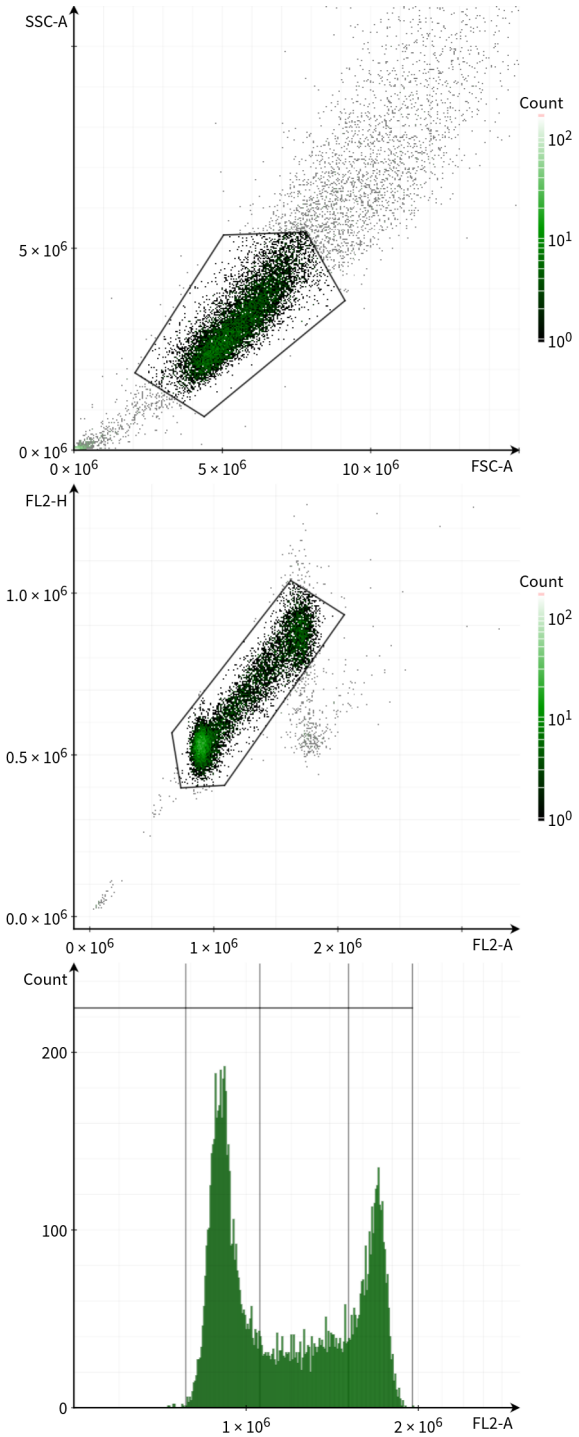

Figure 6.7: Gating in the cell cycle experiments. MCF-7 cells were treated with DMSO for 4 h at 0.5 µM. (Top) The major cell population was selected. (Middle) Aggregates and doublets were removed. (Bottom) The selected cells were gated into four groups based on their PI content detected by the FL2-A detector.

(a) Indpy

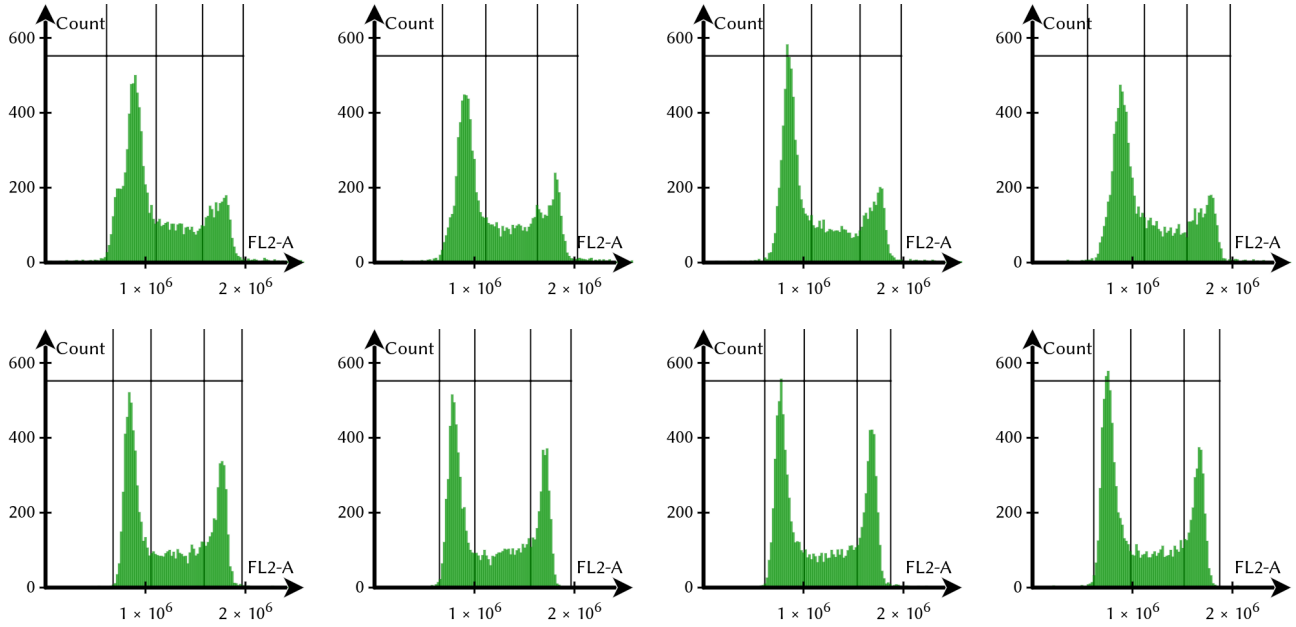

(b) Pice

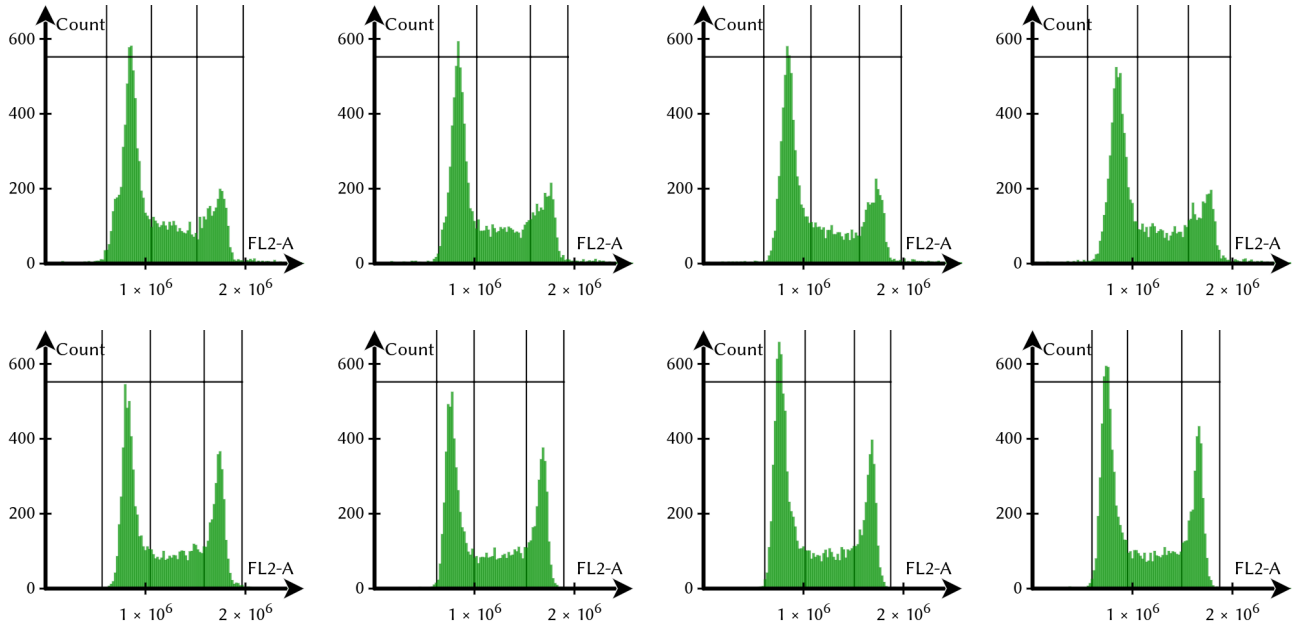

Figure 6.8: Cell Cycle Analysis. Cells were treated with (a) Indpy and (b) Pice. Top row: treatment of HEK-ESR1 cells. Bottom row: Treatment of MCF-7 cells. Each analysis was performed under four conditions: 4 h and 0.1 µM, 4 h and 0.5 µM, 8 h and 0.1 µM, 8 h and 0.5 µM (from left to right).

Table 6.5: Cell cycle analysis. HEK-ESR1 and MCF-7 cells were treated with 0.1 µM or 0.5 µM of Indpy or Pice and incubated for 4 h or 8 h, respectively. DMSO was used as control.

		HEK-ESR1			MCF-7		
Treatment	Phase	DMSO	Indpy	Pice	DMSO	Indpy	Pice
	sub G1 / %	0.2	0.3	0.3	0.2	0.1	0.2
4 h	G1/G0 / %	53.9	54.2	52.3	45.6	46.2	45.4
0.1 µM	S / %	21.2	21.3	22.4	24.6	25.3	24.4
	G2/M / %	24.5	24.0	24.7	29.5	28.3	29.9
	sub G1 / %	0.1	0.4	0.5	0.1	0.2	0.3
4 h	G1/G0 / %	53.4	51.2	51.2	47.9	45.5	44.7
0.5 µM	S / %	19.2	23.1	23.1	24.0	26.6	25.9
	G2/M / %	27.2	25.3	25.2	28.0	27.7	29.1
	sub G1 / %	0.6	1.0	1.1	0.2	0.2	0.2
8 h	G1/G0 / %	53.7	57.0	53.0	46.4	50.1	49.9
0.1 µM	S / %	21.7	20.5	21.9	23.2	23.8	20.5
	G2/M / %	24.0	21.5	24.1	30.1	25.8	29.3
	sub G1 / %	0.2	0.3	0.3	0.2	0.1	0.2
8 h	G1/G0 / %	50.3	53.5	54.0	50.3	47.8	50.9
0.5 µM	S / %	26.9	22.3	21.5	21.5	22.1	21.4
	G2/M / %	22.1	23.8	24.1	28.0	29.9	27.5

7 Summary

In this thesis I investigate the effect of ten compounds associated with microplastic on the human estrogen receptor α. The effects of microplastic on the human health are still unknown. Given the rising amount of microplastic in the oceans, an assessment of their health risk is crucial.

First, I employed virtual screening and molecular docking to screen *in silico* for plastic-associated compounds with a high binding affinity towards the ligand binding domain of the estrogen receptor α. Out of 1845 compounds, I identified four chemically distinct groups of compounds with a high binding affinity: bisphenols, phthalates, organophosphate ester, and polycyclic aromatic hydrocarbons. Second, I verified the binding predicted *in silico* with microscale thermophoresis *in vitro*. Third, I employed cytotoxicity assays, ER activation assays, and cell cycle analyses as *in vitro* cell-based experiments. Finally, I used RNA sequencing and RT-qPCR to reveal the molecular mechanisms induced by the compounds in the cells. I used the human estrogen receptor α positive breast cancer cell line MCF-7 and generated an ESR1-overexpressing HEK293 cell line.

Three of the compound groups represent plasticizers (bisphenols, phthalates, organophosphate ester). Leaching of these plasticizers out of microplastic is currently the biggest concern regarding health issues. The fourth group (polycyclic aromatic hydrocarbons) can adhere to and accumulate on plastic particles, presenting a second threat originating from microplastic. I present the influence of each compound group on the human estrogen receptor α in a separate chapter within this thesis.

In chapter 3, I focus on the binding of bisphenol A, bisphenol B, bisphenol Z, and tetramethyl bisphenol A to the human estrogen receptor α. RNA sequencing reveals that the gene expression pattern of all bisphenol compounds effects cell growth, invasion, migration, apoptosis and cancer development. Of all bisphenols tested, tetramethyl bisphenol A has the strongest effect on the activation of the human estrogen receptor and cell proliferation.

In chapter 4, I demonstrate similar effects of benzyl butyl phthalate, butyl cyclohexyl phthalate and butyl octyl phthalate on the binding and activation of the human estrogen receptor α. The gene expression induced by butyl octyl phthalate suggests an influence on the cell cycle and tumorigenesis with poor chances of survival.

Chapter 5 presents the effect of the organophosphate ester tri-*o*-cresyl phosphate. Besides effects on invasion, metastasis and the cell cycle, the phosphate was found to especially favor tumor growth by upregulating angiogenesis and nutritional supply.

Finally, in chapter 6, I demonstrate the effects of the polycyclic aromatic hydrogens

indeno[1,2,3-*cd*]pyrene and picene. Both compounds interfere with *ESR1*-regulated genes. In comparison with the natural ligand 17-β-estradiol, the effects of both compounds are partly opposed. The gene expression pattern promotes cancer development with poor response to therapy.

In summary, I present in this thesis a detailed study on the effects of three groups of plasticizer compounds and two polycyclic aromatic hydrogen compounds on the human estrogen receptor α. I reveal the molecular effects induced by the compounds on the gene expression pattern in MCF-7 cells. All compounds interfere with estrogen receptor α *in silico*, *in vitro*, and influence the gene expression towards tumorigenesis. Therefore, the investigated compounds, which are all associated with microplastic, are potentially detrimental to the human health due to their interaction with the human estrogen receptor α.

Bibliography

[1] D. K. A. Barnes, F. Galgani, R. C. Thompson, and M. Barlaz. Accumulation and fragmentation of plastic debris in global environments. *Phil Trans R Soc B*, 364(1526):1585–1998, 2009.

[2] J. R. Jambeck, R. Geyer, C. Wileox, T. R. Siegler, M. Perryman, A. Andrady, R. Narayan, and K. L. Law. Plastic waste inputs from land into the ocean. *Science*, 347(6223):768–771, 2015.

[3] M. Gross. Oceans of plastic waste. *Current Biology*, 25(3):R93 – R96, 2015.

[4] I. L. N. Bråte, D. P. Eidsvoll, C. C. Steindal, and K. V. Thomas. Plastic ingestion by atlantic cod (gadus morhua) from the norwegian coast. *Mar Pollut Bull*, 112(1):105–110, 2016.

[5] W. C. Li, H. F. Tse, and L. Fok. Plastic waste in the marine environment: A review of sources, occurrence and effects. *Sci Total Environ*, 566-567:333–349, 2016.

[6] C. C. Wessel, G. R. Lockridge, D. Battiste, and J. Cebrian. Abundance and characteristics of microplastics in beach sediments: Insights into microplastic accumulation in northern Gulf of Mexico estuaries. *Mar Pollut Bull*, 109(1):178–183, 2016.

[7] E. Besseling, B. Wang, M. Lurling, and A. A. Koelmans. Nanoplastic affects growth of *S. obliquus* and reproduction of *D. magna*. *Environ Sci Technol*, 48(20):12336–43, 2014.

[8] M. Cole, P. Lindeque, E. Fileman, C. Halsband, and T. S. Galloway. The impact of polystyrene microplastics on feeding, function and fecundity in the marine copepod *Calanus helgolandicus*. *Environ Sci Technol*, 49(2):1130–7, 2015.

[9] M. Cole, P. Lindeque, E. Fileman, C. Halsband, R. Goodhead, J. Moger, and T. S. Galloway. Microplastic ingestion by zooplankton. *Environ Sci Technol*, 47(12):6646–55, 2013.

[10] C. B. Jeong, E. J. Won, H. M. Kang, M. C. Lee, D. S. Hwang, U. K. Hwang, B. Zhou, S. Souissi, S. J. Lee, and J. S. Lee. Microplastic size-dependent toxicity, oxidative stress induction, and p-JNK and p-p38 activation in the monogonont rotifer (*Brachionus koreanus*). *Environ Sci Technol*, 50(16):8849–57, 2016.

[11] K. W. Lee, W. J. Shim, O. Y. Kwon, and J. H. Kang. Size-dependent effects of micro polystyrene particles in the marine copepod tigriopus japonicus. *Environ Sci Technol*, 47(19):11278–83, 2013.

[12] I. Paul-Pont, C. Lacroix, C. Gonzalez Fernandez, H. Hegaret, C. Lambert, N. Le Goic, L. Frere, A. L. Cassone, R. Sussarellu, C. Fabioux, J. Guyomarch, M. Albentosa, A. Huvet, and P. Soudant. Exposure of marine mussels Mytilus spp. to polystyrene microplastics: Toxicity and influence on fluoranthene bioaccumulation. *Environ Pollut*, 216:724–737, 2016.

[13] R. Sussarellu, M. Suquet, Y. Thomas, C. Lambert, C. Fabioux, M. E. J. Pernet, N. Le Goïc, V. Quillien, C. Mingant, Y. Epelboin, C. Corporeau, J. Guyomarch, J. Robbens, I. Paul-Pont, P. Soudant, and A. Huvet. Oyster reproduction is affected by exposure to polystyrene microplastics. *PNAS*, 113(9):2430–2435, 2016.

[14] H. W. Ng, M. Shu, H. Luo, H. Ye, W. Ge, R. Perkins, W. Tong, and H. Hong. Estrogenic activity data extraction and *in silico* prediction show the endocrine disruption potential of bisphenol A replacement compounds. *Chem Res Toxicol*, 28(9):1784–95, 2015.

[15] J. L. Lyche, A. C. Gutleb, A. Bergman, G. S. Eriksen, A. J. Murk, E. Ropstad, M. Saunders, and J. U. Skaare. Reproductive and developmental toxicity of phthalates. *J Toxicol Environ Health B Crit Rev*, 12(4):225–49, 2009.

[16] Q. Chen, A. Allgeier, D. Yin, and H. Hollert. Leaching of endocrine disrupting chemicals from marine microplastics and mesoplastics under common life stress conditions. *Environ Int*, 130:104938, 2019.

[17] C. J. Foley, Z. S. Feiner, T. D. Malinich, and T. O. Hook. A meta-analysis of the effects of exposure to microplastics on fish and aquatic invertebrates. *Sci Total Environ*, 631-632:550–559, 2018.

[18] C. Alomar, A. Sureda, X. Capo, B. Guijarro, S. Tejada, and S. Deudero. Microplastic ingestion by Mullus surmuletus linnaeus, 1758 fish and its potential for causing oxidative stress. *Environ Res*, 159:135–142, 2017.

[19] F. Murphy, M. Russell, C. Ewins, and B. Quinn. The uptake of macroplastic & microplastic by demersal & pelagic fish in the Northeast Atlantic around Scotland. *Mar Pollut Bull*, 122(1-2):353–359, 2017.

[20] M. A. Nadal, C. Alomar, and S. Deudero. High levels of microplastic ingestion by the semipelagic fish bogue Boops boops (L.) around the balearic islands. *Environ Pollut*, 214:517–523, 2016.

[21] K. Tanaka and H. Takada. Microplastic fragments and microbeads in digestive tracts of planktivorous fish from urban coastal waters. *Sci Rep*, 6:34351, 2016.

[22] A. L. Vendel, F. Bessa, V. E. N. Alves, A. L. A. Amorim, J. Patricio, and A. R. T. Palma. Widespread microplastic ingestion by fish assemblages in tropical estuaries subjected to anthropogenic pressures. *Mar Pollut Bull*, 117(1-2):448–455, 2017.

[23] R. H. Waring, R. M. Harris, and S. C. Mitchell. Plastic contamination of the food chain: A threat to human health? *Maturitas*, 115:64–68, 2018.

[24] S. Kim, J. Chen, T. Cheng, A. Gindulyte, J. He, S. He, Q. Li, B. A. Shoemaker, P. A. Thiessen, B. Yu, L. Zaslavsky, J. Zhang, and E. E. Bolton. Pubchem 2019 update: improved access to chemical data. *Nucleic Acids Res*, 47(D1):D1102–D1109, 2019.

[25] H. M. Berman, J. Westbrook, Z. Feng, G. Gilliland, T. N. Bhat, H. Weissig, I. N. Shindyalov, and P. E. Bourne. The protein data bank. *Nucleic Acids Research*, 28(1):235–242, 2000.

[26] J. D. Stender, J. C. Nwachukwu, I. Kastrati, Y. Kim, T. Strid, M. Yakir, S. Srinivasan, J. Nowak, T. Izard, E. S. Rangarajan, K. E. Carlson, J. A. Katzenellenbogen, X. Q. Yao, B. J. Grant, H. S. Leong, C. Y. Lin, J. Frasor, K. W. Nettles, and C. K. Glass. Structural and molecular mechanisms of cytokine-mediated endocrine resistance in human breast cancer cells. *Mol Cell*, 65(6):1122–1135 e5, 2017.

[27] G. M. Morris, R. Huey, W. Lindstrom, M. F. Sanner, R. K. Belew, D. S. Goodsell, and A. J. Olson. AutoDock4 and AutoDockTools4: Automated docking with selective receptor flexibility. *J Comput Chem*, 30(16):2785–91, 2009.

[28] W. Humphrey, A. Dalke, and K. Schulten. VMD: Visual molecular dynamics. *J. Mol. Graphics.*, 14:33–38, 1996.

[29] M. Böckers, N. W. Paul, and T. Efferth. Bisphenolic compounds alter gene expression in MCF-7 cells through interaction with estrogen receptor α. *Toxicol Appl Pharmacol.*, 399:115030, 2020.

[30] H. Webb, J. Arnott, R. Crawford, and E. Ivanova. Plastic degradation and its environmental implications with special reference to poly(ethylene terephthalate). *Polymers*, 5(1):1–18, 2012.

[31] L. Lebreton, B. Slat, F. Ferrari, B. Sainte-Rose, J. Aitken, R. Marthouse, S. Hajbane, S. Cunsolo, A. Schwarz, A. Levivier, K. Noble, P. Debeljak, H. Maral, R. Schoeneich-Argent, R. Brambini, and J. Reisser. Evidence that the great pacific garbage patch is rapidly accumulating plastic. *Sci Rep*, 8(1):4666, 2018.

[32] J. E. Cooper, E. L. Kendig, and S. M. Belcher. Assessment of bisphenol A released from reusable plastic, aluminium and stainless steel water bottles. *Chemosphere*, 85(6):943–7, 2011.

[33] R. E. Engler. The complex interaction between marine debris and toxic chemicals in the ocean. *Environ Sci Technol*, 46(22):12302–15, 2012.

[34] D. Lithner, A. Larsson, and G. Dave. Environmental and health hazard ranking and assessment of plastic polymers based on chemical composition. *Sci Total Environ*, 409(18):3309–24, 2011.

[35] J. Michalowicz. Bisphenol A–sources, toxicity and biotransformation. *Environ Toxicol Pharmacol*, 37(2):738–58, 2014.

[36] P. Alonso-Magdalena, A. B. Ropero, S. Soriano, M. Garcia-Arevalo, C. Ripoll, E. Fuentes, I. Quesada, and A. Nadal. Bisphenol-A acts as a potent estrogen via non-classical estrogen triggered pathways. *Mol Cell Endocrinol*, 355(2):201–7, 2012.

[37] J. H. Kang, F. Kondo, and Y. Katayama. Human exposure to bisphenol A. *Toxicology*, 226(2-3):79–89, 2006.

[38] L. Y. Cao, X. M. Ren, C. H. Li, J. Zhang, W. P. Qin, Y. Yang, B. Wan, and L. H. Guo. Bisphenol AF and bisphenol B exert higher estrogenic effects than bisphenol A via G protein-coupled estrogen receptor pathway. *Environ Sci Technol*, 51(19):11423–11430, 2017.

[39] L. Grumetto, D. Montesano, S. Seccia, S. Albrizio, and F. Barbato. Determination of Bisphenol A and Bisphenol B residues in canned peeled tomatoes by reversed-phase liquid chromatography. *J. Agric. Food Chem*, 56(22):10633–10637, 2008.

[40] D. Chen, K. Kannan, H. Tan, Z. Zheng, Y. L. Feng, Y. Wu, and M. Widelka. Bisphenol analogues other than BPA: Environmental occurrence, human exposure, and toxicity-a review. *Environ Sci Technol*, 50(11):5438–53, 2016.

[41] O. Keminer, M. Teigeler, M. Kohler, A. Wenzel, J. Arning, F. Kaßner, B. Windshügel, and E. Eilebrecht. A tiered high-throughput screening approach for evaluation of estrogen and androgen receptor modulation by environmentally relevant bisphenol A substitutes. *Science of The Total Environment*, page 134743, 2019.

[42] S. Berthumeyrie, A. Colin, C. Esparcieux, M. Baba, F. Catalina, P.-O. Bussiere, and S. Therias. Photodegradation of tetramethylpolycarbonate (TMPC): Correlation of properties with chemical modifications. *Polymer Degradation and Stability*, 98(10):2081–2088, 2013.

[43] X. C. Chen and P. F. Green. Structure of thin film polymer/nanoparticle systems: polystyrene (PS) coated-au nanoparticle/tetramethyl bisphenol-A polycarbonate mixtures (TMPC). *Soft Matter*, 7(3):1192–1198, 2011.

[44] H. Yoshimizu, T. Murakami, T. Suzuki, and Y. Tsujita. Characterization of the microvoids of a tetramethyl polycarbonate/polystyrene blend system using Xe sorption measurements and 129Xe NMR spectroscopy. *Polymer Journal*, 44(8):827–831, 2012.

[45] R. Lenz, K. Enders, and T. G. Nielsen. Microplastic exposure studies should be environmentally realistic. *Proc Natl Acad Sci U S A*, 113(29):E4121–2, 2016.

[46] R. T. Zoeller, T. R. Brown, L. L. Doan, A. C. Gore, N. E. Skakkebaek, A. M. Soto, T. J. Woodruff, and F. S. Vom Saal. Endocrine-disrupting chemicals and public health protection: a statement of principles from the endocrine society. *Endocrinology*, 153(9):4097–110, 2012.

[47] G. Mileva, S. L. Baker, A. T. Konkle, and C. Bielajew. Bisphenol-A: epigenetic reprogramming and effects on reproduction and behavior. *Int J Environ Res Public Health*, 11(7):7537–61, 2014.

[48] C. M. Klinge. Estrogen receptor interaction with co-activators and co-repressors. *Steroids*, 65(5):227–251, 2000.

[49] P. La Rosa, M. Pellegrini, P. Totta, F. Aconcia, and M. Marino. Xenoestrogens alter estrogen receptor (ER) α intracellular levels. *PLoS ONE*, 9(2), 2014.

[50] A. Sett, B. B. Borthakur, J. D. Sharma, A. C. Kataki, and U. Bora. DNA aptamer probes for detection of estrogen receptor α positive carcinomas. *Transl Res*, 183:104–120 e2, 2017.

[51] J. A. Gustafsson. Estrogen receptor β - a new dimension in estrogen mechanism of action. *J Endocrinol*, 163:379–383, 1999.

[52] M. Jia, K. Dahlman-Wright, and J. A. Gustafsson. Estrogen receptor alpha and beta in health and disease. *Best Pract Res Clin Endocrinol Metab*, 29(4):557–68, 2015.

[53] I. Paterni, C. Granchi, J. A. Katzenellenbogen, and F. Minutolo. Estrogen receptors alpha (ERα) and beta (ERβ): subtype-selective ligands and clinical potential. *Steroids*, 90:13–29, 2014.

[54] J.-F. Arnal, F. Lenfant, R. Metivier, G. Flouriot, D. Henrion, M. Adlanmerini, C. Fontaine, P. Gourdy, P. Chambon, B. Katzenellenbogen, and J. Katzenellenbogen. Membrane and nuclear estrogen receptor alpha actions: From tissue specificity to medical implications. *Physiol Rev*, 97(3):1045–1087, 2017.

[55] B.S. Katzenellenbogen and J.A. Katzenellenbogen. Estrogen receptor transcription and transactivation estrogen receptor alpha and estrogen receptor beta: regulation by selective estrogen receptor modulators and importance in breast cancer. *Breast Cancer Res*, 2:335–344, 2000.

[56] H. Ye, S. Z. Dudley, and I. C. Shaw. Intimate estrogen receptor-α/ligand relationships signal biological activity. *Toxicology*, 408:80–87, 2018.

[57] M. Marino, P. Galluzzo, and P. Ascenzi. Estrogen signaling multiple pathways to impact gene transcription. *Current Genomics*, 7(8):497–508, 2006.

[58] K. A. Burns, Y. Li, Y. Arao, R. M. Petrovich, and K. S. Korach. Selective mutations in estrogen receptor α D-domain alters nuclear translocation and non-estrogen response element gene regulatory mechanisms. *J Biol Chem*, 286(14):12640–9, 2011.

[59] L. Celik, J. D. Dalsgaard Lund, and B. Schiøtt. Exploring interactions of endocrine-disrupting compounds with different conformations of the human estrogen receptor α ligand binding domain: A molecular docking study. *Chem. Res. Toxicol.*, 21(11):2195–2206, 2008.

[60] N. Sharma, K. E. Carlson, J. C. Nwachukwu, S. Srinivasan, A. Sharma, K. W. Nettles, and J. A. Katzenellenbogen. Exploring the structural compliancy versus specificity of the estrogen receptor using isomeric three-dimensional ligands. *ACS Chem Biol*, 12(2):494–503, 2017.

[61] R. N. Hanson, E. McCaskill, P. Tongcharoensirikul, R. Dilis, D. Labaree, and R. B. Hochberg. Synthesis and evaluation of 17α-(dimethylphenyl)vinyl estradiols as probes of the estrogen receptor-α ligand binding domain. *Steroids*, 77(5):471–6, 2012.

[62] C. Berger, Y. Qian, and X. Chen. The p53-estrogen receptor loop in cancer. *Curr Mol Med*, 13(8):1229–40, 2013.

[63] K. Milde-Langosch, H. Röder, B. Andritzky, B. Aslan, G. Hemminger, A. Brinkmann, C.M. Bamberger, T. Löning, and A-M. Bamberger. The role of the AP-1 transcription factors c-Fos, FosB, Fra-1 and Fra-2 in the invasion process of mammary carcinomas. *Breast Cancer Res Treat*, 86:139–152, 2004.

[64] C. Schröder, U. Schumacher, V. Muller, R. M. Wirtz, T. Streichert, U. Richter, D. Wicklein, and K. Milde-Langosch. The transcription factor Fra-2 promotes mammary tumour progression by changing the adhesive properties of breast cancer cells. *Eur J Cancer*, 46(9):1650–60, 2010.

[65] T. L. McCarthy, W. Z. Chang, Y. Liu, and M. Centrella. Runx2 integrates estrogen activity in osteoblasts. *J Biol Chem*, 278(44):43121–9, 2003.

[66] M. Vishal, R. Swetha, G. Thejaswini, B. Arumugam, and N. Selvamurugan. Role of Runx2 in breast cancer-mediated bone metastasis. *Int J Biol Macromol*, 99:608–614, 2017.

[67] Q. Deng, J. Hou, L. Feng, A. Lv, X. Ke, H. Liang, F. Wang, K. Zhang, K. Chen, and H. Cui. PHF19 promotes the proliferation, migration, and chemosensitivity of glioblastoma to doxorubicin through modulation of the SIAH1/β-catenin axis. *Cell Death Dis*, 9(11):1049, 2018.

[68] M. Sauvageau and G. Sauvageau. Polycomb group proteins: multi-faceted regulators of somatic stem cells and cancer. *Cell Stem Cell*, 7(3):299–313, 2010.

[69] A. E. Gururaj, R. R. Singh, S. K. Rayala, C. Holm, P. den Hollander, H. Zhang, S. Balasenthil, A. H. Talukder, G. Landberg, and R. Kumar. MTA1, a transcriptional activator of breast cancer amplified sequence 3. *Proc Natl Acad Sci U S A*, 103(17):6670–5, 2006.

[70] K. Ohshiro and R. Kumar. Evolving pathway-driven biomarkers in breast cancer. *Expert Opinion on Investigational Drugs*, 19:sup1:S51–S56, 2010.

[71] D. C. Allred. Issues and updates: evaluating estrogen receptor-α, progesterone receptor, and HER2 in breast cancer. *Mod Pathol*, 23 Suppl 2:S52–9, 2010.

[72] V. J. Bardou, G. Arpino, R. M. Elledge, C. K. Osborne, and G. M. Clark. Progesterone receptor status significantly improves outcome prediction over estrogen receptor status alone for adjuvant endocrine therapy in two large breast cancer databases. *J Clin Oncol*, 21(10):1973–9, 2003.

[73] J. Yang, Y. Zhang, J. Tong, H. Lv, C. Zhang, and Z. J. Chen. Dysfunction of DNA damage-inducible transcript 4 in the decidua is relevant to the pathogenesis of preeclampsia. *Biol Reprod*, 98(6):821–833, 2018.

[74] Q. Zhou, J. K. Hahn, B. Neupane, P. Aidery, S. Labeit, M. Gawaz, and M. Gramlich. Dysregulated IER3 expression is associated with enhanced apoptosis in titin-based dilated cardiomyopathy. *Int J Mol Sci*, 18(4), 2017.

[75] H. H. Kampinga, J. Hageman, M. J. Vos, H. Kubota, R. M. Tanguay, E. A. Bruford, M. E. Cheetham, B. Chen, and L. E. Hightower. Guidelines for the nomenclature of the human heat shock proteins. *Cell Stress Chaperones*, 14(1):105–11, 2009.

[76] B. De Servi, A. Hermani, S. Medunjanin, and D. Mayer. Impact of PKC δ on estrogen receptor localization and activity in breast cancer cells. *Oncogene*, 24(31):4946–55, 2005.

[77] Y. Huang, Z. Dai, C. Barbacioru, and W. Sadee. Cystine-glutamate transporter SLC7A11 in cancer chemosensitivity and chemoresistance. *Cancer Res*, 65(16):7446–54, 2005.

[78] P. Koppula, Y. Zhang, L. Zhuang, and B. Gan. Amino acid transporter SLC7A11/xCT at the crossroads of regulating redox homeostasis and nutrient dependency of cancer. *Cancer Commun (Lond)*, 38(1):12, 2018.

[79] F. Verrey, E. I. Closs, C. A. Wagner, M. Palacin, H. Endou, and Y. Kanai. CATs and HATs: the SLC7 family of amino acid transporters. *Pflugers Arch*, 447(5):532–42, 2004.

[80] Z. Lin, P. Yin, S. Reierstad, M. O'Halloran, V. J. Coon, E. K. Pearson, G. M. Mutlu, and S. E. Bulun. Adenosine A1 receptor, a target and regulator of estrogen receptorα action, mediates the proliferative effects of estradiol in breast cancer. *Oncogene*, 29(8):1114–22, 2010.

[81] Z. Qiao, Y. Jiang, L. Wang, L. Wang, J. Jiang, and J. Zhang. Mutations in KIAA1109, CACNA1C, BSN, AKAP13, CELSR2, and HELZ2 are associated with the prognosis in endometrial cancer. *Front Genet*, 10:909, 2019.

[82] J.B. Vincent, J. Skaug, and W. Scherer. The human homologue of flamingo, EGFL2, encodes a brain-expressed large cadherin-like protein with epidermal growth factor-like domains, and maps to chromosome 1p13.3-p21.1. *DNA Research*, 7:233–235, 2000.

[83] D. H. Fagan and D. Yee. Crosstalk between IGF1R and estrogen receptor signaling in breast cancer. *J Mammary Gland Biol Neoplasia*, 13(4):423–9, 2008.

[84] A. V. Lee, J. G. Jackson, J. L. Gooch, S. G. Hilsenbeck, E. Coronado-Heinsohn, C. K. Osborne, and D. Yee. Enhancement of insulin-like growth factor signaling in human breast cancer: Estrogen regulation of insulin receptor substrate-1 expression *in vitro* and *in vivo*. *Molecular Endocrinology*, 13(5):787–796, 1999.

[85] J. Riedemann and V. M. Macaulay. IGF1R signalling and its inhibition. *Endocr Relat Cancer*, 13 Suppl 1:S33–43, 2006.

[86] J.Ph. Peyrat and J. Bonneterre. Type 1 IGF receptor in human breast disease. *Breast Cancer Res Tr*, 22:59–67, 1992.

[87] S. J. Chu, J. Zhang, R. Zhang, W. W. Lu, and J. S. Zhu. Evolution and functions of stanniocalcins in cancer. *Int J Immunopathol Pharmacol*, 28(1):14–20, 2015.

[88] Y. Wang, Y. Gao, H. Cheng, G. Yang, and W. Tan. Stanniocalcin 2 promotes cell proliferation and cisplatin resistance in cervical cancer. *Biochem Biophys Res Commun*, 466(3):362–8, 2015.

[89] J. R. Conner, II Smirnova, A. P. Moseman, and A. Poltorak. IRAK1BP1 inhibits inflammation by promoting nuclear translocation of NF-kappaB p50. *Proc Natl Acad Sci U S A*, 107(25):11477–82, 2010.

[90] J. R. Conner, II Smirnova, and A. Poltorak. Forward genetic analysis of toll-like receptor responses in wild-derived mice reveals a novel antiinflammatory role for IRAK1BP1. *J Exp Med*, 205(2):305–14, 2008.

[91] A. J. C. Quaresma, A. Bugai, and M. Barboric. Cracking the control of RNA polymerase II elongation by 7SK snRNP and P-TEFb. *Nucleic Acids Res*, 44(16):7527–39, 2016.

[92] S. Eilebrecht, G. Brysbaert, T. Wegert, H. Urlaub, B. J. Benecke, and A. Benecke. 7SK small nuclear RNA directly affects HMGA1 function in transcription regulation. *Nucleic Acids Res*, 39(6):2057–72, 2011.

[93] Z. Bazi, M. Bertacchi, M. Abasi, S. Mohammadi-Yeganeh, M. Soleimani, N. Wagner, and H. Ghanbarian. Rn7SK small nuclear RNA is involved in neuronal differentiation. *J Cell Biochem*, 119(4):3174–3182, 2018.

[94] Y. Zhang and L. Tang. Inhibition of breast cancer cell proliferation and tumorigenesis by long non-coding RNA RPPH1 down-regulation of mir-122 expression. *Cancer Cell Int*, 17:109, 2017.

[95] Y. Cai, Z. Sun, H. Jia, H. Luo, X. Ye, Q. Wu, Y. Xiong, W. Zhang, and J. Wan. Rpph1 upregulates CDC42 expression and promotes hippocampal neuron dendritic spine formation by competing with miR-330-5p. *Front Mol Neurosci*, 10:27, 2017.

[96] T. Xia, Q. Liao, X. Jiang, Y. Shao, B. Xiao, Y. Xi, and J. Guo. Long noncoding RNA associated-competing endogenous RNAs in gastric cancer. *Sci Rep*, 4:6088, 2014.

[97] G.M. Ku, Z. Pappalardo, C.C. Luo, M.S. German, and M.T. McManus. An siRNA screen in pancreatic beta cells reveals a role for Gpr27 in insulin production. *PLOS Genet*, 8(1), 2012.

[98] N. Li, J. Zheng, H. Li, J. Deng, M. Hu, H. Wu, W. Li, F. Li, X. Lan, J. Lu, and Y. Zhou. Identification of chimeric TSNAX-DISC1 resulting from intergenic splicing in endometrial carcinoma through high-throughput RNA sequencing. *Carcinogenesis*, 35(12):2687–97, 2014.

[99] Q. Y. Ma, L. W. Pang, Z. M. Chen, Y. J. Zhu, G. Chen, and J. Chen. The significance of MAGED4 expression in non-small cell lung cancer as analyzed by real-time fluorescence quantitative PCR. *Oncol Lett*, 4(4):733–738, 2012.

[100] B. F. Kramer, O. Schoor, T. Kruger, C. Reichle, M. Muller, T. Weinschenk, J. Hennenlotter, A. Stenzl, H. G. Rammensee, and S. Stevanovic. MAGED4-expression in renal cell carcinoma and identification of an HLA-A*25-restricted MHC class I ligand from solid tumor tissue. *Cancer Biol Ther*, 4(9):943–8, 2005.

[101] C-T. Huang, G-C. Huang, P-S. Wu, L-W. Wu, S-H. Lin, W-W. Lai, Y-C. Wang, and H-S. Liu. Significance of migration-related genes (S100A9, MAGED4, C8orf30A, IL-8) in esophageal squamous cell carcinoma. *Genomic Medicine, Biomarkers, and Health Sciences*, 4(1-2):16–18, 2012.

[102] X. Wang, M. Ria, P. M. Kelmenson, P. Eriksson, D. C. Higgins, A. Samnegard, C. Petros, J. Rollins, A. M. Bennet, B. Wiman, U. de Faire, C. Wennberg, P. G. Olsson, N. Ishii, K. Sugamura, A. Hamsten, K. Forsman-Semb, J. Lagercrantz, and B. Paigen. Positional identification of TNFSF4, encoding OX40 ligand, as a gene that influences atherosclerosis susceptibility. *Nat Genet*, 37(4):365–72, 2005.

[103] A. Allen, D. A. Hutton, and J. P. Pearson. The MUC2 gene product: a human intestinal mucin. *Int J Biochem Cell Biol*, 30:797–801, 1998.

[104] E. A. Rakha, R. W. Boyce, D. Abd El-Rehim, T. Kurien, A. R. Green, E. C. Paish, J. F. Robertson, and I. O. Ellis. Expression of mucins (MUC1, MUC2, MUC3, MUC4, MUC5AC and MUC6) and their prognostic significance in human breast cancer. *Mod Pathol*, 18(10):1295–304, 2005.

[105] L.K. Diaz, E.L. Wiley, and M. Morrow. Expression of epithelial mucins MUC1, MUC2, and MUC3 in ductal carcinoma in situ of the breast. *The Breast Journal*, 7:40–45, 2001.

[106] M. D. Walsh, M. A. McGuckin, P. L. Devine, B. G. Hohn, and R. G. Wright. Expression of MUC2 epithelial mucin in breast carcinoma. *J clin Pathol*, 46:922–925, 1993.

[107] C. Y. Ying, D. Dominguez-Sola, M. Fabi, I. C. Lorenz, S. Hussein, M. Bansal, A. Califano, L. Pasqualucci, K. Basso, and R. Dalla-Favera. MEF2B mutations lead to deregulated expression of the oncogene BCL6 in diffuse large B cell lymphoma. *Nat Immunol*, 14(10):1084–92, 2013.

[108] N. M. Soldatov. CACNB2: An emerging pharmacological target for hypertension, heart failure, arrhythmia and mental disorders. *Current Molecular Pharmacology*, 8(1):32–42, 2015.

[109] V. Durairaj Pandian, D. R. Giovannucci, G. Vazquez, and S. Kumarasamy. CACNB2 is associated with aberrant RAS-MAPK signaling in hypertensive dahl salt-sensitive rats. *Biochem Biophys Res Commun*, 513(3):760–765, 2019.

[110] P. F. Zhang, J. Wu, Y. Wu, W. Huang, M. Liu, Z. R. Dong, B. Y. Xu, Y. Jin, F. Wang, and X. M. Zhang. The lncRNA SCARNA2 mediates colorectal cancer chemoresistance through a conserved microRNA-342-3p target sequence. *J Cell Physiol*, 234(7):10157–10165, 2019.

[111] E. J. Choi, J. A. Yun, S. Jabeen, E. K. Jeon, H. S. Won, Y. H. Ko, and S. Y. Kim. Prognostic significance of TMEM16A, PPFIA1, and FADD expression in invasive ductal carcinoma of the breast. *World J Surg Oncol*, 12:137, 2014.

[112] V. Astro, C. Asperti, M. G. Cangi, C. Doglioni, and I. de Curtis. Liprin-α1 regulates breast cancer cell invasion by affecting cell motility, invadopodia and extracellular matrix degradation. *Oncogene*, 30(15):1841–9, 2011.

[113] M. Sugiyama, A. Kikuchi, H. Misu, H. Igawa, M. Ashihara, Y. Kushima, K. Honda, Y. Suzuki, Y. Kawabe, S. Kaneko, and T. Takamura. Inhibin βE (INHBE) is a possible insulin resistance-associated hepatokine identified by comprehensive gene expression analysis in human liver biopsy samples. *PLOS ONE*, 13(3):e0194798, 2018.

[114] A. J. Schindler, A. Watanabe, and S. B. Howell. LGR5 and LGR6 in stem cell biology and ovarian cancer. *Oncotarget*, 9(1):1346–1355, 2017.

[115] J. Ke, P. Ma, J. Chen, J. Qin, and H. Qian. LGR6 promotes the progression of gastric cancer through PI3K/AKT/mTOR pathway. *Onco Targets Ther*, 11:3025–3033, 2018.

[116] N. Zhang, X.-M. Zhou, F.-F. Yang, Q. Zhang, Y. Miao, and G. Hou. FAM129A promotes invasion and proliferation by activating FAK signaling pathway in non-small cell lung cancer. *Int J Clin Exp Pathol*, 12(3):893–900, 2019.

[117] Z.Q. Wang, A. Faddaoui, M. Bachvarova, M. Plante, J. Gregoire, M.C. Renaud, A. Sebastianelli, C. Guillemette, S. Gobeil, E. Macdonald, B. Vanderhyden, and D. Bachvarov. BCAT1 expression associates with ovarian cancer progression: possible implications in altered disease metabolism. *Oncotarget*, 6(31):31522–31543, 2015.

[118] L. Zhang and J. Han. Branched-chain amino acid transaminase 1 (BCAT1) promotes the growth of breast cancer cells through improving mTOR-mediated mitochondrial biogenesis and function. *Biochem Biophys Res Commun*, 486(2):224–231, 2017.

[119] W. Zhou, X. Feng, C Ren, X. Jian, W. Liu, W. Huang, Z. Liu, Z. Li, L. Zeng, L. Wang, B. Zhu, J. Shi, J. Liu, C. Zhang, Y. Liu, and K. Yao. Over-expression of BCAT1, a c-Myc target gene, induces cell proliferation, migration and invasion in nasopharyngeal carcinoma. *Mol Cancer*, 12(53), 2013.

[120] G. Jeong, H. Bae, D. Jeong, J. Ham, S. Park, H. W. Kim, H. S. Kang, and S. J. Kim. A kelch domain-containing KLHDC7B and a long non-coding RNA ST8SIA6-AS1 act oppositely on breast cancer cell proliferation via the interferon signaling pathway. *Sci Rep*, 8(1):12922, 2018.

[121] T. W. Kim, Y. J. Kim, H. J. Lee, S. Y. Min, H. S. Kang, and S. J. Kim. Hs.137007 is a novel epigenetic marker hypermethylated and up-regulated in breast cancer. *Int J Oncol*, 36(5):1105–11, 2010.

[122] A. Careghini, A. F. Mastorgio, S. Saponaro, and E. Sezenna. Bisphenol A, nonylphenols, benzophenones, and benzotriazoles in soils, groundwater, surface water, sediments, and food: a review. *Environ Sci Pollut Res Int*, 22(8):5711–5741, 2015.

[123] J. Corrales, L. A. Kristofco, W. B. Steele, B. S. Yates, C. S. Breed, E. S. Williams, and B. W. Brooks. Global assessment of bisphenol A in the environment: Review and analysis of its occurrence and bioaccumulation. *Dose-response*, 13(3):1–29, 2015.

[124] EFSA CEF Panel. Scientific opinion on the risks to public health related to the presence of bisphenol A (BPA) in foodstuffs: Executive summary. *EFSA J.*, 13(1):3978, 2015.

[125] L.G.A. Barboza, A.D. Vethaak, B.R.B.O. Lavorante, A-K. Lundebye, and L. Guilhermino. Marine microplastic debris: An emerging issue for food security, food safety and human health. *Mar Pollut Bull*, 133:336–348, 2018.

[126] S. Rist, B. Carney Almroth, N. B. Hartmann, and T. M. Karlsson. A critical perspective on early communications concerning human health aspects of microplastics. *Sci Total Environ*, 626:720–726, 2018.

[127] S. Sharma and S. Chatterjee. Microplastic pollution, a threat to marine ecosystem and human health: a short review. *Environ Sci Pollut Res Int*, 24(27):21530–21547, 2017.

[128] M. Smith, D. C. Love, C. M. Rochman, and R. A. Neff. Microplastics in seafood and the implications for human health. *Curr Environ Health Rep*, 5(3):375–386, 2018.

[129] M. Bocqué, C. Voirin, V. Lapinte, S. Caillol, and J.-J. Robin. Petro-based and bio-based plasticizers: Chemical structures to plasticizing properties. *Journal of Polymer Science Part A: Polymer Chemistry*, 54(1):11–33, 2016.

[130] U. Heudorf, V. Mersch-Sundermann, and J. Angerer. Phthalates: toxicology and exposure. *Int J Hyg Environ Health*, 210(5):623–34, 2007.

[131] C. Köksal, A. Nalbantsoy, and N. Ü. Karabay Yavasoglu. Cytotoxicity and genotoxicity of butyl cyclohexyl phthalate. *Cytotechnology*, 68(2):213–22, 2016.

[132] A. Paluselli, V. Fauvelle, F. Galgani, and R. Sempere. Phthalate release from plastic fragments and degradation in seawater. *Environ Sci Technol*, 53(1):166–175, 2019.

[133] O. Herrero, R. Planello, and G. Morcillo. The plasticizer benzyl butyl phthalate (BBP) alters the ecdysone hormone pathway, the cellular response to stress, the energy metabolism, and several detoxication mechanisms in chironomus riparius larvae. *Chemosphere*, 128:266–77, 2015.

[134] R. Mankidy, S. Wiseman, H. Ma, and J. P. Giesy. Biological impact of phthalates. *Toxicol Lett*, 217(1):50–8, 2013.

[135] T. Schettler. Human exposure to phthalates via consumer products. *Int J Androl*, 29(1):134–9.

[136] S. Cui, L. Wang, H. Zhao, F. Lu, W. Wang, and Z. Yuan. Benzyl butyl phthalate (BBP) triggers the migration and invasion of hemangioma cells via upregulation of Zeb1. *Toxicol In Vitro*, 60:323–329, 2019.

[137] N. Ü. Yavasoglu, C. Köksal, M. Dagdeviren, H. Aktug, and A. Yavasoglu. Induction of oxidative stress and histological changes in liver by subacute doses of butyl cyclohexyl phthalate. *Environ Toxicol*, 29(3):345–53, 2012.

[138] M. Matsumoto, M. Hirata-Koizumi, and M. Ema. Potential adverse effects of phthalic acid esters on human health: a review of recent studies on reproduction. *Regul Toxicol Pharmacol*, 50(1):37–49, 2008.

[139] N. P. Moore. The oestrogenic potential of the phthalate esters. *Reproductive Toxicology*, 14(3):183–192, 2000.

[140] E. K. Shanle and W. Xu. Endocrine disrupting chemicals targeting estrogen receptor signaling: Identification and mechanisms of action. *Chem. Res. Toxicol.*, 24(1):6–19, 2011.

[141] O. Yang, H. L. Kim, J. I. Weon, and Y. R. Seo. Endocrine-disrupting chemicals: Review of toxicological mechanisms using molecular pathway analysis. *J Cancer Prev*, 20(1):12–24, 2015.

[142] G. Castoria, A. Migliaccio, P. Giovannelli, and F. Auricchio. Cell proliferation regulated by estradiol receptor: Therapeutic implications. *Steroids*, 75(8-9):524–7, 2010.

[143] R. Jäger, N. Friedrichs, I. Heim, R. Büttner, and H. Schorle. Dual role of AP-2γ in ErbB-2-induced mammary tumorigenesis. *Breast Cancer Res Treat*, 90:273–280, 2005.

[144] J. M. Pellikainen and V. M. Kosma. Activator protein-2 in carcinogenesis with a special reference to breast cancer–a mini review. *Int J Cancer*, 120(10):2061–7, 2007.

[145] P. P. Wong, F. Miranda, K. V. Chan, C. Berlato, H. C. Hurst, and A. G. Scibetta. Histone demethylase KDM5B collaborates with TFAP2C and Myc to repress the cell cycle inhibitor p21(cip) (CDKN1A). *Mol Cell Biol*, 32(9):1633–44, 2012.

[146] E. Rosonina, J. Y. Ip, J. A. Calarco, M. A. Bakowski, A. Emili, S. McCracken, P. Tucker, C. J. Ingles, and B. J. Blencowe. Role for PSF in mediating transcriptional activator-dependent stimulation of pre-mRNA processing in vivo. *Mol Cell Biol*, 25(15):6734–46, 2005.

[147] Y. Tao, C. Ma, Q. Fan, Y. Wang, T. Han, and C. Sun. MicroRNA-1296 facilitates proliferation, migration and invasion of colorectal cancer cells by targeting SFPQ. *J Cancer*, 9(13):2317–2326, 2018.

[148] G. Wang, Y. Cui, G. Zhang, A. Garen, and X. Song. Regulation of proto-oncogene transcription, cell proliferation, and tumorigenesis in mice by PSF protein and a VL30 noncoding RNA. *Proc Natl Acad Sci U S A*, 106(39):16794–8, 2009.

[149] B. K. Ward, P. J. Mark, D. M. Ingram, R. F. Minchin, and T. Ratajczak. Expression of the estrogen receptor-associated immunophilins, cyclophilin 40 and FKBP52, in breast cancer. *Breast Cancer Res Treat*, 58:265–280, 1999.

[150] W. S. Yang, H. G. Moon, H. S. Kim, E. J. Choi, M. H. Yu, D. Y. Noh, and C. Lee. Proteomic approach reveals FKBP4 and S100A9 as potential prediction markers of therapeutic response to neoadjuvant chemotherapy in patients with breast cancer. *J Proteome Res*, 11(2):1078–88, 2012.

[151] A. R. Daniel, C. R. Hagan, and C. A. Lange. Progesterone receptor action: defining a role in breast cancer. *Expert Review of Endocrinology & Metabolism*, 6(3):359–369, 2011.

[152] M. R. Boland, E. J. Ryan, E. Dunne, T. M. Aherne, N. R. Bhatt, and A. J. Lowery. Meta-analysis of the impact of progesterone receptor status on oncological outcomes in oestrogen receptor-positive breast cancer. *Br J Surg*, 107(1):33–43, 2020.

[153] Z. Cheng, Y. Dai, Y. Pang, Y. Jiao, Y. Liu, L. Cui, L. Quan, T. Qian, T. Zeng, C. Si, W. Huang, J. Chen, Y. Pang, X. Ye, J. Shi, and L. Fu. Up-regulation of DDIT4 predicts poor prognosis in acute myeloid leukaemia. *J Cell Mol Med*, 24(1):1067–1075, 2020.

[154] F. Du, L. Sun, Y. Chu, T. Li, C. Lei, X. Wang, M. Jiang, Y. Min, Y. Lu, X. Zhao, Y. Nie, and D. Fan. DDIT4 promotes gastric cancer proliferation and tumorigenesis through the p53 and MAPK pathways. *Cancer Commun (Lond)*, 38(1):45, 2018.

[155] I. Tirado-Hurtado, W. Fajardo, and J. A. Pinto. DNA damage inducible transcript 4 gene: The switch of the metabolism as potential target in cancer. *Front Oncol*, 8:106, 2018.

[156] A. Arlt and H. Schäfer. Role of the immediate early response 3 (IER3) gene in cellular stress response, inflammation and tumorigenesis. *Eur J Cell Biol*, 90(6-7):545–52, 2011.

[157] H. Jin, D. S. Suh, T. H. Kim, J. H. Yeom, K. Lee, and J. Bae. IER3 is a crucial mediator of TAp73β-induced apoptosis in cervical cancer and confers etoposide sensitivity. *Sci Rep*, 5:8367, 2015.

[158] D. W. Nebert, T. P. Dalton, A. B. Okey, and F. J. Gonzalez. Role of aryl hydrocarbon receptor-mediated induction of the CYP1 enzymes in environmental toxicity and cancer. *J Biol Chem*, 279(23):23847–50, 2004.

[159] T. Shimada and Y. Fujii-Kuriyama. Metabolic activation of polycyclic aromatic hydrocarbons to carcinogens by cytochromes P450 1A1 and 1B1. *Cancer Science*, 95(1):1–6, 2004.

[160] Y. D. Bhutia, E. Babu, S. Ramachandran, and V. Ganapathy. Amino acid transporters in cancer and their relevance to "glutamine addiction": novel targets for the design of a new class of anticancer drugs. *Cancer Res*, 75(9):1782–8, 2015.

[161] Y. J. Cha, E. S. Kim, and J. S. Koo. Amino acid transporters and glutamine metabolism in breast cancer. *Int J Mol Sci*, 19(3), 2018.

[162] J. Zhou, X. Fan, N. Chen, F. Zhou, J. Dong, Y. Nie, and D. Fan. Identification of CEACAM5 as a biomarker for prewarning and prognosis in gastric cancer. *J Histochem Cytochem*, 63(12):922–30, 2015.

[163] M. J. Duffy. Carcinoembryonic antigen as a marker for colorectal cancer: Is it clinically useful? *Clinical Chemistry*, 47(4):624–630, 2001.

[164] Z. Lin, S. Li, C. Feng, S. Yang, H. Wang, D. Ma, J. Zhang, M. Gou, D. Bu, T. Zhang, X. Kong, X. Wang, O. Sarig, Y. Ren, L. Dai, H. Liu, J. Zhang, F. Li, Y. Hu, G. Padalon-Brauch, D. Vodo, F. Zhou, T. Chen, H. Deng, E. Sprecher, Y. Yang, and X. Tan. Stabilizing mutations of KLHL24 ubiquitin ligase cause loss of keratin 14 and human skin fragility. *Nat Genet*, 48(12):1508–1516, 2016.

[165] M. C. Bolling and M. F. Jonkman. KLHL24: Beyond skin fragility. *J Invest Dermatol*, 139(1):22–24, 2019.

[166] T. Bouras, M. C. Southey, A. C. Chang, R. R. Reddel, D. Willhite, R. Glynne, M. A. Henderson, J. E. Armes, and D. J. Venter. Stanniocalcin 2 is an estrogen-responsive gene coexpressed with the estrogen receptor in human breast cancer. *Cancer Res*, 62(5):1289–1295, 2002.

[167] S. Esseghir, A. Kennedy, P. Seedhar, A. Nerurkar, R. Poulsom, J. S. Reis-Filho, and C. M. Isacke. Identification of NTN4, TRA1, and STC2 as prognostic markers in breast cancer in a screen for signal sequence encoding proteins. *Clin Cancer Res*, 13(11):3164–73, 2007.

[168] H. Wang, K. Wu, Y. Sun, Y. Li, M. Wu, Q. Qiao, Y. Wei, Z. G. Han, and B. Cai. STC2 is upregulated in hepatocellular carcinoma and promotes cell proliferation and migration in vitro. *BMB Rep*, 45(11):629–34, 2012.

[169] M. Böckers, N. W. Paul, and T. Efferth. Organophosphate ester tri-*o*-cresyl phosphate interacts with estrogen receptor α in MCF-7 breast cancer cells promoting cancer growth. *Toxicol Appl Pharmacol.*, 395:114977, 2020.

[170] J. C. Anderson, B. J. Park, and V. P. Palace. Microplastics in aquatic environments: Implications for Canadian ecosystems. *Environ Pollut*, 218:269–280, 2016.

[171] J. L. Conkle, C. D. Baez Del Valle, and J. W. Turner. Are we underestimating microplastic contamination in aquatic environments? *Environ Manage*, 61(1):1–8, 2018.

[172] E. Guzzetti, A. Sureda, S. Tejada, and C. Faggio. Microplastic in marine organism: Environmental and toxicological effects. *Environ Toxicol Pharmacol*, 64:164–171, 2018.

[173] E. Mendenhall. Oceans of plastic: A research agenda to propel policy development. *Marine Policy*, 96:291–298, 2018.

[174] H. Luo, Y. Xiang, D. He, Y. Li, Y. Zhao, S. Wang, and X. Pan. Leaching behavior of fluorescent additives from microplastics and the toxicity of leachate to chlorella vulgaris. *Sci Total Environ*, 678:1–9, 2019.

[175] P. Wu, Z. Cai, H. Jin, and Y. Tang. Adsorption mechanisms of five bisphenol analogues on PVC microplastics. *Sci Total Environ*, 650(Pt 1):671–678, 2019.

[176] H. Zhang, Q. Zhou, Z. Xie, Y. Zhou, C. Tu, C. Fu, W. Mi, R. Ebinghaus, P. Christie, and Y. Luo. Occurrences of organophosphorus esters and phthalates in the microplastics from the coastal beaches in north China. *Sci Total Environ*, 616-617:1505–1512, 2018.

[177] M. Rahman and C. Brazel. The plasticizer market: an assessment of traditional plasticizers and research trends to meet new challenges. *Progress in Polymer Science*, 29(12):1223–1248, 2004.

[178] A. K. Greaves and R. J. Letcher. A review of organophosphate esters in the environment from biological effects to distribution and fate. *Bull Environ Contam Toxicol*, 98(1):2–7, 2017.

[179] P. H. Craig and M. L. Barth. Evaluation of the hazards of industrial exposure to tricresyl phosphate: a review and interpretation of the literature. *J Toxicol Environ Health B Crit Rev*, 2(4):281–300, 1999.

[180] C. Winder and J. C. Balouet. The toxicity of commercial jet oils. *Environ Res*, 89(2):146–64, 2002.

[181] J. X. Chen, Y. J. Sun, P. Wang, D. X. Long, W. Li, L. Li, and Y. J. Wu. Induction of autophagy by TOCP in differentiated human neuroblastoma cells lead to degradation of cytoskeletal components and inhibition of neurite outgrowth. *Toxicology*, 310:92–7, 2013.

[182] D. X. Long, D. Hu, P. Wang, and Y. J. Wu. Induction of autophagy in human neuroblastoma SH-SY5Y cells by tri-ortho-cresyl phosphate. *Mol Cell Biochem*, 396(1-2):33–40, 2014.

[183] H. Y. Xu, P. Wang, Y. J. Sun, L. Jiang, M. Y. Xu, and Y. J. Wu. Autophagy in tri-o-cresyl phosphate-induced delayed neurotoxicity. *J Neuropathol Exp Neurol*, 76(1):52–60, 2017.

[184] F. Song, Y. Yan, X. Zhao, D. Dou, C. Zhang, and K. Xie. Phenylmethylsulfonyl fluoride protects against the degradation of neurofilaments in tri-ortho-cresyl phosphate (TOCP) induced delayed neuropathy. *Toxicology*, 262(3):258–64, 2009.

[185] C. Zou, R. Kou, Y. Gao, K. Xie, and F. Song. Activation of mitochondria-mediated apoptotic pathway in tri-ortho-cresyl phosphate-induced delayed neuropathy. *Neurochem Int*, 62(7):965–72, 2013.

[186] L. L. Xu, C. Y. Long, J. L. Wang, M. Yu, and J. X. Chen. Involvement of oxidative stress in tri-ortho-cresyl phosphate-induced liver injury in male mice. *Hum Exp Toxicol*, 35(10):1093–101, 2016.

[187] J. X. Chen, L. L. Xu, J. H. Mei, X. B. Yu, H. B. Kuang, H. Y. Liu, Y. J. Wu, and J. L. Wang. Involvement of neuropathy target esterase in tri-*ortho*-cresyl phosphate-induced testicular spermatogenesis failure and growth inhibition of spermatogonial stem cells in mice. *Toxicol Lett*, 211(1):54–61, 2012.

[188] E. A. Krumm, V. J. Patel, T. S. Tillery, A. Yasrebi, J. Shen, G. L. Guo, S. M. Marco, B. T. Buckley, and T. A. Roepke. Organophosphate flame-retardants alter adult mouse homeostasis and gene expression in a sex-dependent manner potentially through interactions with ERα. *Toxicol Sci*, 162(1):212–224, 2018.

[189] M. L. Liu, J. L. Wang, J. Wei, L. L. Xu, M. Yu, X. M. Liu, W. L. Ruan, and J. X. Chen. Tri-ortho-cresyl phosphate induces autophagy of rat spermatogonial stem cells. *Reproduction*, 149(2):163–70, 2015.

[190] X. Liu, L. Xu, J. Shen, J. Wang, W. Ruan, M. Yu, and J. Chen. Involvement of oxidative stress in tri-ortho-cresyl phosphate-induced autophagy of mouse leydig TM3 cells in vitro. *Reprod Biol Endocrinol*, 14(1):30, 2016.

[191] S. G. Somkuti, D. M. Lapadula, R. E. Chapin, and M. B. Abou-Donia. Light and electron microscopic evidence of tri-o-cresyl phosphate (TOCP)-mediated testicular toxicity in fischer 344 rats. *Toxicology and Applied Pharmacology*, 107(1):35–46, 1991.

[192] S. G. Somkuti, D. M. Lapadula, R. E. Chapin, J. C. Lamb, and M. B. Abou-Donia. Reproductive tract lesions resulting from subchronic administration (63 days) of tri-o-cresyl phosphate in male rats. *Toxicology and Applied Pharmacology*, 89(1):49–63, 1987.

[193] S. Yang, S. Shao, B. Huang, D. Yang, L. Zeng, Y. Gan, D. Long, J. Chen, and J. Wang. Tea polyphenols alleviate tri-ortho-cresyl phosphate-induced autophagy of mouse ovarian granulosa cells. *Environ Toxicol*, 2019.

[194] L. Hu, T. Peng, J. Huang, T. Su, R. Luo, Y. Zheng, Z. Zhong, P. Yu, K. Nie, and L. Zheng. Tri-ortho-cresyl phosphate (TOCP) induced ovarian failure in mice is related to the Hippo signaling pathway disruption. *Reprod Toxicol*, 83:21–27, 2019.

[195] J. Mathieu-Denoncourt, S. J. Wallace, S. R. de Solla, and V. S. Langlois. Plasticizer endocrine disruption: Highlighting developmental and reproductive effects in mammals and non-mammalian aquatic species. *Gen Comp Endocrinol*, 219:74–88, 2015.

[196] X. Wang, R. Zhang, C. Song, and D. Crump. Computational evaluation of interactions between organophosphate esters and nuclear hormone receptors. *Environ Res*, 182:108982, 2020.

[197] T. Komori. Regulation of skeletal development by the Runx family of transcription factors. *J Cell Biochem*, 95(3):445–53, 2005.

[198] K. Milde-Langosch, S. Janke, I. Wagner, C. Schroder, T. Streichert, A. M. Bamberger, F. Janicke, and T. Loning. Role of Fra-2 in breast cancer: influence on tumor cell invasion and motility. *Breast Cancer Res Treat*, 107(3):337–47, 2008.

[199] T. Akasaka, T. Balasas, L. J. Russell, K. Sugimoto, A. Majid, R. Walewska, E. L. Karran, D. G. Brown, K. Cain, L. Harder, S. Gesk, J. I. Martin-Subero, M. G. Atherton, M. Brueggemann, M. J. Calasanz, T. Davies, O. A. Haas, A. Hagemeijer, H. Kempski, M. Lessard, D. M. Lillington, S. Moore, F. Nguyen-Khac, I. Radford-Weiss, C. Schoch, S. Struski, P. Talley, M. J. Welham, H. Worley, J. C. Strefford, C. J. Harrison, R. Siebert, and M. J. S. Dyer. Five members of the CEBP transcription

factor family are targeted by recurrent IGH translocations in B-cell precursor acute lymphoblastic leukemia (bcp-all). *Blood*, 109(8):3451–3461, 2006.

[200] T. Pabst, B. Mueller, P. Zhang, H. S. Radomska, S. Narravula, S. Schnittger, G. Behre, W. Hiddemann, and D. G. Tenen. Dominant-negative mutations of CEBPA, encoding CCAAT/enhancer binding protein-α (C/EBPα), in acute myeloid leukemia. *Nat Genet*, 27:263–270, 2001.

[201] F. Stossi, V. S. Likhite, J. A. Katzenellenbogen, and B. S. Katzenellenbogen. Estrogen-occupied estrogen receptor represses cyclin G2 gene expression and recruits a repressor complex at the cyclin G2 promoter. *J Biol Chem*, 281(24):16272–8, 2006.

[202] M. Zimmermann, A. P. Arachchige-Don, M. S. Donaldson, T. Patriarchi, and M. C. Horne. Cyclin G2 promotes cell cycle arrest in breast cancer cells responding to fulvestrant and metformin and correlates with patient survival. *Cell Cycle*, 15(23):3278–3295, 2016.

[203] S. Gao, J. J. Ma, and C. Lu. Prognostic value of cyclin E expression in breast cancer: a meta-analysis. *Tumour Biol*, 34(6):3423–30, 2013.

[204] H. C. Hwang and B. E. Clurman. Cyclin E in normal and neoplastic cell cycles. *Oncogene*, 24(17):2776–86, 2005.

[205] S. Santala, A. Talvensaari-Mattila, Y. Soini, and M. Santala. Cyclin E expression correlates with cancer-specific survival in endometrial endometrioid adenocarcinoma. *Anticancer Res*, 35(6):3393–3397, 2015.

[206] E. Tortosa, C. Montenegro-Venegas, M. Benoist, S. Hartel, C. Gonzalez-Billault, J. A. Esteban, and J. Avila. Microtubule-associated protein 1B (MAP1B) is required for dendritic spine development and synaptic maturation. *J Biol Chem*, 286(47):40638–48, 2011.

[207] S. K. Saha, H. Y. Choi, B. W. Kim, A. A. Dayem, G. M. Yang, K. S. Kim, Y. F. Yin, and S. G. Cho. KRT19 directly interacts with β-catenin/RAC1 complex to regulate numb-dependent NOTCH signaling pathway and breast cancer properties. *Oncogene*, 36(3):332–349, 2017.

[208] D. N. Jackson and D. A. Foster. The enigmatic protein kinase Cδ: complex roles in cell proliferation and survival. *FASEB J*, 18(6):627–36, 2004.

[209] E. McKiernan, K. O'Brien, N. Grebenchtchikov, A. Geurts-Moespot, A. M. Sieuwerts, J. W. Martens, V. Magdolen, D. Evoy, E. McDermott, J. Crown, F. C. Sweep, and M. J. Duffy. Protein kinase C δ expression in breast cancer as measured by real-time PCR, western blotting and ELISA. *Br J Cancer*, 99(10):1644–50, 2008.

[210] J. Ikeda, E. Morii, Y. Liu, Y. Qiu, N. Nakamichi, R. Jokoji, Y. Miyoshi, S. Noguchi, and K. Aozasa. Prognostic significance of CD55 expression in breast cancer. *Clin Cancer Res*, 14(15):4780–6, 2008.

[211] Z. Madjd, L. G. Durrant, R. Bradley, I. Spendlove, I. O. Ellis, and S. E. Pinder. Loss of CD55 is associated with aggressive breast tumors. *Clin Cancer Res*, 10(8):2797–2803, 2004.

[212] K. Joensuu, P. Heikkila, and L. C. Andersson. Tumor dormancy: elevated expression of stanniocalcins in late relapsing breast cancer. *Cancer Lett*, 265(1):76–83, 2008.

[213] J. Wu, M. Lai, C. Shao, J. Wang, and J. J. Wei. STC2 overexpression mediated by HMGA2 is a biomarker for aggressiveness of high-grade serous ovarian cancer. *Oncol Rep*, 34(3):1494–502, 2015.

[214] L. Claesson-Welsh and M. Welsh. VEGFA and tumour angiogenesis. *J Intern Med*, 273(2):114–27, 2013.

[215] M. Böckers, N. W. Paul, and T. Efferth. Indeno[1,2,3-*cd*]pyrene and picene mediate actions *via* estrogen receptor α signaling pathway in *in vitro* cell systems, altering gene expression. *Toxicol Appl Pharmacol.*, 396:114995, 2020.

[216] B. Gewert, M. M. Plassmann, and M. MacLeod. Pathways for degradation of plastic polymers floating in the marine environment. *Environ. Sci.: Processes Impacts*, 17:1513–1521, 2015.

[217] M. R. Gregory. Environmental implications of plastic debris in marine settings–entanglement, ingestion, smothering, hangers-on, hitch-hiking and alien invasions. *Philos Trans R Soc Lond B Biol Sci*, 364(1526):2013–25, 2009.

[218] C. Wesch, K. Bredimus, M. Paulus, and R. Klein. Towards the suitable monitoring of ingestion of microplastics by marine biota: A review. *Environ Pollut*, 218:1200–1208, 2016.

[219] M. Kedzierski, B. Lechat, O. Sire, G. Le Maguer, V. Le Tilly, and S. Bruzaud. Microplastic contamination of packaged meat: Occurrence and associated risks. *Food Packag Shelf Life*, 24:100489, 2020.

[220] J. C Prata, J. P. da Costa, I. Lopes, A. C Duarte, and T. Rocha-Santos. Environmental exposure to microplastics: An overview on possible human health effects. *Sci Total Environ*, 702:134455, 2019.

[221] P. Zuccarello, M. Ferrante, A. Cristaldi, C. Copat, A. Grasso, D. Sangregorio, and G. O. Conti. Exposure to microplastics (<10 μm) associated to plastic bottles mineral water consumption: The first quantitative study. *Water Res*, 157:365–371, 2019.

[222] M. Fisner, S. Taniguchi, F. Moreira, M. C. Bicego, and A. Turra. Polycyclic aromatic hydrocarbons (PAHs) in plastic pellets: variability in the concentration and composition at different sediment depths in a sandy beach. *Mar Pollut Bull*, 70(1-2):219–26, 2013.

[223] C. R. Nobre, M. F. M. Santana, A. Maluf, F. S. Cortez, A. Cesar, C. D. S. Pereira, and A. Turra. Assessment of microplastic toxicity to embryonic development of the sea urchin lytechinus variegatus (echinodermata: Echinoidea). *Mar Pollut Bull*, 92(1-2):99–104, 2015.

[224] T. S. Galloway, M. Cole, and C. Lewis. Interactions of microplastic debris throughout the marine ecosystem. *Nat Ecol Evol*, 1(5):116, 2017.

[225] V. Foulon, F. Le Roux, C. Lambert, A. Huvet, P. Soudant, and I. Paul-Pont. Colonization of polystyrene microparticles by vibrio crassostreae: Light and electron microscopic investigation. *Environ Sci Technol*, 50(20):10988–10996, 2016.

[226] J. Reisser, J. Shaw, G. Hallegraeff, M. Proietti, D. K. A. Barnes, M. Thums, C. Wilcox, B. D. Hardesty, and C. Pattiaratchi. Millimeter-sized marine plastics: A new pelagic habitat for microorganisms and invertebrates. *PLOS ONE*, 9(6):e100289, 2014.

[227] E. R. Zettler, T. J. Mincer, and L. A. Amaral-Zettler. Life in the "plastisphere": microbial communities on plastic marine debris. *Environ Sci Technol*, 47(13):7137–46, 2013.

[228] L. Liu, R. Fokkink, and A. A. Koelmans. Sorption of polycyclic aromatic hydrocarbons to polystyrene nanoplastic. *Environ Toxicol Chem*, 35(7):1650–5, 2016.

[229] M. Cole, P. Lindeque, C. Halsband, and T. S. Galloway. Microplastics as contaminants in the marine environment: a review. *Mar Pollut Bull*, 62(12):2588–97, 2011.

[230] J. P. Frias, P. Sobral, and A. M. Ferreira. Organic pollutants in microplastics from two beaches of the portuguese coast. *Mar Pollut Bull*, 60(11):1988–92, 2010.

[231] L. M. Rios, C. Moore, and P. R. Jones. Persistent organic pollutants carried by synthetic polymers in the ocean environment. *Mar Pollut Bull*, 54(8):1230–7, 2007.

[232] Lorena M. Rios Mendoza and Patrick R. Jones. Characterisation of microplastics and toxic chemicals extracted from microplastic samples from the North Pacific Gyre. *Environmental Chemistry*, 12(5):611, 2015.

[233] C. M. Rochman, E. Hoh, B. T. Hentschel, and S. Kaye. Long-term field measurement of sorption of organic contaminants to five types of plastic pellets: implications for plastic marine debris. *Environ Sci Technol*, 47(3):1646–54, 2013.

[234] A. A. Koelmans, A. Bakir, G. A. Burton, and C. R. Janssen. Microplastic as a vector for chemicals in the aquatic environment: Critical review and model-supported reinterpretation of empirical studies. *Environ Sci Technol*, 50(7):3315–26, 2016.

[235] R. Lohmann. Microplastics are not important for the cycling and bioaccumulation of organic pollutants in the oceans-but should microplastics be considered POPs themselves? *Integr Environ Assess Manag*, 13(3):460–465, 2017.

[236] C. Scopetani, A. Cincinelli, T. Martellini, E. Lombardini, A. Ciofini, A. Fortunati, V. Pasquali, S. Ciattini, and A. Ugolini. Ingested microplastic as a two-way transporter for PBDEs in talitrus saltator. *Environ Res*, 167:411–417, 2018.

[237] M. A. Browne, S. J. Niven, T. S. Galloway, S. J. Rowland, and R. C. Thompson. Microplastic moves pollutants and additives to worms, reducing functions linked to health and biodiversity. *Curr Biol*, 23(23):2388–92, 2013.

[238] K. Fent and R. Bätscher. Cytochrome P4501A induction potencies of polycyclic aromatic hydrocarbons in a fish hepatoma cell line: Demonstration of additive interactions. *Environmental Toxicology and Chemistry*, 19(8):2047–2058, 2000.

[239] S. W. Rogers, S. K. Ong, B. H. Kjartanson, J. Golchin, and G. A. Stenback. Natural attenuation of polycyclic aromatic hydrocarbon-contaminated sites: Review. *Practice Periodical of Hazardous, Toxic, and Radioactive Waste Management*, 6(3):141–155, 2002.

[240] B.S. Katzenellenbogen, I. Choi, R. Delage-Mourroux, T. R. Ediger, P. G. V. Martini, M. Montano, J. Sun, K. Weis, and J.A. Katzenellenbogen. Molecular mechanisms of estrogen action: selective ligands and receptor pharmacology. *The Journal of Steroid Biochemistry and Molecular Biology*, 74(5):279–285, 2000.

[241] K. Skupinska, I. Misiewicz-Krzeminska, K. Lubelska, and T. Kasprzycka-Guttman. The effect of isothiocyanates on CYP1A1 and CYP1A2 activities induced by polycyclic aromatic hydrocarbons in MCF7 cells. *Toxicol In Vitro*, 23(5):763–71, 2009.

[242] D. C. Spink, S. J. Wu, B. C. Spink, M. M. Hussain, D. D. Vakharia, B. T. Pentecost, and L. S. Kaminsky. Induction of CYP1A1 and CYP1B1 by benzo(k)fluoranthene and benzo(a)pyrene in T-47D human breast cancer cells: roles of PAH interactions and PAH metabolites. *Toxicol Appl Pharmacol*, 226(3):213–24, 2008.

[243] C. F. Vogel, W. L. Chang, S. Kado, K. McCulloh, H. Vogel, D. Wu, T. Haarmann-Stemmann, G. Yang, P. S. Leung, F. Matsumura, and M. E. Gershwin. Transgenic overexpression of aryl hydrocarbon receptor repressor (AhRR) and AhR-mediated induction of CYP1A1, cytokines, and acute toxicity. *Environ Health Perspect*, 124(7):1071–83, 2016.

[244] S. Ahmed, S. Al-Saigh, and J. Matthews. FOXA1 is essential for andryl hydrocarbon receptor-dependent regulation of cyclin G2. *Mol Cancer Res*, 10(5):636–48, 2012.

[245] S. Hua, R. Kittler, and K. P. White. Genomic antagonism between retinoic acid and estrogen signaling in breast cancer. *Cell*, 137(7):1259–71, 2009.

[246] X. H. Tang and L. J. Gudas. Retinoids, retinoic acid receptors, and cancer. *Annu Rev Pathol*, 6:345–64, 2011.

[247] G. W. Woodfield, A. D. Horan, Y. Chen, and R. J. Weigel. TFAP2C controls hormone response in breast cancer cells through multiple pathways of estrogen signaling. *Cancer Res*, 67(18):8439–43, 2007.

[248] J. M. Gee, J. J. Eloranta, J. C. Ibbitt, J. F. Robertson, I. O. Ellis, T. Williams, R. I. Nicholson, and H. C. Hurst. Overexpression of TFAP2C in invasive breast cancer correlates with a poorer response to anti-hormone therapy and reduced patient survival. *J Pathol*, 217(1):32–41, 2009.

[249] M. Lacroix and G. Leclercq. About GATA3, HNF3A, and XBP1, three genes co-expressed with the oestrogen receptor-α gene (ESR1) in breast cancer. *Mol Cell Endocrinol*, 219(1-2):1–7, 2004.

[250] L. Romero-Ramirez, H. Cao, D. Nelson, E. Hammond, A.-H. Lee, H. Yoshida, K. Mori, L. H. Glimcher, N. C. Denko, A. J. Giaccia, Q.-T. Le, and A. C. Koong. XBP1 is essential for survival under hypoxic conditions and is required for tumor growth. *Cancer Research*, 64(17):5943–5947, 2004.

[251] P. Chan, A. Möller, M. C. P. Liu, J. E. Sceneay, C. S. F. Wong, N. Waddell, K. T. Huang, A. Dobrovic, E. K. A. Millar, S. A. O'Toole, C. M. McNeil, R. L. Sutherland, D. D. Bowtell, and S. B. Fox. The expression of the ubiquitin ligase SIAH2 (seven in absentia homolog 2) is mediated through gene copy number in breast cancer and is associated with a basal-like phenotype and p53 expression. *Breast Cancer Research*, 13(1):R19, 2011.

[252] K. Nakayama, J. Qi, and Z. Ronai. The ubiquitin ligase Siah2 and the hypoxia response. *Mol Cancer Res*, 7(4):443–51, 2009.

[253] M. P. Jansen, K. Ruigrok-Ritstier, L. C. Dorssers, I. L. van Staveren, M. P. Look, M. E. Meijer-van Gelder, A. M. Sieuwerts, J. Helleman, S. Sleijfer, J. G. Klijn, J. A. Foekens, and E. M. Berns. Downregulation of SIAH2, an ubiquitin E3 ligase, is associated with resistance to endocrine therapy in breast cancer. *Breast Cancer Res Treat*, 116(2):263–71, 2009.

[254] N. Bretschneider, S. Kangaspeska, M. Seifert, G. Reid, F. Gannon, and S. Denger. E2-mediated cathepsin D (CTSD) activation involves looping of distal enhancer elements. *Mol Oncol*, 2(2):182–90, 2008.

[255] V. Krishnan, X. Wang, and S. Safe. Estrogen receptor-Sp1 complexes mediate estrogen-induced cathepsin D gene expression in MCF-7 human breast cancer cells. *J Biol Chem*, 269(22):15912–15917, 1994.

[256] M. Wolf, I. Clark-Lewis, C. Buri, H. Langen, M. Lis, and L. Mazzucchelli. Cathepsin D specifically cleaves the chemokines macrophage inflammatory protein-1α, macrophage inflammatory protein-1β, and SLC that are expressed in human breast cancer. *The American Journal of Pathology*, 162(4):1183–1190, 2003.

[257] S. Lal, A. Mahajan, W. Ning Chen, and B. Chowbay. Pharmacogenetics of target genes across doxorubicin disposition pathway: A review. *Current Drug Metabolism*, 11(1):115–128, 2010.

[258] R. El Ansari, M. L. Craze, I. Miligy, M. Diez-Rodriguez, C. C. Nolan, I. O. Ellis, E. A. Rakha, and A. R. Green. The amino acid transporter SLC7A5 confers a poor prognosis in the highly proliferative breast cancer subtypes and is a key therapeutic target in luminal B tumours. *Breast Cancer Res*, 20(1):21, 2018.

[259] A. Gattelli, I. Nalvarte, A. Boulay, T. C. Roloff, M. Schreiber, N. Carragher, K. K. Macleod, M. Schlederer, S. Lienhard, L. Kenner, M. I. Torres-Arzayus, and N. E. Hynes. Ret inhibition decreases growth and metastatic potential of estrogen receptor positive breast cancer cells. *EMBO Mol Med*, 5(9):1335–50, 2013.

[260] M. Nguyen, S. Miyakawa, J. Kato, T. Mori, T. Arai, M. Armanini, K. Gelmon, R. Yerushalmi, S. Leung, D. Gao, G. Landes, M. Haak-Frendscho, K. Elias, and A. D. Simmons. Preclinical efficacy and safety assessment of an antibody-drug conjugate targeting the c-RET proto-oncogene for breast carcinoma. *Clin Cancer Res*, 21(24):5552–62, 2015.

[261] X. Sun, G. Cheng, M. Hao, J. Zheng, X. Zhou, J. Zhang, R. S. Taichman, K. J. Pienta, and J. Wang. CXCL12 / CXCR4 / CXCR7 chemokine axis and cancer progression. *Cancer Metastasis Rev*, 29(4):709–22, 2010.

[262] E. Castro-Rivera, S. Ran, P. Thorpe, and J. D. Minna. Semaphorin 3B (SEMA3B) induces apoptosis in lung and breast cancer, whereas VEGF165 antagonizes this effect. *Proc Natl Acad Sci U S A*, 101(31):11432–7, 2004.

[263] A. Sakurai, C. L. Doci, and J. S. Gutkind. Semaphorin signaling in angiogenesis, lymphangiogenesis and cancer. *Cell Res*, 22(1):23–32, 2012.

[264] K. Dabanaka, S. Chung, H. Nakagawa, Y. Nakamura, T. Okabayashi, T. Sugimoto, K. Hanazaki, and M. Furihata. PKIB expression strongly correlated with phosphorylated Akt expression in breast cancers and also with triple-negative breast cancer subtype. *Med Mol Morphol*, 45(4):229–33, 2012.

[265] J.-B. Zhang, W. Song, Y.-Y. Wang, M.-G. Liu, M.-M. Sun, and H. Liu. Study on correlation between PKIB and pAkt expression in breast cancer tissues. *Eur Rev Med Pharmacol Sci*, 21(6):1264–1269, 2017.

[266] A. S. Pfister, K. Tanneberger, A. Schambony, and J. Behrens. Amer2 protein is a novel negative regulator of wnt/β-catenin signaling involved in neuroectodermal patterning. *J Biol Chem*, 287(3):1734–41, 2012.

[267] V. Vasiliou, A. Pappa, and D. R. Petersen. Role of aldehyde dehydrogenases in endogenous and xenobiotic metabolism. *Chemico-Biological Interactions*, 129(1-2):1–19, 2000.

[268] J. J. Duan, J. Cai, Y. F. Guo, X. W. Bian, and S. C. Yu. ALDH1A3, a metabolic target for cancer diagnosis and therapy. *Int J Cancer*, 139(5):965–75, 2016.

[269] P. Pappas, M. Sotiropoulou, P. Karamanakos, A. Kostoula, S. Levidiotou, and M. Marselos. Acute-phase response to benzo[a]pyrene and induction of rat ALDH3A1. *Chem Biol Interact*, 143-144:55–62, 2003.

[270] J. D. Karkera, J. S. Lee, E. Roessler, S. Banerjee-Basu, M. V. Ouspenskaia, J. Mez, E. Goldmuntz, P. Bowers, J. Towbin, J. W. Belmont, A. D. Baxevanis, A. F. Schier, and M. Muenke. Loss-of-function mutations in growth differentiation factor-1 (GDF1) are associated with congenital heart defects in humans. *Am J Hum Genet*, 81(5):987–94, 2007.

[271] S.-J. Lee. Identification of a novel member (GDF-1) of the transformin growth factor-β superfamily. *Molecular Endocrinology*, 4(7):1034–1040, 1990.

[272] S. P. Khare, A. Sharma, K. K. Deodhar, and S. Gupta. Overexpression of histone variant H2A.1 and cellular transformation are related in N-nitrosodiethylamine-induced sequential hepatocarcinogenesis. *Exp Biol Med*, 236(1):30–5, 2011.

[273] R. K. Singh, D. Liang, U. R. Gajjalaiahvari, M. H. Kabbaj, J. Paik, and A. Gunjan. Excess histone levels mediate cytotoxicity via multiple mechanisms. *Cell Cycle*, 9(20):4236–44, 2010.

[274] M. E. Harris, R. Böhni, M. H. Schneiderman, L. Ramamurthy, D. Schümperli, and W. F. Marzluff. Regulation of histone mRNA in the unperturbed cell cycle:

evidence suggesting control at two posttranscriptional steps. *Molecular and Cellular Biology*, 11(5):2416–2424, 1991.

Publications and presentations

Peer-reviewed journal articles

- M. Böckers, N. W. Paul, T. Efferth
  Bisphenolic compounds alter gene expression in MCF-7 cells through interaction with estrogen receptor α
  Toxicol. Appl. Pharmacol. **399**:115030 (2020)
- M. Böckers, N. W. Paul, T. Efferth
  *Indeno[1,2,3-*cd*]pyrene and picene mediate actions* via *estrogen receptor α signaling pathway in* in vitro *cell systems, altering gene expression*
  Toxicol. Appl. Pharmacol. **396**:114995 (2020)
- M. Böckers, N. W. Paul, T. Efferth
  *Organophosphate ester tri-*o*-cresyl phosphate interacts with estrogen receptor α in MCF-7 breast cancer cells promoting cancer growth*
  Toxicol. Appl. Pharmacol. **395**:114977 (2020)
- S. Abdelfatah,* M. Böckers,* M. Asensio, O. Kadioglu, A. Klinger, E. Fleischer, T. Efferth (* Authors contributed equally)
  Isopetasin and S-isopetasin as novel P-glycoprotein inhibitors against multidrug-resistant cancer cells
  Phytomedicine, *in press* (2020)
- S. Abdelfatah, A. Berg, M. Böckers, T. Efferth
  A selective inhibitor of the Polo-box domain of Polo-like kinase 1 identified by virtual screening
  J. Adv. Res. **16** (2019)

Journal articles in preparation

- M. Böckers, N. W. Paul, T. Efferth
  Butyl octyl phthalate interacts with estrogen receptor α in MCF-7 breast cancer cells promoting cancer development

Editorial

- M. Böckers, M. Saeed, T. Efferth
  Second Career for Grayanotoxins?
  Med. Aromat. Plants **5.1** (2016)

Talk

- *Life Sciences - Life Writing*
  Entanglements of Mind and Matter, Machines and Microbes
  M. Böckers, O. Kuchenbuch, J. Pötzsch
  Blue Skies – Bodies in Trouble, PACT Zollverein, July 2019, Essen, Germany

Posters

- *A selective inhibitor of the Polo-box domain of Polo-like kinase 1 identified by virtual screening*
  S. Abdelfatah, A. Berg, M. Böckers, T. Efferth
  14th Charles Rodolphe Brupbacher Symposium, January 2019, Zurich, Switzerland
- *Plastic in the Ocean - Just Far Away?*
  Molecular Mechanisms of Estrogenic Xenobiotica
  M. Böckers, T. Efferth, M. Banerjee
  Inspection of the DFG research training group *Life Sciences – Life Writing*, March 2018, Mainz, Germany